

NTIS # PB2011-

SSC-460

**EFFECT OF WELDED PROPERTIES
ON ALUMINUM STRUCTURES**



This document has been approved
For public release and sale; its
Distribution is unlimited

SHIP STRUCTURE COMMITTEE
2011

Ship Structure Committee

RADM P.F. Zukunft
U. S. Coast Guard Assistant Commandant,
Assistant Commandant for Marine Safety, Security
and Stewardship
Co-Chair, Ship Structure Committee

Mr. H. Paul Cojeen
Society of Naval Architects and Marine Engineers

Mr. Christopher McMahon
Director, Office of Ship Construction
Maritime Administration

Mr. Kevin Baetsen
Director of Engineering
Military Sealift Command

Mr. Jeffrey Lantz,
Commercial Regulations and Standards for the
Assistant Commandant for Marine Safety, Security
and Stewardship
Mr. Jeffery Orner
Deputy Assistant Commandant for Engineering and
Logistics

RDML Thomas Eccles
Chief Engineer and Deputy Commander
For Naval Systems Engineering (SEA05)
Co-Chair, Ship Structure Committee

Dr. Roger Basu
Senior Vice President
American Bureau of Shipping

Mr. Victor Santos Pedro
Director Design, Equipment and Boating Safety,
Marine Safety,
Transport Canada

Dr. Neil Pegg
Group Leader - Structural Mechanics
Defence Research & Development Canada - Atlantic

Mr. Edward Godfrey
Director, Structural Integrity and Performance Division

Dr. John Pazik
Director, Ship Systems and Engineering Research
Division

SHIP STRUCTURE SUB-COMMITTEE

AMERICAN BUREAU OF SHIPPING (ABS)

Mr. Craig Bone
Mr. Phil Rynn
Mr. Tom Ingram

MARITIME ADMINISTRATION (MARAD)

Mr. Chao Lin
Mr. Richard Sonnenschein

NAVY/ONR / NAVSEA/ NSWCCD

Mr. David Qualley / Dr. Paul Hess
Mr. Erik Rasmussen / Dr. Roshdy Barsoum
Mr. Nat Nappi, Jr.
Mr. Malcolm Witford

UNITED STATES COAST GUARD

CAPT John Nadeau
CAPT Paul Roden
Mr. Jaideep Sirkar
Mr. Chris Cleary

DEFENCE RESEARCH & DEVELOPMENT CANADA ATLANTIC

Dr. David Stredulinsky
Mr. John Porter

MILITARY SEALIFT COMMAND (MSC)

Mr. Michael W. Touma
Mr. Jitesh Kerai

TRANSPORT CANADA

Natasa Kozarski
Luc Tremblay

SOCIETY OF NAVAL ARCHITECTS AND MARINE ENGINEERS (SNAME)

Mr. Rick Ashcroft
Mr. Dave Helgerson
Mr. Alex Landsburg
Mr. Paul H. Miller

Member Agencies:

*American Bureau of Shipping
Defence Research and Development Canada
Maritime Administration
Military Sealift Command
Naval Sea Systems Command
Office of Naval Research
Society of Naval Architects & Marine Engineers
Transport Canada
United States Coast Guard*



**Ship
Structure
Committee**

Address Correspondence to:

COMMANDANT (CG-5212/SSC)
ATTN (EXECUTIVE DIRECTOR/SHIP
STRUCTURE COMMITTEE)
US COAST GUARD
2100 2ND ST SW STOP 7126
WASHINGTON DC 20593-7126
Website: <http://www.shipstructure.org>

**SSC – 460
SR – 1460**

JANUARY 5, 2011

EFFECT OF WELDED PROPERTIES ON ALUMINUM STRUCTURES

The design of a high-speed vessel is a constant trade-off analysis between reducing structural weight versus maintaining sufficient strength to prevent failure. The result has been widespread use of aluminum throughout vessel structures for its strength performance and reduced structural weight. Welding aluminum can result in significant modifications to the material properties in the area around the weld creating a heat-affected zone or HAZ with up to 50 percent reductions in base material strength. Consequently, typical analysis of vessel aluminum structure assumes a uniform reduction of material strength throughout the vessel and provides a safe, but conservative approach. This approach can underestimate the strength of welded structure and impose a significant weight penalty on the final vessel design.

This report presents a basis for the design of aluminum structures to minimize the HAZ penalty on scantling selection, provides a comparison of proposed design methods and suggests where additional research and development is warranted. Welded aluminum stiffened panels were analyzed to determine the reduction in strength in the HAZ using finite element and closed-form methods. Twelve combinations of plate and stiffener structures were analyzed for tension, compression, and bending. The structures considered within this project have material properties of all base metal, all HAZ metal, and a combination of base metal and HAZ metal.

We thank the authors and Project Technical Committee for their dedication and research toward completing the objectives and tasks detailed throughout this paper and continuing the Ship Structure Committee's mission to enhance the safety of life at sea.


P.F. ZUKUNFT
Rear Admiral, U.S. Coast Guard
Co-Chairman, Ship Structure Committee


T. J. ECCLES
Rear Admiral, U.S. Navy
Co-Chairman, Ship Structure Committee

1. Report No. SSC-460	2. Government Accession No.	3. Recipient's Catalog No.	
4. Title and Subtitle Effect of Welded Properties on Aluminum Structures		5. Report Date	
		6. Performing Organization Code	
7. Author(s) Sensharma, P.; Collette, M.; Harrington, J.		8. Performing Organization Report No. SR-1460	
9. Performing Organization Name and Address BMT Designers & Planners 2120 Washington Blvd, Suite 200 Arlington, VA 22204		10. Work Unit No. (TRAIS)	
		11. Contract or Grant No. DTMA1C09001	
12. Sponsoring Agency Name and Address COMMANDANT (CG-5212/SSC) ATTN (SHIP STRUCTURE COMMITTEE) US COAST GUARD 2100 2ND ST SW STOP 7126 WASHINGTON DC 20593-7126		13. Type of Report Final Report	
		14. Sponsoring Agency Code CG - 5	
15. Supplementary Notes The research completed by the above author for the Ship Structure Committee was reviewed by the Project Technical Committee for satisfactory completion of the objectives outlined in the Statement of Work developed and approved for funding by the Principal Members of the Ship Structure Committee. Sponsored by the Ship Structure Committee. Sponsored by the Ship Structure Committee and its member agencies			
16. Abstract The current commercial and military interest in large high-speed vessels has resulted in the development of monohulls, catamarans, and trimarans designs between 70m and 130m in length for transportation and combat roles. In this design space, deadweight is restricted, and the vessel operates under a constant tradeoff between cargo capacity, achievable speed, and achievable range quite unlike conventional displacement vessels. Given these restrictions, minimization of lightship weight, and hence structural weight, is of great significance in the design of the vessels. Most existing vessels in this category have been constructed out of aluminum to reduce structural weight. Welding aluminum results in significant modifications to the material properties in the area around the weld. The 5xxx-series and the 6xxx-series alloys obtain a significant portion of their strength either from cold working or thermal processing, processes that are impacted by the heat input from welding. The area impacted by the heat input from the welding process is termed as heat-affected zone or HAZ. For high-strength 5xxx and 6xxx-series alloys joined by fusion welding, the HAZ is typically 30%-50% weaker than the base material. The 30 to 50 percent decrease in the strength of the HAZ in aluminum has not been investigated sufficiently. Current design methods assume that all metal will have this reduced strength, whereas the localized weakening has been shown to have less effect on overall strength in compression and in tension. This approach may seriously underestimate the strength of welded structure, and if so, it imposes a significant weight penalty on the final vessel design. This study intends to provide a basis for modification to design standards. Fine mesh finite element models are developed and analyzed for different plate-stiffener combinations and for AL5083 and AL6082. Nonlinear stress-strain curves are used. These fine mesh models are analyzed using the properties of : a). Base metal, b). HAZ, c). Base metal and HAZ (extending 3*thickness of the plate). These models are analyzed for tension, compression and bending loads. For each of these three cases, limit state criteria are developed to compare the results.			
17. Key Words Aluminum , ultimate strength, heat affected zone, HAZ, Finite Element Analysis		18. Distribution Statement National Technical Information Service U.S. Department of Commerce Springfield, VA 22151 Ph. (703) 487-4650 / www.ntis.gov	
19. Security Classif. (of this report) Unclassified	20. Security Classif. (of this page) Unclassified	21. No. of Pages 794	22. Price

CONVERSION FACTORS
(Approximate conversions to metric measures)

To convert from	to	Function	Value
LENGTH			
inches	meters	divide	39.3701
inches	millimeters	multiply by	25.4000
feet	meters	divide by	3.2808
VOLUME			
cubic feet	cubic meters	divide by	35.3149
cubic inches	cubic meters	divide by	61,024
SECTION MODULUS			
inches ² feet ²	centimeters ² meters ²	multiply by	1.9665
inches ² feet ²	centimeters ³	multiply by	196.6448
inches ⁴	centimeters ³	multiply by	16.3871
MOMENT OF INERTIA			
inches ² feet ²	centimeters ² meters	divide by	1.6684
inches ² feet ²	centimeters ⁴	multiply by	5993.73
inches ⁴	centimeters ⁴	multiply by	41.623
FORCE OR MASS			
long tons	tonne	multiply by	1.0160
long tons	kilograms	multiply by	1016.047
pounds	tonnes	divide by	2204.62
pounds	kilograms	divide by	2.2046
pounds	Newtons	multiply by	4.4482
PRESSURE OR STRESS			
pounds/inch ²	Newtons/meter ² (Pascals)	multiply by	6894.757
kilo pounds/inch ²	mega Newtons/meter ² (mega Pascals)	multiply by	6.8947
BENDING OR TORQUE			
foot tons	meter tons	divide by	3.2291
foot pounds	kilogram meters	divide by	7.23285
foot pounds	Newton meters	multiply by	1.35582
ENERGY			
foot pounds	Joules	multiply by	1.355826
STRESS INTENSITY			
kilo pound/inch ² inch ^{1/2} (ksi√in)	mega Newton MNm ^{3/2}	multiply by	1.0998
J-INTEGRAL			
kilo pound/inch	Joules/mm ²	multiply by	0.1753
kilo pound/inch	kilo Joules/m ²	multiply by	175.3

TABLE OF CONTENTS

1	INTRODUCTION	5
2	OBJECTIVE AND SCOPE OF INVESTIGATION.....	7
3	ALUMINUM ALLOYS AND METALLURGY	10
4	LITERATURE SURVEY	15
4.1	Research on Aluminum Welds and Weld Effects.....	15
4.1.1	Local Studies of Welds	15
4.1.2	Impact of Welds on Tensile Response.....	18
4.1.3	Impact of Welds on Compression Response	20
4.1.4	Impact of Welds on Bending Response and Lateral Load Response	27
4.2	Aluminum Structural Design Standards	29
4.2.1	Aluminum Association	29
4.2.2	Eurocode 9	31
4.2.3	Classification Society Rules	34
4.3	Summary	38
5	ONR SIMPLIFIED APPROACH.....	42
6	FINITE ELEMENT MODELING.....	47
6.1	Model Matrix	47
6.2	Stress-Strain Relationships	48
6.3	Finite Element Models.....	49
6.4	Failure Criteria.....	52
7	RESULTS	54
7.1	Compression Load case	54
7.2	Tension Load Case.....	63
7.3	Pressure Load Case.....	67
7.4	Paik's Closed Form Solution	69
8	CONCLUSIONS AND RECOMMENDATIONS	74
9	REFERENCES	77

APPENDIX A: Panel Geometry selection for FEA

APPENDIX B: Ultimate Strength for Compressive Load Case

APPENDIX C: Compression Load Case - FEA Stress & Deflection Plots

APPENDIX D: Tension Load Case - Yield Point and Stress Plots

APPENDIX E: Pressure Load Case - Stress, Deflection and Strain Plots

LIST OF FIGURES

1. Figure 2-1: Material curves for plate-stiffener and HAZ (Rigo et al. 2003)	8
2. Figure 3-1: Comparison of Stress-Strain Curves in 6061 and 5083 Materials	13
3. Figure 6-1: Stress-Strain Relationships for AL5083 & AL 6082	49
4. Figure 6-2: Heat Affected Zone (HAZ) for Plate and stiffener (Paik 2005)	50
5. Figure 6-3: Finite element model of the Stiffened-plate	51
6. Figure 6-4: Finite element model with HAZ	51
7. Figure 6-5: Finite element model with HAZ for extruded panels	52
8. Figure 6-6: Boundary conditions applied to the finite element model	52
9. Figure 7-1: Comparison of Ultimate Strength (FEA Results)	55
10. Figure 7-2: Comparison of Ultimate Strength: Combined properties versus reduced base metal properties	61
11. Figure 7-3: Comparison of Ultimate Strength for Model 11: Combined properties versus increased HAZ properties (25% higher proof stress)	61
12. Figure 7-4: Strength Reduction vs. Failure Stress divide by HAZ Proof Stress	62
13. Figure 7-5: Strength Reduction vs. HAZ/Base Ratios of Tangent Modulus at Average Failure Stress	62
14. Figure 7-6: Comparison of yield points for tension load case	64
15. Figure 7-7: Plot of lateral pressure at the yield point	68
16. Figure 7-8: Percentage difference in lateral pressure wrt. combined case	68
17. Figure 7-9: Assumed softening zone (Paik 2005)	69
18. Figure 7-10: Cross section of the plate-stiffener combination with softening zones (Paik 2005)	69
19. Figure 7-11: Comparison of ultimate strength	73

LIST OF TABLES

1. Table 3-1: Impact of Welds on 6061 and 5083 Aluminum Alloys – 2”/50mm Gauge Length	12
2. Table 4-1: HAZ Width Specified by <i>Eurocode 9</i>	32
3. Table 4-2: Comparison of Welder Qualification Required Cross-Weld Ultimate Strengths	35
4. Table 4-3: Comparison of Given Proof Strengths for Welded Aluminum	36
5. Table 4-4: Comparison of Proposed Design Methods	41
6. Table 6-1: Matrix of Models to be analyzed.....	48
7. Table 6-2: Ramberg-Osgood Parameters.....	49
8. Table 7-1: Ultimate strength comparison for model 1, 5, & 9.....	56
9. Table 7-2: Ultimate strength comparison for model 2, 6, & 10.....	56
10. Table 7-3: Ultimate strength comparison for model 3, 7, & 11.....	57
11. Table 7-4: Ultimate strength comparison for model 4, 8, & 12.....	57
12. Table 7-5: Yield point comparison of Models 1,5 & 9.....	65
13. Table 7-6: Yield point comparison of Models 2,6 & 10.....	65
14. Table 7-7: Yield point comparison of Models 3,7 & 11.....	66
15. Table 7-8: Yield point comparison of Models 4,8 & 12.....	66
16. Table 7-9: Coefficients depending on the levels of initial deflections of plating and stiffeners (Paik 2005).....	72
17. Table 7-10: Comparison of Ultimate Strengths	72

ACKNOWLEDGEMENT

This study was sponsored by the interagency Ship Structures Committee. The authors are grateful for the guidance of the Project Technical Committee, especially the Chairman, Kim Tran of the Naval Surface Warfare Center, Carderock (NSWCCD).

EXECUTIVE SUMMARY

The US Ship Structures Committee Project, SR-1460, “Effect of Welded Properties on Aluminum Structures,” was awarded to BMT Designers & Planners (D&P) and Science Application International Corporation (SAIC). The objective of this project is to provide a basis for the design of aluminum structures that will minimize the penalty on scantling selection and to provide a basis for modification to design standards. The project was divided into the following 8 tasks:

Task 1. Creation of Draft and Final Project Plans

Task 2. Literature Survey

Task 3. Develop Matrix of Plate Stiffeners Models to be Analyzed

Task 4. Develop/Obtain Stress-Strain Relationship

Task 5. Develop and Analyze Fine Mesh Models

Task 6. Perform Volumetric Yield Strength calculations

Task 7. Recommend changes to Design Standard

Task 8. Preparation of Final Report

Tasks 1, 4, 5, and 6 were conducted primarily by D&P. SAIC conducted tasks 2 & 3 with contributions from D&P. Tasks 7 and 8 were performed with contributions from both the organizations. The main contributors from each organization are:

D&P	SAIC
Dr. Pradeep Sensharma	Dr. Matthew Collette
Joey Harrington	

The 5xxx-series and 6xxx-series aluminum alloys are extensively used for marine structures. Generally, 5xxx-series alloys possess excellent corrosion resistance when immersed in seawater whereas 6xxx-series are inferior. Traditionally, 5xxx-series alloys are used in deck and hull plating whereas 6xxx-series alloys are used as structural reinforcements, bulkheads, and

stiffeners that do not come in direct contact with seawater. Welding aluminum results in significant modifications to the material properties in the area around the weld. The area impacted by the heat input from the welding process is termed as heat-affected zone or HAZ. For high-strength 5xxx and 6xxx-series alloys joined by fusion welding, the HAZ is typically 30%-50% weaker than the base material.

The 30 to 50 percent decrease in the strength of the HAZ in aluminum has not been investigated sufficiently. Current design methods assume that all metal will have this reduced strength, whereas the localized weakening has been shown to have less effect on overall strength in compression and in tension. This approach may seriously underestimate the strength of welded structure and it may impose a significant weight penalty on the final vessel design. Alternative approaches to design are possible.

To study the impact of HAZ on load carrying capability of stiffened panels, twelve (12) combinations of plate and stiffeners are analyzed. Each model consists of three bays and four stiffeners. The finite element analyses are performed for models built with 5083-H116 and 6082-T6 aluminum alloys (hereafter AL5083 and AL6082). In models 1 through 4, both plate and stiffeners are AL5083. In model 5 through 8, plate is AL5083 and stiffeners are AL6082. For models 1 through 8 HAZ is modeled at the plate-stiffener junction. In models 9 through 12 both plate and stiffeners are considered extruded AL6082 and HAZ is modeled at the junction of two extruded elements. The HAZ softening is also modeled at the transverse frame location between the bays. Welds are not modeled as the analyses are performed with plate elements. This analysis also ignores effect of residual stresses. Each of the 12 plate stiffener combinations is analyzed for three different loadings (tension, compression, & bending). For each panel, three separate FE models were made consisting of:

1. All base metal throughout the model – no separate HAZ regions
2. All HAZ metal throughout the model – no separate HAZ regions
3. Base metal & HAZ metal.

Based on the literature review and simulations run, the following conclusions and suggestion for future work seem justified:

1. Modeling aluminum structures as all-HAZ material is overly conservative and will result in a substantial weight penalty. Thus, the marine community is advised that developing HAZ-specific strength formulations to remove this penalty is essential.
2. The generally good agreement between the simplified methods studied and the FE results suggests that it is possible to develop reasonable HAZ-specific strength models. Furthermore, reducing the material strength by 10% appears to be a good first step for including conventional HAZ in 5xxx-series alloy structures. On the other hand, simplified methods based on ratios of average failure stresses to HAZ proof stresses as well as associated stiffness were inconclusive.
3. HAZ impacts 6xxx-series are generally larger than that of 5xxx-series alloys.
4. With existing commercial FE codes, it is not straightforward to model extensive strain localization and material failure with the types of shell-element models used in the marine field. This significantly impacts the ability of the structural naval architect to model strain localization for tensile and bending load cases. Given previous literature on the subject, there is reason to be concerned about decrease in energy absorption and global-strain-to-failure in HAZ-impacted structures. Practical design approaches to quantify these effects are needed.
5. Further analysis of the all-6xxx series panels would be beneficial to separate out the impact of alloy type and HAZ location on the large reductions in strength seen for these panels. Furthermore, in extrusion design, it is possible to locate welds at other locations on the plate. The best location for such welds would be an interesting area of study, including any impact on the extrusions process by having an unbalanced die.

1 INTRODUCTION

The current commercial and military interest in large high-speed vessels has resulted in the development of monohulls, catamarans, and trimarans designs between 70 m and 130 m in length for transportation and combat roles. In this design space, deadweight is restricted, and the vessel operates under a constant tradeoff between cargo capacity, achievable speed, and achievable range quite unlike conventional displacement vessels. Given these restrictions, minimization of lightship weight, and hence structural weight, is of great significance in the design of the vessels. Most existing vessels in this category have been constructed out of aluminum to reduce structural weight.

The 5xxx-series and 6xxx-series aluminum alloys are extensively used for marine structures. Generally, 5xxx-series alloys possess excellent corrosion resistance when immersed in seawater whereas 6xxx-series are inferior. Traditionally, 5xxx-series alloys are used in deck and hull plating whereas 6xxx-series alloys are used as structural reinforcements, bulkheads, and stiffeners that do not come in direct contact with seawater. Welding aluminum results in significant modifications to the material properties in the area around the weld. The 5xxx-series and the 6xxx-series alloys obtain a significant portion of their strength either from cold working or thermal processing, processes that are impacted by the heat input from welding. The area impacted by the heat input from the welding process is termed as heat-affected zone or HAZ. For high-strength 5xxx and 6xxx-series alloys joined by fusion welding, the HAZ is typically 30%-50% weaker than the base material. Friction stir welding typically has a smaller HAZ with higher strengths. As the underlying metallurgy of the 5xxx and 6xxx-series alloys are significantly different, the HAZ for these two alloys behave in different ways. Additionally, for high-Mg 5xxx-series alloys, the heat input near the weld may cause portions of the HAZ to become susceptible to inter-granular corrosion.

The 30 to 50 percent decrease in the strength of the HAZ in aluminum has not been investigated sufficiently. Current design methods assume that all metal will have this reduced strength, whereas the localized weakening has been shown to have less effect on overall strength in

compression and in tension. This approach may seriously underestimate the strength of welded structure and it may impose a significant weight penalty on the final vessel design. Alternative approaches to design are possible. For example Paik et al. (2005) proposed equivalent yield strength based on the plate volume. Although the concept of equivalent yield strength has been used in research reports, the full implications for design standards have not been investigated.

This research study intends to provide a basis for modification to design standards by analyzing the impact of the HAZ on the strength of aluminum stiffened panels under compressive, tensile, and bending loads.

2 OBJECTIVE AND SCOPE OF INVESTIGATION

The objective of this project is to provide a basis for the design of aluminum structures that will minimize the penalty on scantling selection and to provide a basis for modification to design standards. To accomplish the above mentioned objectives, following tasks were proposed:

Task 1: Creation of Draft and Final Project Plans

A draft project plan will be created from the proposal, and circulated to members of the project technical committee before the project kick-off meeting. Based on the comments received during the project kick-off meeting, subject to the limitations of the overall budget and timeline agreed during contract negotiations, the draft project plan will be revised and a final project plan will be issued.

Task 2: Literature Survey

A two-part literature survey will be conducted. First, previous technical studies which address the impact of welds on the strength of aluminum structures will be reviewed. This will cover studies from both marine and non-marine fields, with a focus on the 5xxx and 6xxx series alloys typically used in vessel construction. Second, current aluminum design standards from the marine and civil engineering communities will be reviewed, and their approaches to determining the strength of welded aluminum structures compared. Both phases of the literature survey will be documented for the final report, and the findings used in developing the matrix of finite element models that will be investigated in this study.

Task 3: Develop Matrix of Plate Stiffeners Models to be Analyzed

The effect of HAZ on the strength of aluminum will be studied for various stiffener-plate combinations and also for extruded elements. These models will include at least two transverse frames. Transverse frame spacing will have to be chosen very carefully. Sample Stress-Strain

curves for aluminum are shown in Figure 2-1. For the materials chosen for this task, contractors will select the model geometries such that the ultimate strength of the models selected are in the non-linear region of the curves. That will ensure that the models are sensitive to HAZ. The parameters primarily influencing the ultimate strength is the slenderness ratio of the beam-column.

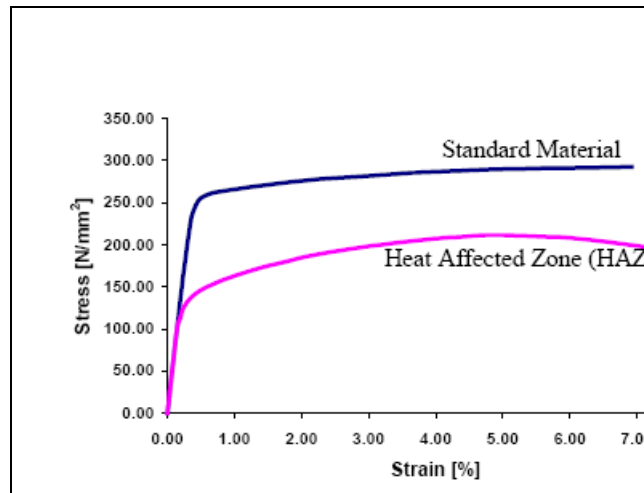


Figure 2-1: Material curves for plate-stiffener and HAZ (Rigo et al. 2003)

Task 4: Develop/Obtain Stress-Strain Relationship

Non-linear stress-strain data for the selected Al alloys will be obtained from the existing literature or using the Ramberg – Osgood relationship as shown below:

$$\varepsilon = \frac{\sigma}{E} + 0.002 \left(\frac{\sigma}{\sigma_{0.2}} \right)^n$$

Where :

ε Strain

σ Applied stress

E Elastic modulus

$\sigma_{0.2}$ 0.2% offset proof stress

n Exponent

Task 5: Develop and Analyze Fine Mesh Models

Fine mesh models for all the plate-stiffener combinations identified under Task 3 will be developed with plate elements using the finite element code FEMAP/NASTRAN. Mesh density will be optimized. Non-linear stress-strain curves from Task 4 will be used. These fine mesh models will be analyzed using the properties of :

- a). Base metal,
- b). HAZ,
- c). Base metal and HAZ (extending $3 \times$ thickness of the plate).

These models will be analyzed for tension, compression and bending loads. For each of these three cases, limit state criteria will be developed to compare the results.

Task 6: Perform Volumetric Yield Strength calculations

Ultimate strength will be calculated for all models developed under Task 3 using the closed-form solution developed by Dr. Paik for volumetric equivalent yield strength. These results will also be compared with the results obtained under Task 5.

Task 7: Recommend changes to Design Standard

Based on the results of the analyses performed under Task 5 and task 6, recommendations will be made to change the existing design standard to better suit aluminum structure design.

Task 8: Preparation of Final Report

The reports produced under the previous tasks will be integrated into a final report, following the style guidelines and template for the Ship Structure Committee. The draft report will be circulated for review by the project technical committee, and suggested revisions to the report will be implemented in a final draft, which will be delivered to the Ship Structure Committee in accordance with the terms of the contract.

3 ALUMINUM ALLOYS AND METALLURGY

As a structural material, aluminum alloys have noticeable differences from steel. The basic metallurgy and structural design process with aluminum has been reviewed in several standard texts (Kissell and Ferry 2002, Mazzolani 1995). In the marine community, alloys of the 5xxx-series and 6xxx-series are primarily used. These alloys have good corrosion resistance, weldability, and are economical. The 5xxx-series alloys are primarily alloys of Aluminum and Magnesium, and gain strength through strain-hardening at the mill. 5xxx-series alloys are used in rolled plates and much less frequently can be found in extrusions (Alcan 5383 extruded stiffener profiles being one of the few 5xxx-extrusions for marine use.) The 6xxx-series alloys are precipitation-hardened alloys with both Magnesium and Silicon alloying elements. The 6xxx-series alloys gain their strength via heat treatment. The 6xxx-series alloys can be extruded much more easily than the 5xxx-series and can be extruded into complex shapes with enclosed voids. The material differences between the marine aluminum alloys and steel alloys in terms of ultimate limit strength analysis (ignoring corrosion and fatigue mechanisms) can be briefly summarized as:

- The elastic moduli of the aluminum alloys are roughly 1/3 the elastic modulus of steel. Thus, an aluminum structure of similar geometry to a steel structure will be more susceptible to elastic buckling, and any strength methods or rules of thumb that do not explicitly consider the elastic modulus of the material developed for steel (such as limiting b/t ratios for plating) will not be conservative for aluminum.
- The shape of the aluminum stress-strain curve is generally more rounded than that of steel. Typically, no defined yield point can be identified in the material stress-strain curve, and a 0.2% offset proof stress used in place of the yield stress. The 0.2% offset proof stress is defined as the stress where the plastic component of the strain is 0.2%. The 5xxx-series alloys have a particularly rounded stress-strain curve, and their local tangent modulus may fall significantly below the elastic modulus before the proof stress is reached. This

indicates that these alloys may be more prone to buckling in the inelastic regime than equivalent steel or 6xxx-series alloy structures. As the 5xxx-series alloys are strain hardened, the proof stress is often higher in tension than compression, a fact often overlooked in marine structural analysis. The 6xxx-series generally has a stress-strain curve closer to the elastic perfectly-plastic assumption often used for steel structures. However, after the extrusion process the material may show a pronounced anisotropy, with generally lower strength and ductility in samples taken at a right angle to the direction of extrusion.

- Both 5xxx and 6xxx series alloys become weaker in a local region near the weld when welded by fusion welding. This local weak region is known as the heat-affected zone (HAZ). For 5xxx-series alloys, the HAZ material is typically similar to anneal material. For the 6xxx-series, the HAZ is typically an over-aged region in terms of the precipitation hardening. The extent of the HAZ is typically on the order of 25mm or 3 times the thickness of the plate from the weld centerline.

To capture the rounded shape of the stress-strain curve of aluminum, the Ramberg-Osgood equation is typically used. While this relation may not always capture the profile of the entire stress-strain curve, it has the advantage of being simple and useful for both analysis and design activities, where the type of data required for more advanced models may not always be available. The Ramberg-Osgood relation relates applied stress, σ , to strain, ε , via the material's elastic modulus, E , a proof stress $\sigma_{0.2}$, and an exponent, n :

$$\varepsilon = \frac{\sigma}{E} + 0.002 \left(\frac{\sigma}{\sigma_{0.2}} \right)^n$$

Equation 3-1

Stress-strain curves for both base material and weld metal in 6061-T6 and 5083-H116 tempers are shown in Figure 3-1. The properties used in the generation of these curves are listed in Table 3-1, the proof strengths for the various alloys and weld conditions come from the *Aluminum Design Manual* (Aluminum Association, 2005) while the Ramberg-Osgood exponent is based on experimental data presented by Zha and Moan (2001), and the approximation used by Zha and Moan that the reduction in the exponent is proportional to the reduction in proof stress is used to estimate the properties of the HAZ material. The alloy-exact elastic modulus are used in this comparison, in general, a median value of 70,000 MPa can also be used as a generic elastic modulus for all aluminum alloys.

Table 3-1: Impact of Welds on 6061 and 5083 Aluminum Alloys – 2”/50mm Gauge Length

Alloy	Tensile Proof Stress	Tensile Ultimate Stress	Elastic Modulus	Ramberg-Osgood Exponent, n
6061-T6	240	260	69600	39.3
6061-T6 HAZ	105	165	69600	17.2
5083-H116	215	305	71700	15.4
5083-H116 HAZ	115	270	71700	8.2

Table 3-1 shows that the strength reduction in the HAZ is quite severe for higher-strength aluminum alloys, such as the –H116 or –T6 tempers. Given that the proof strength of aluminum in the HAZ is 50%-60% less than that of the base material, it is clear that fusion welds are marked by pronounced inhomogeneity in material strength. This is also referred to as an under-matched weld, as the weld is weaker than the surrounding structure. Furthermore, this inhomogeneity occurs over a much smaller distance than the other dimensions of the structure, such as the panel length, that is normally on the order of 1 meter, and the vessel breadth and depth, that are on the order of 10 meters. One feature of the response of a structure with under-matched welds is that the plastic flow of the structure in the post-elastic tensile regime is

concentrated in the under-matched region, a situation known as strain concentration. As this region is small compared to the overall dimensions of the structure, it is often possible to see ductile rupture in these regions when the average global strains of the overall structure are still quite low. This reduction in overall ductility indicates that failure modes – such as rupture in tension – that are often not investigated for steel vessels may be important for aluminum vessels. Examining Figure 3-1 and Table 3-1 in more detail, it is further clear that the 6061-T6 alloy suffers a larger reduction in ultimate tensile strength than the 5083-H116 alloy. This is a result of the different metallurgy of the two alloys, the 5xxx-series alloys are strain-hardened, so they regain much of their pre-welded strength via cold working when the welds are loaded plastically. However, the 6061-T6 is a precipitation-hardened alloy that does not significantly work-harden when re-loaded, and loses much of its ultimate tensile strength as well as its proof stress when welded. This means that welds in the 6061-T6 material, or similar 6xxx-T6 alloys such as 6082-T6, are especially vulnerable to strain localization in under-matched welds.

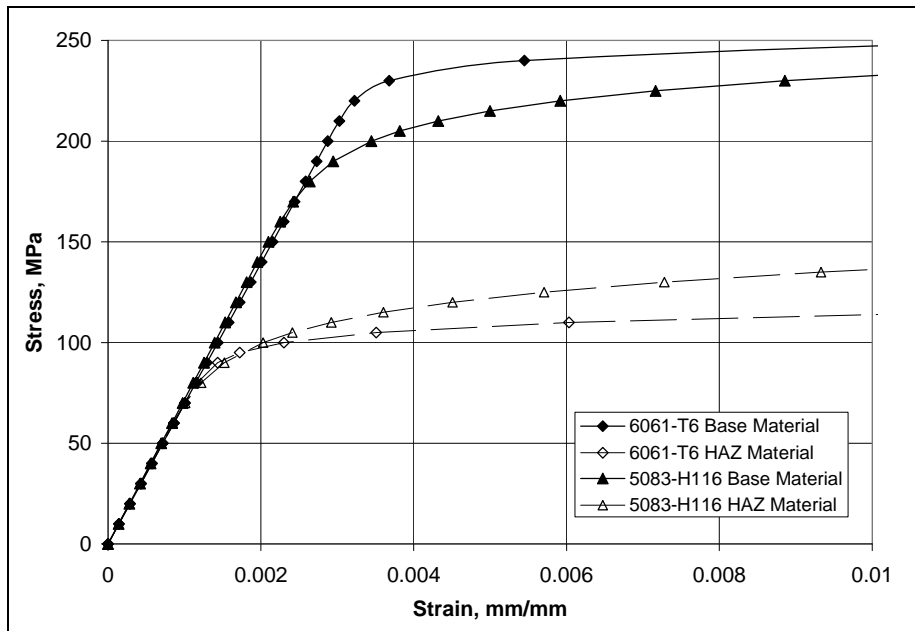


Figure 3-1: Comparison of Stress-Strain Curves in 6061 and 5083 Materials

One interesting effect of the under-matched welds in aluminum is that the cross-welded proof stress, determined by testing specimens with a weld perpendicular to the applied load, is sensitive to the gauge length used during the test. The proof stress is determined when the

average plastic strain component reaches 0.2% over the gauge length, but the strain is not uniformly distributed along the length of the gauge because of the under-matched weld. Therefore, increasing the gauge length will increase the reported proof stress as more low-strain base material is added to the gauge, dropping the average strain reported even though the specimen is otherwise identical. In the past, both 10"/250mm and 2"/50mm gauge length have been used (Sielski 2008), with the later consisting mainly of weld or HAZ material for most plate thicknesses and welding processes. The difference between the 10"/250mm and 2"/50mm gauge lengths can be quite large. For example, in previous versions of the *Aluminum Design Manual*, 10"/250mm gauge length proof stresses were given for welded alloys, but these would be reduced by 25% to be equivalent to 2"/50mm gauge lengths when used in tensile yield limit states (Kissell and Ferry, 2002.) Thus, for cross-weld specimens, both the 0.2% proof stress and the associated gauge length must be specified to uniquely define the material's strength. Other approaches to avoid this gauge length dependence have been tried, such as cutting samples parallel to the weld direction to obtain all-HAZ material in the tensile test specimen, although with this approach it is not possible to test all regions of the weld and HAZ in a single test.

4 LITERATURE SURVEY

Given the large strength impact fusion welding has on aluminum structures, researchers have devoted a significant amount of effort to investigating the strength of welds and the impact of welds and HAZ on the overall response of aluminum structures. This body of previous work was reviewed by conducting a literature survey at the start of the current project, which is presented in this section. The literature survey is divided into two parts, first numerical and experimental studies of aluminum welds and structural responses are reviewed. These studies are further divided into four groups, studies that focused primarily on the local response of weld and HAZ materials, studies that focused on the impact of welds on tensile response, studies that focused on the impact of welds on compressive response, and studies that focused on the impact of welds on bending response and lateral loads. The second part of the literature survey is a review of how welds are handled in four design codes for aluminum structures, including the *Aluminum Design Manual* and the *Eurocode 9* standard from the civil engineering community, and the ABS and DNV classification approaches from the marine community.

4.1 Research on Aluminum Welds and Weld Effects

4.1.1 Local Studies of Welds

To understand the overall response of a welded aluminum structure, it is first necessary to understand the local response of the weld and HAZ material under load. This section of the literature review focuses on studies whose primary focus was to describe or observe the response of individual welds in aluminum alloys. One of the first major studies into fusion welding of aluminum alloys was conducted by Nelson and Howell (1952). Nelson and Howell experimentally determined the strength of both butt and fillet welds in aluminum structures, including examining the reduction in overall ductility that resulted from using under-matched welding. While the alloys tested did not conform to the naming system currently in use, their chemical make-up was close to modern 5xxx and 6xxx series alloys, though with slightly lower

in Magnesium content than modern 5083 or 5383 alloys. The work of Nelson and Howell was further extended by Hill, Clark and Brungraber (1960), who published a comprehensive paper on the strength of welds that underlies much of the current *Aluminum Design Manual* strength formulations that will be reviewed in the design code section following this part of the literature review. The focus of this paper was to remove some of the conservatism in initial design code proposal covering the use of welded 6061-T6 alloy members in construction. Hill, Clark, and Brungraber looked at the strength reduction across welds and proposed modeling this region as a single HAZ block. Based on a compilation of test data for butt and fillet welds in a wide number of alloys, they initially proposed to assume an effective HAZ breadth of 1.5"/37.5mm from the weld centerline, which they termed the reduced-strength zone. Yield strengths for welded components were reported using a 10"/250mm gauge length for a wide range of aluminum alloys, weld types, and material thicknesses. Formulas for the strength of butt welds and fillet welds were developed. Going beyond simple welds, strength formulas for structural members such as columns, beams, and plates were proposed, including proposals for methods of handling welds in the mid-region of columns in compression.

A study of welds in two common marine alloys, 5083 and 6082, was made by Scott and Gittos (1983.) Scott and Gittos studied welds made with both 4043 and 5556 weld filler metals in 3mm and 13mm thick plates. Efforts were made to characterize the strength of the base material and weld material, with tension tests on specimens composed entirely of base material and weld material carried out along with cross-weld tension tests. Post-weld heat-treatments were also carried out on the 6082 welds. In general, fairly low elongations were observed, for the 3mm plate, overall elongations of 3% over a 5"/125mm gauge length were reported in the as-welded condition, reducing to as little as 1% if additional artificial aging was applied in post-weld heat treatment. This shows how strain localization can impact the deformation capacities of 6xxx-series aluminum welds. Center crack, crack-tip opening displacement and Charpy impact tests were also carried out, with ductile, stable failure mechanisms recorded in all cases. Post-test analysis showed that the dominant failure mode was micro-void coalescence for the Charpy and CTOD failures. Scott and Gittos also derived acceptable flaw sizes and drew conclusions based on the test results.

Further tests on 6082-T6 welds were carried out by Matusiak (Matusiak and Larsen 1998, Matusiak 1999.) Matusiak carried out tests on both butt welds and load-bearing fillet welds, using 6082-T6 material welded with 5183 filler metal. For the butt welds, both 8mm and 20mm plate were used. As a part of this study, a series of small tensile specimens with cross-section dimensions 3mm x 4mm were cut parallel to the butt weld. Specimens were taken every 4mm off the weld centerline, allowing the material properties through the thickness of the HAZ to be studied. These specimens revealed that close to the weld metal the HAZ had significantly less ductility than either the weld metal or the HAZ more remote to the weld. A series of cross-weld tension tests were developed, with the weld run at different angles to the applied stress. As expected, the case with the weld perpendicular to the applied stress had the lowest strength and deformation. Matusiak further investigated strength predictions using both simplified formulations and non-linear finite element studies. A key conclusion from the finite element study for the butt weld is that a tri-axial stress state is present in the weakest zone of the HAZ, and the strength of the weld is higher than the minimum material strength measured in the HAZ via the small material specimens. This tri-axial stress state is set up by the constraint of the surrounding, stronger, material. Similar constraint strengthening has long been observed in narrow under-matched welds in steel; see for example Satoh and Toyoda (1970.)

Interest in modeling aluminum welds has continued, with increasing focus on using numeric modeling tools to evaluate the properties of welds. Zhang et al. (2001) combined a welding simulation that could predict the post-weld microstructure and material properties with non-linear finite element simulation of the deformation and strength capacity of the weld. This allowed an entirely numerical prediction of weld strength given material and welding parameters. In limited experimental validation, the results of this approach were quite promising. Zheng et al. (2009) took a slightly different approach, developing a numerical fracture model that can be rapidly calibrated from a single cross-weld test, removing the need to perform expensive micro-tensile tests of the different strength regions in HAZ. This model also showed good results in limited experimental verification, and has been extended to look at dynamic fracture under crash and impact loading.

Another major numerical study on weld strength prediction was performed at NTNU by Wang (Wang 2006, Wang et al. 2006, 2007a, 2007b.) Using a mixture of new hardness measurements and the micro-tensile test carried out previously by Matusiak (1998), Wang studied numerical failure prediction in welds of 6082-T6, including load-bearing fillet welds, beam-column connections, and welded beams in bending. Using the non-linear finite element code LS-DYNA and shell element models, estimates of ductility and fracture loads were estimated, with generally good agreement between the experiments and the simulations. The Weak Texture Model using anisotropic yield criterion of Barlat and Lian was used to capture the material parameters of the base material and HAZ regions in the model. However, the shell modeling approach proved to be mesh-sensitive, as the through-thickness stabilization stresses from constraint are not included. Wang developed and tested a non-local thinning model in LS-DYNA to capture this effect that significantly reduced the mesh sensitivity. Wang also proposed a simple analytical model for butt weld failure in rectangular plates. In general, the finite element approach proposed by Wang performed well, however identification of material parameters and use of the non-local thinning approach mean that the method requires significant set-up and analysis time to be applied to a weld joint.

4.1.2 Impact of Welds on Tensile Response

In addition to studying the local response of weld and HAZ material, several previous studies have been made into the overall tensile response of welded aluminum structures, examining how strain localization impacts ductility and strength. Several studies were made into 6082 beam-truss frameworks used in the oil industry on offshore platforms, including those of Övreas, Thaulow, and Hval (1992) and Hval, Johnsen, Thaulow (1995). These two studies contain both experimental and numeric studies on welded connections, ranging from simple butt welds to complex beam joints under tensile loading. The welds were in 6082 material in both rolled and extruded conditions with plate thickness of 16mm, 35mm, and 50mm, joined with 5183 filler metal. Both studies addressed the concept of strain localization, and examined how the lower overall ductility in these structures may conflict with classical plastic design rules. Constraint and tri-axial stress effects were seen to raise the strength of the joints, which were deeper and narrower than conventional vessel joints as the plates were much thicker than is typically seen in

aluminum vessel construction. Hval, Johnsen and Thaulow also noted that leaving the weld bead on the weld raised the amount of constraint in the HAZ near the weld, and notably increased the strength of the weld. Hval, Johnsen, and Thaulow also present a summary of the shortcomings of then-existing design codes in assuring equal safety between conventional steel structures and aluminum structures with under-matched welds, along with recommendations for designing aluminum structures that will minimize the impact of strain localization.

Chan and Porter Goff (2000) investigated similar issues in welded plate-and-finger connections in tension members in a welded 7xxx-series alloy structure. Although 7xxx-series alloys have not been widely or successfully used in marine construction to date, the weldable 7xxx-series alloys have similar under-matched welds to 6061-T6 or 6082-T6 alloys. Chan and Porter Goff showed how strain localization impacts this type of tensile connector. Chan and Porter Goff proposed a simple analytical model of a finger-type tension connection joint, including characteristics of the base metal and different regions of the HAZ. This model was compared to finite element simulations of the joint and a number of experimental tension tests on similar joints, with generally good agreement.

Collette (2007) examined the impact of welds on aluminum vessel structures, including a review of two simplified formulas to predict the tensile limit states of welded plates and panels. One model was a simple series spring-type model that uses strain and force continuity along with an idealization of the HAZ and base material to predict the strength and overall ductility of welded structures. A second model, based on a steel under-matched weld model proposed by Satoh and Toyoda (1970) was also used, and the results of the two models were compared to the cross-weld strength and ductility results presented in Scott and Gittos (1983.) Neither method could predict all of the experimentally-observed responses. The impact of welds on hull-girder collapse limit states was also assessed via an incremental-curvature collapse model of an aluminum box girder. This study revealed that different types of idealization of the welds in the tension flange in the box girder could have a significant impact on the ultimate resisting bending moment developed by the box girder, and thus tensile weld limit states are important when capturing global responses.

4.1.3 Impact of Welds on Compression Response

The impact of welding on compressive response has also been studied extensively in the past. In this section of the literature review compressive collapse tests that focus on welded aluminum structures in marine-type alloys will be reviewed. Some initial welded columns and beams were presented by Hill, Clark and Brungraber (1960), along with simplified strength formulations, as has been discussed in the first section of the literature review. About two decades later, Mofflin (1983) tested a series of 5083 and 6082 plates under uni-axial compressive. A total of 76 plates were tested, with breadth-to-thickness ratios ranging from 20 to 85. The 5083 material was provided in the older N8 specification, which is quite loose in terms of the allowable strength properties, and generally weaker than modern 5083-H116 temper. The 6082 plate material was in the older –TF temper, which is roughly equivalent to the modern –T6 temper. All plates had four to one aspect ratio, with compressive loads applied to the short edges of the plate. Plates were tested with and without welds along the long (unloaded) edges, and a series of plates were also tested with a central, transverse weld. No plates had welds along their short, loaded edges, which later work indicates may adversely impact strength. The presence of longitudinal welds was shown to reduce plate strength roughly 10%-15% for all 6082 plates, with similar reductions for the stockier 5083 plates. The presence of a transverse weld in the mid-region of the plate reduced the 6082 plate strength by roughly 30%. The 5083 and 6082 plates behaved differently, owing to their different material stress-strain curve. In general, the Mofflin test results establish an experimental baseline that shows that HAZ regions, even when not perpendicular to the applied stress can significantly impact the plate strength. It is possible that the welded strength reductions would be larger for the 5083 plate if the supplied material had been in a higher temper, equivalent to a modern –H116 temper.

Clarke and Swan (1985) and Clarke (1987) report on the compressive test results of five stiffened panels in 5083 aluminum alloy designed for naval use. The tests featured a $\frac{1}{2} + 2 + \frac{1}{2}$ bay experimental set up, with the transverse frames restrained so that buckling would occur between frames. While the panels were welded, no explicit study of the impact of the welds on the panels were made. Experimental residual stress measurements were made, along with measures of plate and stiffener imperfections.

The plates investigated by Mofflin were further investigated by Hopperstad, Langseth, and Hanssen (1997) using the non-linear finite element code ABAQUS. A mesh of roughly 96x24 shell elements was used to model the plates. The model was locally refined in the HAZ regions, though the exact number of elements in the HAZ was not given. Both the weaker HAZ regions and residual stresses were included in the finite element model, and the results agreed very well with the experimental results, confirming that non-linear finite elements can be used with reasonable meshes to predict the compressive collapse of welded aluminum structures.

Edlund (2000) studied the compressive behavior of beam-columns loaded primarily in compression, but with some load eccentricity as well. All of the beam columns were open tee-sections, and were made from 6082-T6 alloy. Both non-welded and welded beams were tested. The welded beams featured welds and HAZ impacting the entire beam cross-section at end, quarter, or mid points of the span. The strength reduction from welding was shown to be potentially significant, but highly dependent on the weld location and the amount of eccentricity applied. Strength reductions between 0% and 25% of the compressive strength were found when comparing welded beam-columns with un-welded beam columns. Edlund also compared his results to both finite element analysis, with good agreement. Comparisons were also made with the *Eurocode 9*, and made a series of suggestions on ways to improve the code were given.

A numeric study of plate collapse was made by Kristensen (2001). Using material properties from the Mofflin (1983) experiments and the non-linear code ABAQUS, Kristensen examined plates under uni-axial compression, bi-axial compression and shear loads. After a mesh convergence study, most plates were meshed using a 4-noded shell element with square mesh with element sides of 12.5mm. This gives two elements across the width of a typical HAZ. More refined meshes were used for convergence studies and some load combination cases. A wide-ranging parameter study was made, including the impacts of HAZ softening with and without residual stresses, boundary conditions, aspect ratios, initial deflections, and material properties. Both a 5083 and a 6082 material were used in the analysis. Regression equations were fit to the results to allow designers to estimate the strength of such plates. Based on his parameter study, Kristensen concluded that the most damaging HAZ for plates in compression is the HAZ along the short, loaded edge. Kristensen's strength formulas propose a linear relation

between HAZ softening and plate strength, and HAZ breadth and plate strength. Kristensen also noted that the impact of HAZ regions on plate strength did not vary with the relative slenderness of the plate – thin plates were as sensitive to welding as thicker plates.

Two additional experimental studies of aluminum panels in compression were also made in 2001. Zha and Moan (2001) studied a series of flat-bar stiffened panels that mainly failed via stiffener tripping via single-bay experimental panel tests. These panels were three stiffeners wide made from both 5083-H116 and 6082-T6 alloys. In addition to the experimental results, a number of ABAQUS finite-element simulations were also made. Using the ABAQUS simulations, the impact of the HAZ on the ultimate failure load of the panels was assessed by running numerical models with and without the HAZ. These studies showed that the HAZ had a larger impact on the 6082-T6 panels than the 5083-H116 panels, with a 15% average reduction in strength for the 6082-T6 panels. Additionally, the transverse HAZ at the end of the panels is shown to make the dominant contribution to strength reduction, further confirming Kristensen's (2001) conclusion about the importance of transverse HAZ. Aalberg, Langseth, and Larsen (2001) also tested a series of 6082-T6 extrusion-type panels, including both closed and open shaped stiffeners. While experimental strengths, including cross-HAZ coupon tests were reported, no parametric study of the HAZ on panel strength was made. These panels also lacked the transverse HAZ at the loaded edges of the panels.

Rigo et al. (2003, 2004) performed a similar study numerically at the stiffened panel level. Several non-linear finite element models were made of a single stiffened panel. Two different type of panel models were made, a full 3-bay model including four transverse frames, and $\frac{1}{2} + 1 + \frac{1}{2}$ bay model that used symmetry boundary conditions for the half-bay end panels. All panel models were five stiffeners in width, and assumed 6082-T6 material. In the original study, the 3-bay model was used with initial imperfections introduced by simulating a lateral pressure (stresses from lateral pressure we not present during the compressive collapse analysis). A sensitivity study was made on this panel, examining the impact of different HAZ extents, severity, and location, as well as other panel parameters. A number of finite element codes were investigated, with generally good agreement between all codes. Meshes varied, but generally two to four shell elements were used across the width of the HAZ, with 40x10 shell element

meshes covering the plating between stiffeners. It is not clear how or if transverse HAZ were added at transverse frames. Three patterns of welds were studied:

- Conventional construction where a HAZ is present at the edges of the plate between stiffeners and in the stiffener web, simulating stiffeners attached to plating by fillet welding, these HAZ regions were parallel to the applied stress,
- Extruded construction where the stiffener and half a plate bay on each side of the stiffener are assumed to be extruded as an integral unit. In this model, HAZ is present in the middle of the plate span between stiffeners where abutting extrusions would be joined by welding, these HAZ regions were parallel to the applied stress,
- Transverse weld at the L/4 and L/2 position between transverse frame, these HAZ regions were perpendicular to the applied stress.

For the panels tested, the extruded-type HAZ pattern had a strength reduction of 1%-6% compared to an all-base material panel. The conventional construction HAZ pattern had a large strength loss of 13%-17%. It is important to note that failure did appear to be initiated by plate buckling, as increasing the plate thickness made a large impact on the failure stress. Thus, the location of the welds in the plate may have a large impact on the failure stress of this type of panel. Kristensen (2001) found that if HAZ are added at transverse frames, the difference between extruded and conventional construction HAZ patterns is significantly reduced. Of course, in a stiffened panel construction, conventional HAZ pattern further reduces the panel strength by impacting the stiffener web, which was not considered in Kristensen's plate-only study. Transverse weld in the quarter or mid-span region reduced strength by 7%-12%. Rigo et al. also studied different HAZ extents, running the model with 25mm, 50mm, 75mm, and 100mm HAZ breadths, however, the largest strength reduction was observed when going from no HAZ to 25mm HAZ, with additional reductions shrinking for every 25mm of HAZ added. In 2004, Rigo et al. expanded the study to include the $\frac{1}{2} + 1 + \frac{1}{2}$ bay model, and also initial imperfections introduced by buckling Eigen-modes instead of lateral pressure. These changes reduced the peak strength of the panel, but they also reduced the strength loss from the presence

of HAZ regions in the model. This supports the use of the 3-bay model for the sensitivity analysis, if not for the peak strength calculation.

Xiao and Menzemer (2003) also used finite element analysis to study both simply-supported and outstand plates with and without welds by simulating a series of stub-columns with I or H cross sections, so that both simply-supported and outstand plates were present in each analysis. This approach gave results in line with previous experiments and design codes, however, a sensitivity study to the HAZ parameters was not made, so it is difficult to draw any general conclusions about weld modeling from this study. Similar to the Rigo et al. work reviewed above, it appears that the calculation meshes used by Xiao and Menzemer used two to four shell elements across the width of the HAZ regions.

Paik and Duran (2004) also used non-linear finite elements to study the compressive collapse of marine aluminum plates and stiffened panels, concentrating on the then newly-introduced proprietary alloy 5383 in the -H116 temper. In this study, conventional construction was assumed, with stiffeners attached to plates by fillet welds, which is typical of 5xxx-series construction as the 5xxx alloys are difficult to extrude into complex or large shapes. HAZ regions were also modeled at the short, loaded edges of plates and at the transverse frames regions of stiffened panels. HAZ widths were set to three times the plate thickness in the unstiffened plates, and 1"/25mm in the stiffened panel models. Imperfections were introduced into both the plate and stiffened panel models; however, residual stresses were not included in the analysis. Paik and Duran carried out a systematic study, varying plate and panel parameters over 23 different plates and 50 different stiffened panels. Regression equations were fitted to the ultimate strength results. These equations use modified versions of the standard plate and column slenderness factors β and λ computed using a volume-averaged material proof stress that included the base material and HAZ regions of the structure. For stiffened panels, the volume averaging only includes HAZ regions running parallel with the stiffeners; the cross-panel HAZ along the loaded panel edges is not included. The proposed equations are shown to fit the finite element simulations well.

Wang et al. (2005) conducted finite element studies of aluminum plates and stiffened panels. Meshes used 12 to 13 shell elements across the width of the HAZ, with a coarser mesh outside of the HAZ regions. In this study, the width of the HAZ was taken as three times the plate thickness for plates thinner than 0.30in/7.5mm and 0.78in/20mm plus one third the thickness for thicker plates. A parametric study was carried out varying the geometric parameters of the plates and stiffened panels, and the strength reduction in the HAZ. A modification factor to Faulkner's (1975) classic plate strength equation was proposed. This factor reduces the plate strength, with increasing reductions occurring as the material strength in the HAZ is reduced from the base material strength. The strength reduction is also increased as the plate becomes stockier, with a higher buckling stress, a slightly different result than Kristensen who proposed a constant proportion reduction regardless of plate strength. The formula proposed by Wang et al. was shown to agree very strongly with their finite element results. A modified panel buckling approach is also presented where the HAZ strength reduction only impacts the plate in the stiffened panel. To fully compute the ultimate strength of the panel, an extension to the method outlined in the paper is required (Collette et al. 2008).

Zhu and Young (2006a, 2006b, 2007) examined aluminum columns, focusing on rectangular and circular hollow columns with and without welded end plates made from the 6063-T5 and 6061-T6 alloys. Extensive experimental material tests were reported, including 1¹/₂in/25mm gauge-length specimens taken between two parallel welds, and 10¹/₂in/250mm gauge length cross-weld specimens. A series of experimental collapse tests and parametric finite element studies were made of the columns. Results were compared to civil engineering design codes and a cold-formed steel structure direct strength method with generally good results and some suggestions to improve the methods. The approaches developed are not of direct use as formulated for plate and panel type structures, though the experiments do provide some interesting background.

More recently, the Ship Structure Committee has commissioned a large number of panel tests in two consecutive projects run by Professor Paik at Pusan National University in Korea. In the first study, SSC-451 (Paik et al. 2008), 78 stiffened panels made from 5083, 5383, and 6082 alloys were tested in uni-axial compression. The majority of the panels were single-bay specimens with welded end plates (hence ensuring that there would be HAZ perpendicular to the

applied load), and were four stiffeners in width. A smaller number of three-bay panels were also tested. Detailed information on the welding process used, along with initial deformations introduced by welding, the softening in the HAZ, and the HAZ width were reported. Most of the HAZ widths were reported close to 1"/25mm in size. The HAZ strength measurements showed mean values fairly close to code requirements, but significant variability from this mean value. Approximate values were given for slight, average, and severe levels of HAZ weakening for the 5083 and 5383 plates, and average values for the 5383 and 6082 stiffeners. Parametric non-linear finite element models were run to investigate a variety of modeling approaches. The presence of HAZ was shown to be significant for the panel strength in the finite element models as expected. Attempts to use an elastic-perfectly-plastic material law in place of the Ramberg-Osgood type equation showed reasonable results for panel-type structures, which is in contrast to results for un-stiffened plates where the rounding of the stress-strain curve has been shown to be significant. One shell element was used to represent the HAZ width in the finite element models, with roughly 10 shell elements (including HAZ) between stiffeners and 6 elements on the stiffener web. Based on a comparative study of several different finite element approaches, multi-bay finite element models appeared to be more reliable than single bay models. It was noticed that the different finite element idealizations gave very different strength predictions, indicating that proper selection of the finite element modeling approach is critical. Closed-form strength equations were also proposed based on both the experimental results and additional finite element studies.

More recently, Professor Paik has extended his studies of aluminum panels to include friction stir welded (FSW) panels under a following Ship Structure Committee study. Although such welds will not be considered in the present work, this study presents a variety of valuable information on both FSW and fusion welded structures. A working final draft of the report for this project was made available for this literature review (Paik 2009.) In this study, 10 additional panels were tested and compared to the results from the previous fusion-welded panel study presented in SSC-451. Eight of these panels were joined by friction stir welding, including joining multiple extrusions by butt welding, and joining extruded profiles to plates by a plunging lap-type weld where the FSW tool penetrates through the thickness of the plate to join the bottom of the stiffener web to the plate. Paik (2009) presents an extensive literature review of

FSW technology, along with extensive material tests on both friction stir and fusion welds. Materials investigated include 5083 in the unusual –H112 temper, as well as 5383 and 6082. 2”/50mm gauge length cross-weld tests were made in both FSW and fusion welded butt joints; the FSW joints showed significantly more ductility as well as higher strengths. Interestingly, base material tension coupons were repeated after the collapse testing, using plate material that had failed during the collapse. These coupons showed significantly reduced strength and ductility. Initial imperfections and residual stresses were measured, the later via a hole-drilling approach. In the FSW panels initial imperfections were generally much smaller than in the fusion welded panels. Residual stresses and HAZ material properties were also improved in the FSW panels, but by a smaller amount. The FSW HAZ width appeared to be roughly twice the FSW tool shoulder diameter, which was less than the 1 inch (25mm) typically assumed in fusion welding. Collapse testing revealed that many of the friction stir welds suffered a delamination-type failure, with the stiffener section separating from the plate over a short length of the panel. Most of these occurred in the post-ultimate strength region, but a few of these occurred before the ultimate strength was reached. Conclusions about improving NDT inspection and other FSW parameters were presented. Non-linear finite element analysis was used to analyze the collapse data. Three-bay models were investigated by Paik, these featured 16 4-node shell elements between stiffeners and a single shell element across the width of the HAZ. The finite element models were run with residual stresses and HAZ regions, and without. Adding the residual stresses and HAZ regions reduced the strength of the panels, but the reduction was much larger for the fusion welded panels than the friction stir welded panels. This study further confirms the importance of including the HAZ when estimating the strength of aluminum shell structures in compression.

4.1.4 Impact of Welds on Bending Response and Lateral Load Response

Aluminum welds also impact the strength of structures undergoing bending loads, such as plates resisting hydrostatic or cargo pressure, as well as beams bending between points of support. Compared to other aspects of structural response, these bending loads have not been as well investigated to date. Significant work on aluminum beam-columns has been performed, concentrating on the ability of aluminum to develop plastic moments as it is not as ductile as

steel, but only a handful of studies have extended these concerns to welds. The aforementioned work of Övreas, Thaulow, and Hval (1992) and Hval, Johnsen, Thaulow (1995) was designed to investigate aluminum beam-column framework, but most of their analysis concentrated on the tensile response local to individual welds. This could be extended to investigate bending response using either simple beam models or finite element simulation to predict the local tensile stresses and strains at welds. Moen, Hopperstad, and Langseth (1999) investigated the rotational capacity of several aluminum beams, including some I-beams with mid-span welds. The materials used were 6082 alloy in the –T4 and –T6 tempers, and 7108-T7. The higher-temper –T6 and –T7 beams showed some ductility limits when tested under increasing bending moments without welds, with some material failures recorded in the tension flange before the full plastic capacity of the beam was realized. However, the welded I-beams failed via tensile fracture in HAZ before any other failure modes had developed, showing that strain localization is a major concern for limit state design of such beams. Abildgaard, Hansen, and Simonsen (2001) investigated lateral loads acting on aluminum plates with and without HAZ. The HAZ were placed at the plate boundaries, reflecting conventional construction. Lateral loading was assumed to be a concentrated patch load at the center of plate, and both finite element simulations and a modified version of yield-line theory were used to predict the response of the plates. Compared to experiments, both methods provided fair agreement with some difficulty matching the experimental results. These methods showed that the allowable load for an equivalent level of lateral deformation was reduced by roughly 10%-25% by the presence of HAZ in the plate. More recently, Wang (2006) investigated beam-column joints as part of her previously-discussed study on local weld models, as well as attachments on the tension flanges of aluminum beams under bending that were originally tested by Matusiak (1999.) While these studies focused on the details of the weld response, they supported the concern that strain localization can significantly impact the strength of welded aluminum members under bending, and could also be used as the starting point in the investigation of similar beams.

4.2 Aluminum Structural Design Standards

4.2.1 Aluminum Association

The U.S. Aluminum Association publishes a set of civil engineering design codes referred to as the *Aluminum Design Manual* (Aluminum Association 2005) which is available in both allowable-stress and load and resistance factor design (LRFD) formats. The general format of the code in either case is a series of strength requirements for given types of structures and loads, expressed in non-dimensional form. These expressions use alloy-dependent material constants so that the same basic expression form can cover a wide range of aluminum alloys with different material stress-strain curve shapes and notch sensitivities. The code also has one set of safety factors for normal building design, and a second more conservative set for bridge design. A good overview of the code is given by Kissell and Ferry (2002.) Material properties are given for both base material and welded material properties, with tensile ultimate strengths and yield strengths, compressive yield strengths, and shear yield strengths. Starting in the 2005 edition, the yield strengths for welded alloys are specified to be measured at 0.2% offset over a 2"/50mm gauge length. The specified ultimate tensile strength for the welded alloys corresponds with the requirements in the American Welding Society (AWS) standard D1.2 (AWS 2008.), and a table of allowable filler metals is given in the *Aluminum Design Manual*.

When the structure is welded, strength reductions are specified according to Section 7 of the code. This section specifies that the heat-affected zone is to be taken as 25mm in width, with properties as outline above. Strength reductions for welding depend on the locations of welds in the structures, for the following types structures:

- Members loaded in tension with HAZ impacting the entire cross-section,
- Bearing stress at HAZ regions,
- Columns and Beams with HAZ impacting their entire cross-section but no more than 0.05L from the end of the column or beam,

- Flat element of columns or beams with welds only at supported edges,

Calculations are allowed to use base-material properties provided that the resulting strength is lower than the tensile or compressive proof strength of the HAZ region. This allows beams where the maximum bending moment occurs in a non-HAZ region, or overall buckling problems where the welds will not impact the buckling, to be designed using the higher base material strength. For columns or beams with welds more than 0.05L from the end, the code requires the calculation to be made as if the entire structural member was composed of HAZ material.

For other types of structures, where the HAZ impacts only part of the cross-section but extends over the entire length of the member, such as a built-up I or T stiffener with welds joining the web and flange, the *Aluminum Design Manual* takes a weighted-area approach, where the strength of the member is given by the following formula:

$$F_{PW} = F_{NW} - \frac{A_w}{A} (F_{NW} - F_w) \quad \text{Equation 4-1}$$

Where F_{PW} is the strength of the part-welded member, F_{NW} is the strength as if the member had no welds, and F_w is the strength as if the member was entirely comprised of HAZ material. A_w is the HAZ material area in the cross section, and A is the total cross-sectional area. For cases where the HAZ area is less than 15% of the total area for compression cases, or less than 15% of the flange area, defined as the material more than 2/3 of the distance from the neutral axis to the extreme fiber for flexure cases, this correction can be ignored. For beams, this approach allows welds to be located in low-stress areas of beams (provided the shear limit states are also met), allowing the base material strength to be utilized in the highly-stressed regions. Thus when assessing the strength impact of HAZ, the Aluminum Association approach considers the location of the HAZ as well as the material strength reduction. Ductility in the welds is not

specifically addressed in this approach; the details of the welder and weld procedure qualification are left to the AWS D1.2 standard. A specific gauge length is specified for cross-weld proof stresses.

4.2.2 Eurocode 9

The *Eurocode 9* is a pan-European building code for structures using aluminum as a material. It is a part of a number of Eurocodes developed by the European Committee for Standardization (CEN.) The goal of these codes is to eventually replace national codes in the European Union, and they consist of a set of codes for structures made of steel, concrete, timber, aluminum and several other materials. While the codes differ in their formulations to reflect the limit states associated with each structural material, they all follow a common format and have the same LRFD philosophical approach. While the core code is standardized across Europe, national annexes to the Eurocodes are allowed with additional information or requirements. In this review, the focus will be on the pan-European code, without reference to any particular national annex, focusing on the treatment of welds as outline in *EN 1999 1-1:2007 Eurocode 9 Design of Aluminum Structures, General Structural Rules* (CEN 2007.) In addition to the Eurocode itself, the European Aluminium Association (EAA) has prepared comprehensive training materials covering aluminum design under *Eurocode 9*, known as TALAT, which is freely available online (EAA 2009). From the TALAT website, the lectures *2301 Design of Members* and *2302 Design of Joints* are especially useful for the current topic though some material applies to earlier drafts of *Eurocode 9*. More recently, the European Commission held a workshop on all of the Eurocodes that has significant additional information on *Eurocode 9* (European Commission 2008.). From this website, the presentation entitled *Strength and stability of aluminium members according to EN 1999-1-1-Eurocode 9* (Höglund 2008) is particularly useful.

Eurocode 9 takes a slightly unusual effective thickness approach to deal with both local buckling of structural members as well as the effect of HAZ. In this approach, a reduction factor, ρ , is computed to account for either local buckling before a member reaches its material proof stress,

or the strength reduction in the HAZ near welds. The effective thickness of the member is then determined by multiplying the original thickness by the reduction factor ρ :

$$t_e = \rho t$$

Equation 4-2

Where t is the original thickness and t_e is the effective thickness. For local buckling of a member, the effective thickness reduction applies to the entire cross-section of the member. For HAZ, the reduction factor only applies within the HAZ width. Unlike the U.S. Aluminum Association approach, the HAZ width is dependent on the thickness of the material being joined. Additionally, for thinner material, the welding process used (TIG or MIG) is also considered. The HAZ widths used in *Eurocode 9* are shown in Table 4-1.

Further guidance is given in the code regarding inter-pass cooling for multi-pass welds, as well as the extent of HAZ for members of dissimilar thicknesses, and welding on near free edges where the welding heat may not be able to be conducted away from the weld area as easily. *Eurocode 9* specifies two thickness reduction factors, ρ , in the HAZ, one for the reduction of proof stress, and one for the reduction of ultimate tensile strength. For example, for thin 6082-T6 extrusions, the ρ factors are 0.5 on proof stress, and 0.64 on ultimate strength.

Table 4-1: HAZ Width Specified by *Eurocode 9*

Thickness, t, range, mm	HAZ Width, mm
$0 < t \leq 6$	20 MIG welds, 30 TIG welds
$6 < t \leq 12$	30
$12 < t \leq 25$	35
$t > 25$	40

For members in built up structures, applying the HAZ rules in *Eurocode 9* is straightforward. When dealing with welds running parallel to the applied stress, several checks need to be made to determine the impact of the HAZ. First, the member that is welded – such as the web or flange of a beam – must be checked for local buckling. The local buckling constants in *Eurocode 9* depend on alloy type, boundary condition, and the presence of welds. If the member is slender, a buckling thickness reduction factor, ρ , will be determined; otherwise this factor is taken as 1.0. Next, the ρ factor for the proof stress in the HAZ is determined based on the weld parameters. Within the HAZ region, the thickness of the material is then reduced to an effective thickness based on the most severe ρ factor from the HAZ or buckling concerns. Outside of the HAZ, the thickness is only modified for local buckling. The effective section and its associated properties such as area of moment of inertia are then used in the *Eurocode 9* strength formulations, which directly give an as-welded strength. For welds perpendicular to the applied stress, the normal strength formulations are applied as well as a rupture check on both the HAZ and weld metal using a ρ factor based on ultimate strength and higher partial safety factors corresponding to the increased severity of this type of failure. For overall buckling failures of assemblies of individual element, such as built-up beam-column structures, the presence of HAZ is also accounted for through a supplemental series of HAZ-factors. For longitudinal welds, these are based on the ratio of HAZ material to base material in the section, while for transverse welds typically the ultimate strength of the beam-column at the location of the weld, considering the local moments and forces at the weld, is used. While this approach is significantly more complex than the *Aluminum Design Manual* rules reviewed in the previous section, this formulation allows for the consideration of welds at any point along the length of the beam-column without resorting to treating the entire structure as if it was HAZ material. Höglund (2008) gives several examples of using these formulations to examine beam-columns. While this approach is attractive, more work would be required to extend it to general shell-type structures with welds in the middle of plating fields away from transverse frames or longitudinal stiffeners. *Eurocode 9* also discusses using plastic design approaches for aluminum structures, noting that only certain aluminum alloys have the ductility required to develop plastic hinges. The code also notes that transverse welds on the tension side of beams at the location of plastic

hinges should prohibit plastic analysis. This further confirms the importance of strain localization in inelastic tension response.

4.2.3 Classification Society Rules

In addition to the civil engineering design codes reviewed previously, two marine classification society rules were reviewed, the DNV *Rules of Classification of High Speed, Light Craft and Naval Surface Craft* (DNV 2009) and the ABS *Guide for Building and Classing High Speed Naval Craft* (ABS 2007). Both of these approaches follow an allowable-stress approach for aluminum high-speed vessels. In both documents, stresses in the vessel's structure are estimated either by direct finite-element analysis or suitable structural idealization models. The resulting stresses are compared to allowable stresses based on the vessel's material, the type of load effect, and the type of structure under consideration. In general, reduced stresses are specified for welded aluminum, with the exception of some specific checks where the higher base material properties are used.

Both the ABS and DNV approaches partially rely on the International Association of Classification Societies (IACS) unified requirements for aluminum materials (W25 – IACS 2006) and welding consumables (W26 – IACS 2005). Interestingly, while both the ABS and DNV rule specify allowable stresses based on the proof or yield stress in the welded condition, the IACS, DNV, and ABS welder and weld procedure qualifications only require that a certain ultimate tensile strength is reached. Where proof or yield stresses are given, they are not a requirement for qualification, and the corresponding gauge length is also not specified. A comparison between the required tensile ultimate strengths is given in Table 4-2 below. The different code documents are in close agreement. Ductility of the welds is assured through a series of weld bend tests specified by ABS or DNV. Minimum elongations over given gauge lengths is not specified by either DNV or ABS for cross-weld tests, though it is required for base materials.

Table 4-2: Comparison of Welder Qualification Required Cross-Weld Ultimate Strengths

Base Material	IACS Requirement ¹ – W26, Table 3	DNV Requirement ² - Pt.2 Ch.3 Sec.5 J Table J2	ABS Requirement ³ – Pt. 2, Ch. 5, Appendix 1 – Table 2
5083-H116	275 MPa	270 MPa	276 MPa
5383-H116	290 MPa	290 MPa	290 MPa
5456-H116	290 MPa	Not Given	290 MPa
6061-T6	170 MPa	165 MPa	165 MPa
6082-T6	170 MPa	170 MPa	Not Given

Notes:

- 1) IACS does not specify tempers corresponding to these strengths. Filler metal not specified – fillers must obtain these strengths plus other requirements in W26.
- 2) All alloys but 5383 can be welded with either 5183 or 5356 fillers, 5383 alloys require 5183 fillers
- 3) ABS requirements are in document “Rules for Materials and Welding – Part 2” dated 2006 and included in the HSNC Guide by reference.

Table 4-3 presents the same data for proof strengths. Note that no firm gauge length value is given for these tests in either the ABS or DNV specifications, so it is difficult to directly compare these figures to each other or to other design codes. The issues surrounding gauge lengths have been discussed and presented previously in Ship Structure Committee work (Sielski 2008). The classification society approaches typically can only be compared on the basis of the final structure, as safety factors may be applied at different points in different rule sets, the differences in proof stress may not translate into similar differences in the final structural requirements. However, it is interesting to note that there are significant differences between the values.

Table 4-3: Comparison of Given Proof Strengths for Welded Aluminum

Base Material	DNV Requirement - Pt.2 Ch.3 Sec.5 J Table J2	ABS Requirement ² – Pt. 2, Ch. 5, Appendix 1 – Table 2
5083-H116	115 MPa (5356 Filler) 125 MPa (5183 Filler)	165 MPa
5383-H116	145 MPa (5183 Filler)	165 MPa
5456-H116	Not Given	179 MPa
6061-T6	115 MPa ¹	138 MPa ³
6082-T6	115 MPa ¹	Not Given

Notes:

- 1) May use either 5183 or 5356 fillers.
- 2) ABS requirements are in document “Rules for Materials and Welding – Part 2” dated 2006 and included in the HSNC Guide by reference. Note than in the HSNC guide in Pt. 3. Ch. 1 Section 2 – 1.5, the properties of 6000-series alloys are further restricted to a welded yield strength of 55 MPa unless special approval is given.
- 3) For material less than 9.5mm in thickness

Design for both the DNV and ABS rules follows a similar pattern. In the DNV rules, a material factor, f_l , is defined as:

$$f_l = \frac{\sigma_f}{240}$$

Equation 4-3

Where σ_f is the yield stress of the material in MPa, which is not to be taken as more than 70% of the material’s ultimate strength. Values of f_l are given in both the base material and welded

condition for a number of approved marine aluminum alloys. For aluminum alloys joined by welding, the as-welded f_l values are generally used to support allowable stress calculations. The calculations can be either simple plate or beam models of the structure as laid out in the rules, or the interpretation of stresses from a finite element model of the vessel. Allowable stress is given as a multiple of f_l based on the type of loading and structure under consideration. In certain areas, base material properties are used in place of welded material properties, including:

- Minimum thickness formulas for plating and plates in web frames and girders.
- Buckling considerations for the structure in Pt. 3, Ch. 3, Sec. 10 of the rules, however, DNV notes that if extensive or critically-located HAZ are present, the as-welded properties may have to be used.

ABS follows a conceptually similar approach, although the implementation is slightly different. No intermediate material factor is used in the ABS HSNC Guide. Allowable stresses are given as fractions of the as-welded proof stress of the alloy under consideration, the structural member under consideration, and the type of load applied. This approach applies to both simplified strength models, and to the result of finite element analysis where combined stresses are typically evaluated using a von-Mises stress approach. Similar to the DNV rules, there are some special circumstances where base material properties can be used in place of welded properties, including:

- Global strength that depends on a Q-factor, which in turn depends on base material yield strength and the ultimate strength of welded material. This is used in both Pt. 3 Ch. 1 Sec. 3 and Pt. 3. Ch. 2 Sec. 1.
- Uniaxial compressive buckling considerations, with the same exception for critical or extensive HAZ regions as DNV includes. Shear buckling relies on welded proof stresses in all cases.

In terms of the approach to modeling welds in aluminum structures, the ABS and DNV approaches are conceptually equal. Both rely on a reduced allowable stress for welded structures, with a few exceptions. Neither method requires an explicit consideration of the size of the HAZ or location of the HAZ in the structure. Weld strength is assured by listing allowable consumables and establishing requirements for the ultimate tensile strength of welds as part of the weld procedure and welder qualification. Ductility is not specified beyond performing certain bend radius tests for welder and weld procedure qualifications.

4.3 Summary

The strength reduction in the HAZ of common aluminum alloys has received extensive research attention to date, although not all aspects of interest for marine applications have been adequately covered. Previous studies published in journal articles, reports, and similar sources have been reviewed across four main categories – local weld response, tensile response, compressive response, and bending and lateral load response. Additionally, four design codes have been reviewed. From these studies, the following conclusions and areas of disagreement stand out:

- The width and strength in the HAZ can be quite variable. Care needs to be taken to ensure that a gauge length is given when comparing cross-weld proof stresses measured to a given offset.
- The local material failure of the HAZ is a complex problem, with constraint leading to tri-axial stress states. Finite element analysis has shown some promise in modeling this, but extensive material models and very detailed weld models are still required.
- HAZ can significantly (10% - 25%) impact the compressive buckling strength of aluminum structures.
- Both Kristensen (2001) and Zha and Moan (2001) note that the transverse HAZ perpendicular to the applied loading appears to be the most damaging HAZ for

compressive response. This is not fully supported by the limited data from Rigo et al. (2003, 2004.) This HAZ was not included in all experimental and numerical analysis reviewed, so care should be taken when comparing test results or methods between sources.

- For plate structures, Kristensen (2001) notes that the strength reduction from HAZ is constant regardless of plate slenderness, while Wang et al. (2005) propose that the HAZ impact is larger on stockier plates.
- While tensile limit states beyond gross yielding are not commonly considered in ship design, it is clear that the potential for strain localization in HAZ under inelastic loads exists, and both the ductility and strength of these regions requires careful consideration.
- The 6xxx-series alloys appear more susceptible to such tensile strain localization than the 5xxx-series alloys.
- Very little data is available for plates acting under lateral pressure, or bending structures. The limited data available indicates that the HAZ will significantly impact the carrying ability of these structures. It is clear that strain localization must be considered for these cases.

In terms of finite element modeling, modeling of the tensile failure of local welds can be achieved with both shell and solid elements. However, such meshes require extensive material properties and highly detailed local weld models. Therefore, such approaches are probably not suited for design purposes for quite some time. Good compressive collapse predictions for ship-like stiffened panels have been made with finite element models featuring roughly 10-25 four-node shell elements spanning the distance between longitudinal stiffeners, and a sufficient number of elements between transverse frames to ensure that the aspect ratio of the elements is near one. The HAZ can be modeled with one to four shell elements with reasonable accuracy for compressive collapse. Several previous studies have accepted slightly large aspect ratios for the elements in the HAZ to allow local mesh refinement. Modeling details for bending and lateral

load responses have not yet been established, if rigorous treatment of the strain localization phenomenon in the HAZ is to be made, detailed models are probably required. However, based on the compressive collapse results reviewed, it would appear that first yield and analysis for lateral loads with relatively small levels of plastic strain could be carried out with similar meshes to the compressive collapse meshes.

Several design approaches have been proposed by both authors and code writing bodies. These are compared in Table 4-4 below. Many approaches rely on a weighted-average concept for welds running in the direction of the applied stresses, whether it is applied to material properties, affected areas, or calculated strengths. The design approaches can be divided into two broad categories: simplified weld models and modified allowable stress approaches. The simplified weld models are used in all of the research papers reviewed, and in the *Eurocode 9* and *Aluminum Design Manual*. While the complexity of these approaches varies, they all try to take into account the amount of HAZ material and its strength relative to the base material when calculating the overall structural strength. These approaches range from simple volume-averaging like that proposed by Paik and Duran (2004) where the locations of the HAZ are assumed within the method through fairly complex approaches such as that used in *Eurocode 9*, where the location of the HAZ can be considered in addition to its breadth and strength. The second category of approaches is the modified allowable stress approaches used by ABS and DNV. These approaches apply a blanket strength reduction to the allowable stresses in the structure to account for HAZ regions, largely removing the need to consider the location, extent, and strength reduction in the HAZ. While this makes design much simpler and does allow greater freedom for locating structural welds as well as pipe attachments, construction lifting lugs and other potential HAZ locations commonly required in vessel construction, the penalty is presumably a heavier more conservative structure.

Table 4-4: Comparison of Proposed Design Methods

Method	Applicable Limit States	HAZ Model	Approach to	
			Welds Parallel to Dominant Stress	Welds Perpendicular to Dominant Stress
Wang (2006)	Local tensile failure across butt weld.	Multi-zone with independent properties.	Not applicable.	A rigid - plastic model of linked regions by the weld is proposed.
Collette (2007)	Local tensile failure across butt weld.	Single material strength, various widths.	Not applicable.	Treated either as series of non-linear springs or a notch following the approach of Satoh and Toyoda (1970).
Paik and Duran (2004)	Compressive collapse of plates and stiffened panels.	Formula allows variable width and HAZ strength within bounds of underlying finite element database .	Volume-averaged proof stress is used to predict plate and column slenderness factors that are used in a regression equation, thereby accounting for HAZ breadth and strength reduction. Transverse and longitudinal HAZ are not treated separately, only longitudinal HAZ is analyzed for panel failures. HAZ at boundaries of panel only.	
Wang et al. (2005)	Compressive collapse of plates and stiffened panels.	HAZ width determined by BS8118 standard, strength can vary between 40% and 100% of base metal strength.	Regression model for plate failure with different HAZ strengths, assumed welds at boundary of plate only. Panel collapse strength is impacted by HAZ only via reduced plate strength.	
Abildgaard, Hansen, and Simonsen (2001)	Lateral patch loads on plates.	HAZ width fixed, strength variable.	Modified yield line theory for HAZ at plate boundaries for permanent set of plate under lateral patch load.	
Aluminum Association (2005)	In-plane and lateral loads.	HAZ width fixed at 1" / 25mm. HAZ strength fixed per design values.	Area-averaged approach used with strengths of un-welded and all-HAZ members.	Not allowed except at end supports of beam/columns. Stress at supports checked for yield of welded material.
Eurocode 9 (CEN 2007)	In-plane and lateral loads.	HAZ width varies by thickness and welding process. Strength fixed per design values.	Effective thickness approach used, some related buckling constants change if member has welds. A limited number of these constants also use welded/un-welded area ratio.	Checked for rupture, not yield with higher safety factors and ultimate tensile strength of HAZ and weld. Procedures for handling welds at any location on beam or column.
DNV (2009)	In-plane and lateral loads.	None.	Approaches use allowable stress design, with stress reduced for welded aluminum. No explicit consideration of HAZ locations, breadth, or strength.	
ABS (2007)				

5 ONR SIMPLIFIED APPROACH

A simplified approach to predicting the compressive collapse of aluminum stiffened panel and extrusions was under development under a separate research contract at the time of this work. An early version of this method was used in the current project to both help develop the panel design and to provide a basis of comparison for the FEA results. The background to this method, as applied on this project, is briefly presented here. The method falls into the category of “plate separation” approaches to collapse problem, in that each individual plate component of the stiffened panel is first modeled independently. The basis for this theory is Hopperstad et al.’s (1999) extension of Stowell’s (1948) unified buckling theory. Stowell’s theory proposes that the uni-axial buckling stress can be expressed as:

$$\sigma_{Buckle} = \eta \sigma_{Elastic} \quad \text{Equation 5-5-1}$$

Where $\sigma_{elastic}$ is the elastic buckling stress and η is used to correct for plastic effects in stocky sections. The elastic buckling stress for plate-like objects can be found from the equation:

$$\sigma_{Elastic} = k \frac{\pi^2 E}{12(1-\nu^2)} \left(\frac{t}{b} \right)^2 \quad \text{Equation 5-5-2}$$

Where ν is the elastic Poisson’s ratio for the material, taken as 0.3 for aluminum, t is the thickness of the member, b is the breadth, E is the Young’s modulus, and k is buckling geometry coefficient. For the flat plates simply-supported on all four edges investigated in this report, k was taken as 4 for all values. The η factor also changes based on plate geometry. Stowell [2] proposed the following for simply-supported flat plates:

$$\eta = \frac{E_{SEC}}{E} \left(\frac{1}{2} + \frac{1}{2} \sqrt{\frac{1}{4} + \frac{3 E_{TAN}}{4 E_{SEC}}} \right)$$

Equation 5-5-3

Where E_{SEC} and E_{TAN} are the secant and tangent modulus of the material's stress-strain curve. As both the secant and tangent modulus depend on the instantaneous stress level, an iterative approach is required to calculate the buckling stress via Equation 5-5-1 and Equation 5-5-3. This approach has been shown to be reasonably accurate at predicting the initial buckling stress in both the elastic and plastic regions; however, it does not include any post-buckling strength. Such post-buckling strength can be significant when the initial buckling occurs at stress levels below the material proof stress in slender sections. Hopperstad et al. (1999) extended Stowell's theory so that the entire compressive load-shortening curve of the plate in compression could be predicted, thus including any post-buckling strength that may occur. The basis for the approach is the effective width approach, where the nominal width of the plate is reduced as buckling occurs to account for the loss of stiffness and resisting force associated with buckling. Thus, for any instantaneous average compressive stress, the effective width, b_{eff} , can be found as:

$$b_{eff} = b \frac{\sigma_{avg}}{\sigma_e}$$

Equation 5-5-4

Where σ_{avg} is the average axial compressive stress across the plate, and σ_e is the current edge stress, which is equal to the stress obtained from the material compressive stress-strain curve at the current value of axial strain. Hopperstad et al.'s approach fundamentally assumes that the effective width of the plate once the edge stress of the plate has surpassed the initial buckling stress can be found by calculating the width of the plate that would first buckle at the current edge stress value. An effective width of plating is then defined as this calculated width divided by the actual width of the plate. Thus, the stress after the onset of buckling can be evaluated as:

$$\sigma = \sqrt{\eta \sigma_{Elastic} \sigma_e} \leq \sigma_e$$

Equation 5-5-5

Where the buckling coefficient η is calculated now at the current edge-stress value, and the elastic buckling stress is the same one from Equation 5-5-2, calculated with the original plate geometry. The inequality simply enforces an effective breath equal to or less than one. The ultimate strength of the plate is now found numerically as the maximum value on the stress-strain curve. This method was further extended to account for:

1. Initial imperfections, by a regression term derived from the additional plate bending caused by the maximum value of the imperfection and Mofflin's (1983) plate test data set.
2. Residual stresses, by using a simple strain – offset approach to account for the compressive residual stress already present in the plate at the start of loading.
3. HAZ running in the direction of the applied load by reducing the stress carried by the HAZ to account for yielding in the HAZ.

This approach gave fairly accurate predictions of both the peak compressive stress and the shape of the compressive load-shortening curve when compared to the plates tested by Mofflin (1983).

The behavior of the stiffened panel composed of such plate elements was determined by a modification of the classical panel column buckling approach developed and presented by Faulkner et al. (1973) for steel panels, and extension to predict the entire load-shortening curve by Gordo and Guedes Soares (1993). In this approach, the strength of a steel plate and stiffener combination in compression can be determined as:

$$\frac{\sigma_C}{\sigma_Y} = \frac{\sigma_{CB}}{\sigma_Y} \left(\frac{A_S + b_e t}{A_S + bt} \right)$$

Equation 5-5-6

Where σ_C is the column failure stress, σ_Y is the yield stress of the steel, σ_{CB} is the column buckling stress, b is the plate width, b_e is the effective plate width at failure, t is the plate thickness, and A_S is the stiffener cross-section area. The second term in this expression assumes that the plate between stiffeners will buckle before the overall panel fails, and thus an area reduction factor for this must be included. In this approach, the column buckling stress is calculated using the Johnson-Ostenfeld interaction approach to transition from elastic buckling to in-elastic buckling as:

$$\frac{\sigma_{CB}}{\sigma_Y} = 1 - \frac{1}{4} \frac{\sigma_Y}{\sigma_E}, \quad \sigma_E \geq 0.5\sigma_Y$$

$$\frac{\sigma_{CB}}{\sigma_Y} = \frac{\sigma_E}{\sigma_Y}, \quad \sigma_E < 0.5\sigma_Y$$

Equation 5-5-7

Where σ_E is the Euler column buckling stress that is distinct from the edge stress, σ_e , used above with a lower-case e subscript. The edge stress can be found by entering the applied strain into the panel's material law. σ_E is found as:

$$\sigma_E = \frac{\pi^2}{a^2} E \frac{I_{EFF}'}{A_S + b_e t}$$

Equation 5-5-8

Where a is the panel length between support, and I_{EFF}' is a tangent effective moment of inertia, calculated assuming the plate between stiffeners has a tangent effective width related to the instantaneous compressive modulus of the plate accounting for its buckling failure. Following the approach of Gordo and Guedes Soares (1993), this method was extended to predict the entire load-shortening curve, using the following assumptions:

1. At strains below the peak compressive strain predicted by the Faulkner approach, the resisting force of the stiffened panel is found by adding up the individual stress-strain responses of all the plate elements in the panel
2. At the peak compressive strain, the resisting force of the stiffened panel is equal to that predicted by the Faulkner approach
3. At strains above the column failure strain, the resisting stress is approximated by applying Equation 5-5-6 at the instantaneous value of edge strain.

The proposed method provides a rapid approach to calculate the compressive response of aluminum panels, accounting for material-specific stress-strain laws and the HAZ. However, the version used in this study has some limitations:

- The plate data set used for development did not include any plates welded on all four edges, only plates welded in the direction of the applied compressive load. Thus, the impact of the transverse HAZ on plate strength cannot be studied or included.
- The effect of initial column imperfections is not explicitly included, but implicit in the use of the Johnson-Ostenfeld approach.
- The column-collapse approach as implemented often predicts too-rapid decreases in strength after the peak load is reached.

Ongoing research is addressing these areas.

6 FINITE ELEMENT MODELING

6.1 Model Matrix

Twelve (12) combinations of plate and stiffeners are analyzed for this study. These are shown in Table 6-1. These parameters are chosen based on the calculation shown in Appendix A. Each model consists of three bays and four stiffeners. The finite element analyses are performed for models built with 5083-H116 and 6082-T6 aluminum alloys (hereafter AL5083 and AL6082). In models 1 through 4, both plate and stiffeners are AL5083. In model 5 through 8, plate is AL5083 and stiffeners are AL6082. For models 1 through 8 HAZ is modeled at the plate-stiffener junction. In models 9 through 12 both plate and stiffeners are considered extruded AL6082 and HAZ is modeled at the junction of two extruded elements. The HAZ softening is also modeled at the transverse frame location between the bays. The welds are not modeled as the analyses are performed with plate elements only. This analysis also ignores effect of residual stresses. Each of the plate stiffener combinations listed in Table 6-1 is analyzed for three different loadings (tension, compression, & bending). Finally, for each panel, three separate FE models were made consisting of:

4. All base metal throughout the model – no separate HAZ regions
5. All HAZ metal throughout the model – no separate HAZ regions
6. Base metal & HAZ metal.

Where the first two model types are to evaluate the impact of ignoring HAZ by assuming either base or HAZ material properties throughout. Thirty six (36) finite element models are created and each model is analyzed for three load cases. All together one hundred and eight (108) models are analyzed.

Table 6-1: Matrix of Models to be analyzed

Model	Plate	Stiffener	Weld Location
1	Light (4mm)/ 5083	Light (60x3/30x6)/5083	Plate stiffeners connection
2	Heavy (6mm)/ 5083	Light (60x3/30x6)/5083	Plate stiffeners connection
3	Heavy (6mm)/ 5083	Heavy (100x6/40x10)/5083	Plate stiffeners connection
4	Light (4mm)/ 5083	Heavy (100x6/40x10)/5083	Plate stiffeners connection
5	Light (4mm)/ 5083	Light (60x3/30x6)/6082	Plate stiffeners connection
6	Heavy (6mm)/ 5083	Light (60x3/30x6)/6082	Plate stiffeners connection
7	Heavy (6mm)/ 5083	Heavy (100x6/40x10)/6082	Plate stiffeners connection
8	Light (4mm)/ 5083	Heavy (100x6/40x10)/6082	Plate stiffeners connection
9	Light (4mm)/ 6082	Light (60x3/30x6)/6082	Weld between two extruded
10	Heavy (6mm)/ 6082	Light (60x3/30x6)/6082	Weld between two extruded
11	Heavy (6mm)/ 6082	Heavy (100x6/40x10)/6082	Weld between two extruded
12	Light (4mm)/6082	Heavy (100x6/40x10)/6082	Weld between two extruded

6.2 Stress-Strain Relationships

Non-linear stress-strain data for the AL5083 and AL6082 are developed using the Ramberg – Osgood relationship shown below:

$$\varepsilon = \frac{\sigma}{E} + 0.002 \left(\frac{\sigma}{\sigma_{0.2}} \right)^n$$

Where :

ε Strain

σ Applied stress

E Elastic modulus

$\sigma_{0.2}$ 0.2% offset proof stress

n Exponent

These relationships are shown in Figure 6-1 and parameters used to develop these relationships are shown in Table 6-2.

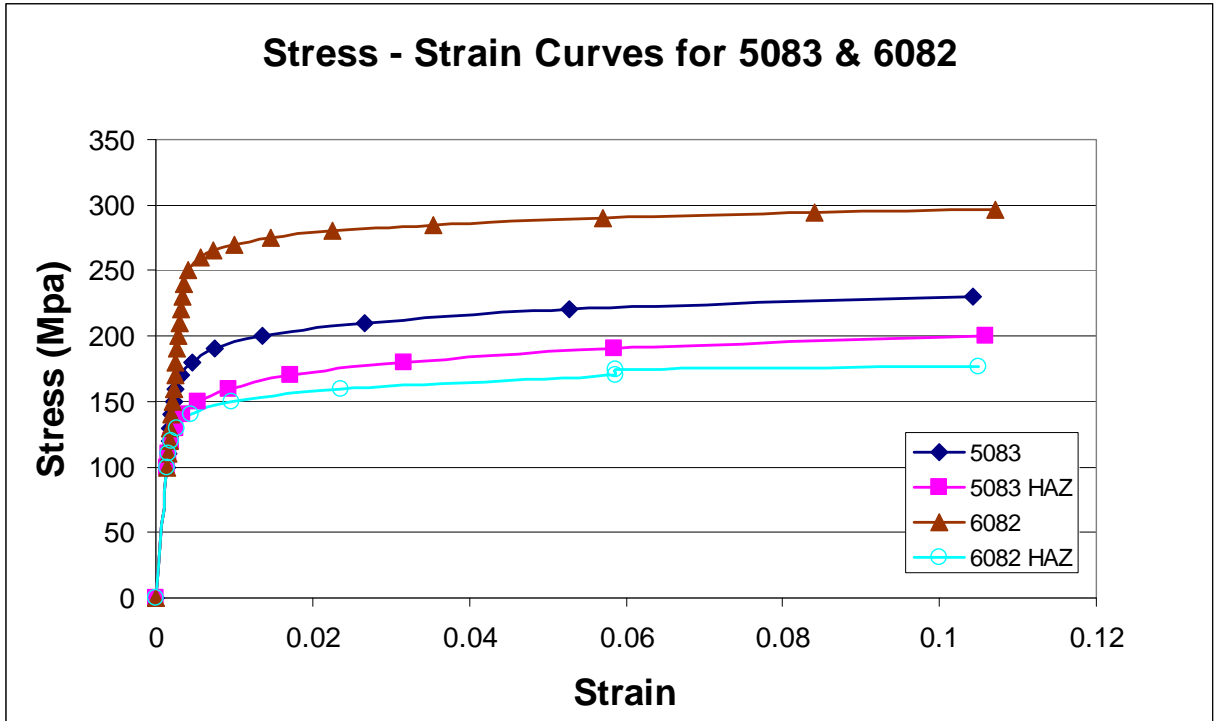


Figure 6-1: Stress-Strain Relationships for AL5083 & AL 6082

Table 6-2: Ramberg-Osgood Parameters

Material	5083	5083 HAZ	6082	6082 HAZ
0.2% Stress (N/mm ²)=	180	144	260	138
Young's Modulus (N/mm ²)	70000	70000	70000	70000
n =	16	12	30	16

6.3 Finite Element Models

The finite element models are developed for all plate-stiffener combinations shown in Table 6-1. These models are developed using the pre/post processor FEMAP using plate elements only. For this study the HAZ is assumed to be 3 times the thickness of the plate. The extent of HAZ is shown in Figure 6-2. In this figure b_p' ($3 \cdot t$) is the breadth of softening (HAZ) in plate and b_s' ($3 \cdot t_w$) is the breadth of softening (HAZ) in stiffener web. As mentioned before that the welds and residual stresses are not modeled. Each model consists of 3 bays and 4 stiffeners. This is shown in Figure 6-3. The stiffener spacing is 225 mm and bays are 1000 mm long. The overall size of the model is 900 mm x 3000 mm. The HAZ at the stiffener-plate junction is

shown in Figure 6-4 and HAZ for the extruded plate is shown in Figure 6-5. The boundary conditions are shown in Figure 6-6. The transverse frames are modeled solely to account for the plate softening due to welding. To simulate stiff transverse frames, these transverse frames are constrained in the vertical direction. The initial imperfection was accounted for by applying 2 mm deflection to both plate and stiffeners between the transverse frames.

All plates are meshed with 4-noded shell elements. The literature search indicated that 1 to 4 shell elements are adequate in modeling the HAZ. For this study we used 4 HAZ elements for 4mm plate and 6 HAZ elements for the 6mm plate. These HAZ elements have four to one aspect ratio. Both transverse and longitudinal HAZ are modeled. In other areas 12mm x 12mm square elements are used. Each model has about 40,000-50,000 nodes. These models are analyzed with NX\NASTRAN advanced nonlinear static solver. For compression load cases, the maximum applied displacement is 10 mm and this is applied over 50 steps (step size 0.2mm). For the tension case the applied displacements ranged from 10 mm to 15 mm and the step size was 0.2mm. Lateral pressure is used to simulate bending of the stiffened plate panels. Applied pressure ranged from 0.1 N/mm² (2088 psf) to 0.15 N/mm² (3132 psf). All pressure cases are run for 100 iterations. Model run time was between 3 to 4 hrs on a 32 bit PC (4GB RAM) and 2 to 3 hrs on a 64 bit machine (8GB RAM).

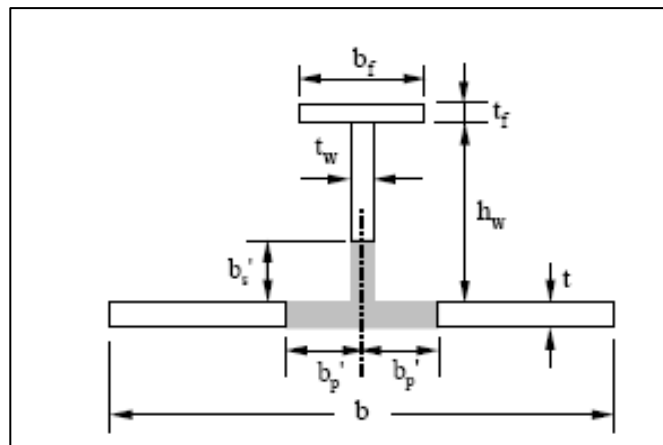


Figure 6-2: Heat Affected Zone (HAZ) for Plate and stiffener (Paik 2005)

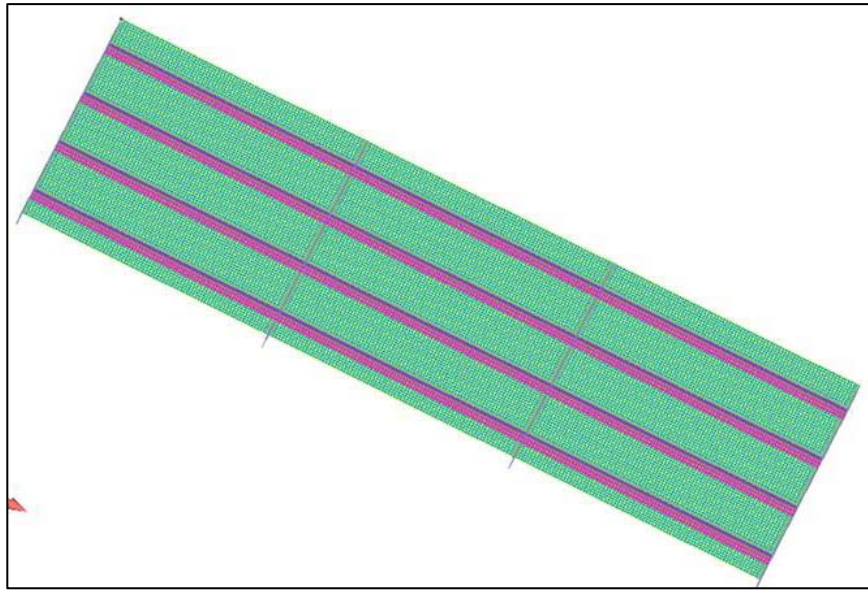


Figure 6-3: Finite element model of the Stiffened-plate

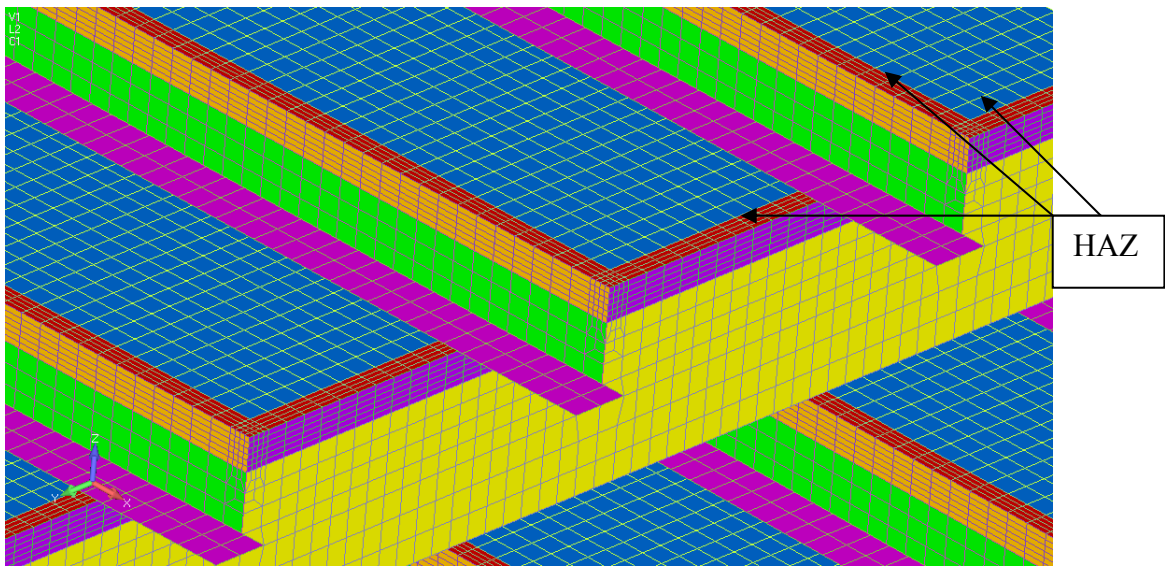


Figure 6-4: Finite element model with HAZ

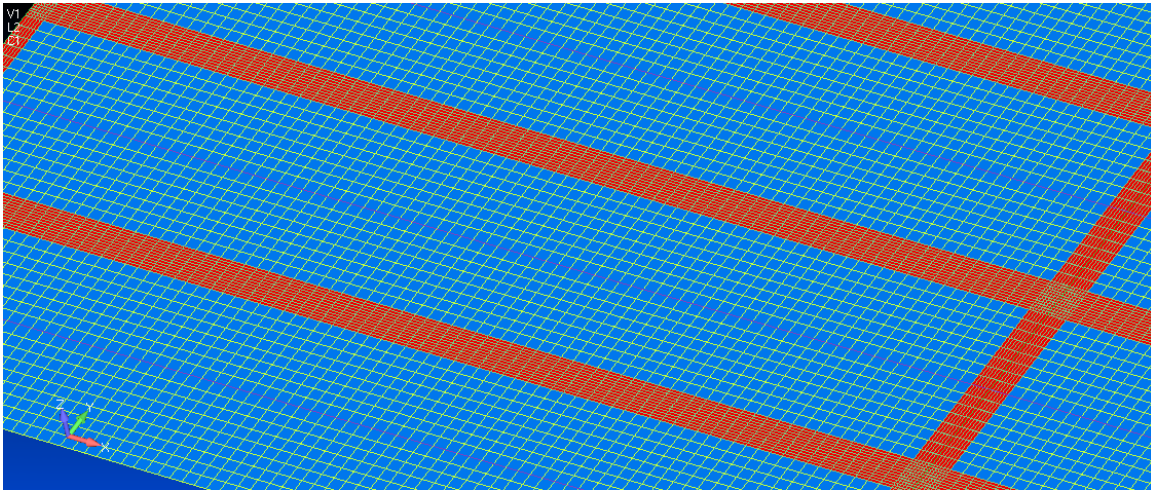


Figure 6-5: Finite element model with HAZ for extruded panels

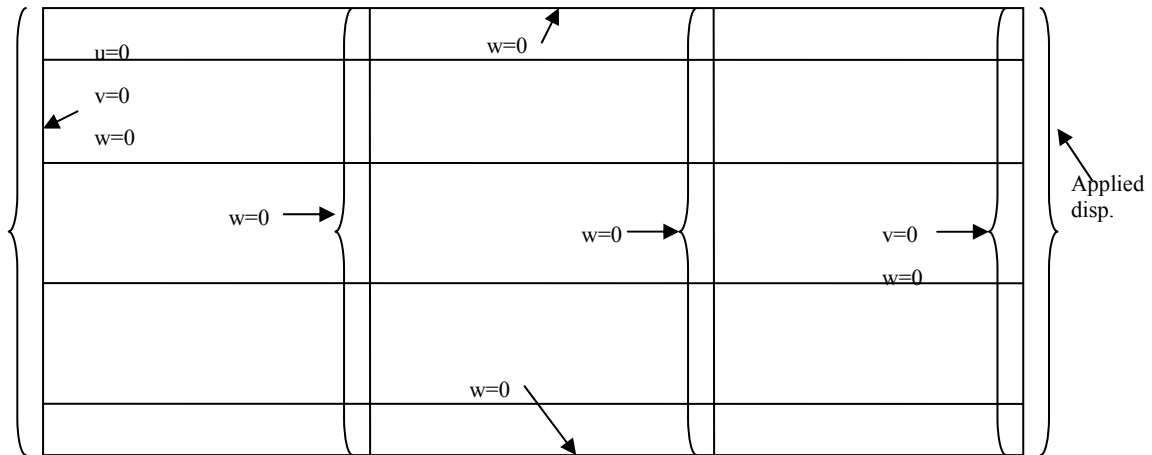


Figure 6-6: Boundary conditions applied to the finite element model

6.4 Failure Criteria

The compressive loads have a distinct and a well defined ultimate strength. However, tension and bending cases do not have distinct peaks and it is not quite obvious when to stop the analysis. Literature survey indicate that analysis can be stopped if the finite element results indicate:

- i) fracture in the weld
- ii) limiting stress, and/or
- iii) limiting strain or overall deflection

As mentioned before only plate elements are used for this study and welds are not modeled. Due to absence of the weld in the finite element models, and a lack of information on detailed material failure parameters, fracture analysis could not be performed. Most classification societies use proof stress as the limiting stress. This study also used the limiting stress as the failure criteria and compared overall tensile forces and lateral pressures for each model that caused at least 5% of the base plate or 5% of the HAZ to reach proof stress. These proof stresses are shown in Table 6-2.

7 RESULTS

As discussed before the finite element analyses are done for three load cases:

1. Compression (enforced displacement)
2. Tension (enforced displacement)
3. Bending (lateral pressure)

For each load case models are run using the properties of: a). Base metal, b). HAZ, and c). combined base metal and HAZ. These results are discussed below. Thirty six finite element models are analyzed for each of the three load cases.

7.1 Compression Load case

For compression load case, the maximum applied displacement is 10 mm and this is applied over 50 steps (step size 0.2mm). The average stress and strain values are calculated and plotted. These plots have distinct peaks that indicate the ultimate strength of the model. These plots are shown in Appendix B. The FEA results are also compared against the ONR simplified approach (Chapter 5). The ultimate strength values (peak values) for these two approaches are summarized in the tabular form in Table 7-1 through Table 7-4 . Results for models 1, 5, and 9 (2,6, and 10, etc) are clustered in one table as these models have same scantlings but different material and weld locations. In this section, results for the combined model (model with both Base metal and HAZ properties) are designated with 'C', for models with base metal only are designated with 'B', and for models with HAZ properties are designated with 'HZ'. Stresses and displacements for all 12 models are plotted at the point where the ultimate strength reaches peak value and also at the maximum applied displacement (step 50) and are shown in Appendix C. The ultimate strengths of all twelve models are compared in Figure 7-1.

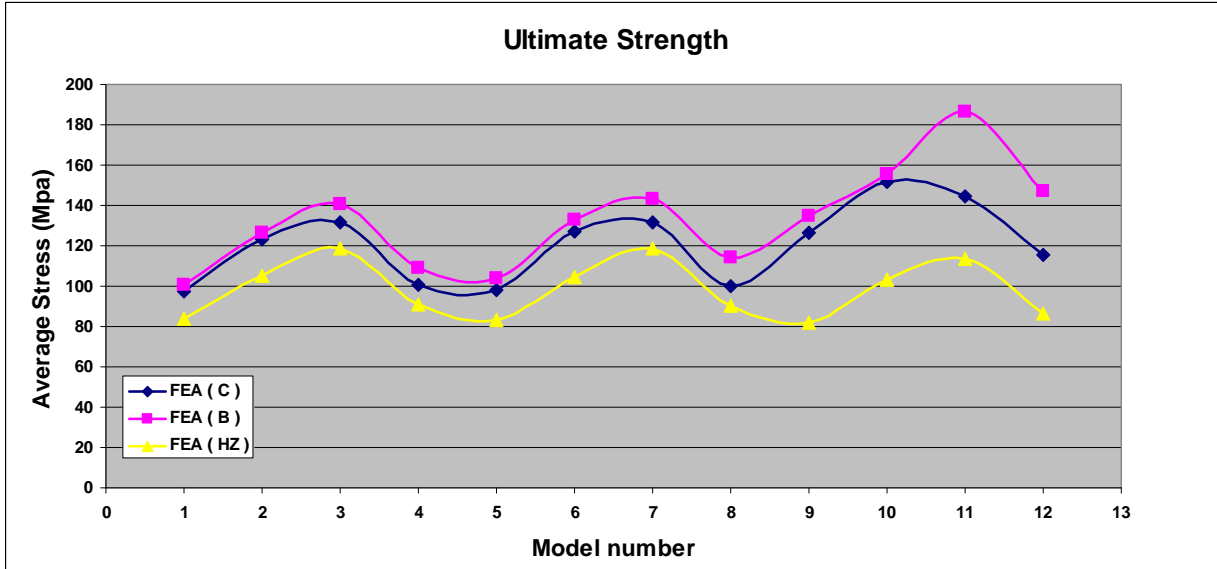


Figure 7-1: Comparison of Ultimate Strength (FEA Results)

The results from the FEA analysis of Model11 (5083 Light plate + 5083 Light Stiffeners) show that the ultimate strength of the stiffened plate is 96.9 Mpa when modeled with properties of both base metal and HAZ. When only base metal properties are used, the ultimate strength (100.8 Mpa) is over predicted by about 4% and when only HAZ properties are used then the ultimate strength (83.6 Mpa) is under predicted by about 14%. In Model2 (5083 Heavy plate + 5083 Light stiffeners) plate thickness is increased from 4 mm to 6mm and the ultimate strength for the combined model increases to 123 Mpa compared to 96.9 MPa for the Model11. The effect of using properties of only base plate and only HAZ are very similar to that of Model11. The finite element model with base plate properties over predict the ultimate strength by about 3% and with HAZ properties under predicts the strength by about 14%. The ultimate strength of Model3 (5083 Heavy plate + 5083 Heavy stiffener) is calculated as 131.8 Mpa which is slightly higher than that of Model2. This increase is due to heavier stiffeners used in Model3 compared to Model2. In this case the model with base properties over predicts the strength by about 7% and the model with HAZ properties under predicts the strength by about 10%. The ultimate strength of Model4 (5083 Light plate + 5083 Heavy stiffener) is calculated as 100.4 Mpa. The effect of using only base metal properties and only HAZ properties are very similar to Model3. Comparing model4 results with the results of Model11 we can see that increasing the

Table 7-1: Ultimate strength comparison for model 1, 5, & 9

Model1						
	FEA			Simplified		
	Strain	Stress	% difference	Strain	Stress	% difference
Combined	0.002000	96.9	-	0.001985	105.0	-
base only	0.002000	100.8	4.1%	0.001985	107.1	2.0%
HAZ only	0.001667	83.6	-13.7%	0.001533	87.8	-16.4%

Model5						
	FEA			Simplified		
	Strain	Stress	% difference	Strain	Stress	% difference
Combined	0.002000	96.9	-	0.001985	106.3	-
base only	0.002200	103.6	6.8%	0.002030	108.7	2.3%
HAZ only	0.001667	83.5	-13.9%	0.001533	88.1	-17.1%

Model9						
	FEA			Simplified		
	Strain	Stress	% difference	Strain	Stress	% difference
Combined	0.002667	126.5	-	0.002980	142.7	-
base only	0.002667	134.6	6.4%	0.003025	146.8	2.8%
HAZ only	0.001467	81.9	-35.3%	0.001533	89.5	-37.3%

Table 7-2: Ultimate strength comparison for model 2, 6, & 10

Model2						
	FEA			Simplified		
	Strain	Stress	% difference	Strain	Stress	% difference
Combined	0.002400	123.0	-	0.002121	131.2	-
base only	0.002400	126.3	2.6%	0.002166	134.8	2.7%
HAZ only	0.002200	105.5	-14.3%	0.001804	105.3	-19.8%

Model6						
	FEA			Simplified		
	Strain	Stress	% difference	Strain	Stress	% difference
Combined	0.002267	127.2	-	0.002302	139.3	-
base only	0.002333	132.9	4.5%	0.002302	143.2	2.8%
HAZ only	0.002133	104.4	-18.0%	0.001759	104.8	-24.8%

Model10						
	FEA			Simplified		
	Strain	Stress	% difference	Strain	Stress	% difference
Combined	0.002933	151.4	-	0.002889	173.9	-
base only	0.002667	155.3	2.6%	0.002889	182.0	4.7%
HAZ only	0.002067	103.1	-31.9%	0.001714	104.0	-40.2%

Table 7-3: Ultimate strength comparison for model 3, 7, & 11

Model3						
FEA			Simplified			
	Strain	Stress	% difference	Strain	Stress	% difference
Combined	0.002000	131.8	-	0.002302	140.9	-
base only	0.002067	140.8	6.8%	0.002302	144.0	2.2%
HAZ only	0.002000	118.8	-9.8%	0.002166	117.9	-16.3%

Model7						
FEA			Simplified			
	Strain	Stress	% difference	Strain	Stress	% difference
Combined	0.002000	131.4	-	0.002935	156.2	-
base only	0.002133	143.2	9.0%	0.002980	162.7	4.1%
HAZ only	0.002000	118.6	-9.7%	0.002030	115.0	-26.4%

Model11						
FEA			Simplified			
	Strain	Stress	% difference	Strain	Stress	% difference
Combined	0.002733	144.8	-	0.003161	191.8	-
base only	0.002533	186.5	28.8%	0.003161	198.4	3.4%
HAZ only	0.001867	113.3	-21.8%	0.002121	116.3	-39.4%

Table 7-4: Ultimate strength comparison for model 4, 8, & 12

Model4						
FEA			Simplified			
	Strain	Stress	% difference	Strain	Stress	% difference
Combined	0.001733	100.4	-	0.002256	122.4	-
base only	0.001867	109.2	8.7%	0.002256	124.0	1.3%
HAZ only	0.001667	90.8	-9.6%	0.001894	100.4	-17.9%

Model8						
FEA			Simplified			
	Strain	Stress	% difference	Strain	Stress	% difference
Combined	0.001667	99.9	-	0.003161	152.3	-
base only	0.002000	114.0	14.0%	0.003161	156.5	2.8%
HAZ only	0.001533	90.0	-9.9%	0.001804	99.7	-34.6%

Model12						
FEA			Simplified			
	Strain	Stress	% difference	Strain	Stress	% difference
Combined	0.001933	115.3	-	0.003251	172.5	-
base only	0.002267	146.8	27.3%	0.003206	175.8	1.9%
HAZ only	0.001200	86.7	-24.8%	0.001804	100.1	-42.0%

stiffener scantlings do not have large impact on the ultimate strength under compressive loading where as increasing the plate thickness increases the ultimate strength significantly (Model1 vs. Model2, Model3 vs. Model4).

As shown in Table 6-2, the reduction in strength in the HAZ for AL5083 material is about 20% (180 Mpa for base metal compared to 144 Mpa for the HAZ). However, the actual reduction in the stiffened panel strength when modeled with the combined properties of base and HAZ, is about 3-14% depending on the scantlings of the stiffened panels.

The results of ONR simplified study show similar ultimate strength values, however, the behavior of the stress/strain curve in the post buckling region are very different. Most of the results of the current study indicate a gradual decrease in the ultimate strength from its peak values but the ONR study indicates sudden drop in ultimate strength for models 1 through 3 and more gradual reduction in Model4.

The results of models 5 through 8 where AL5083 stiffeners are replaced by AL6082 stiffeners are very similar to that of models 1 through 4. AL6082 base metal is stronger than AL5083 base metal but has inferior HAZ properties (Table 6-2). The results indicate that replacing 5083 stiffener with 6082 stiffener virtually has no influence on the ultimate strength of the stiffened panels.

In models 9 through 12, the plate stiffeners combinations are assumed to be of extruded AL6082 and welds and corresponding HAZ are located between the two extruded panels. When these models are analyzed with properties of only base metal and only HAZ, the results follow the similar pattern discussed above , i.e., the ultimate strength increase with scantlings of plate and stiffener. Model9 (light plate + light stiffener) and Model11 (Heavy plate + heavy stiffener) have the lowest and highest ultimate strength, respectively. However, when these stiffened panels are modeled with combined properties of base metal and HAZ, heavier stiffeners seem to adversely affect the ultimate strength. Ultimate strength for Model9 is 126.5 Mpa compared to ultimate strength of Model12, 115.3 Mpa. Similarly, ultimate strength of Model10 (151.4 Mpa) is higher than that of Model11 (144.8 Mpa). When these extruded

stiffened panels are modeled with properties of HAZ, these models under predict the ultimate strength by 20-30%. When these panels are modeled with the properties of base metal, they over predict the strength by 3-6% for models 9 and 10, and about 28% for models 11 and 12. This large difference is due to heavier plate used for models 11 and 12.

As shown in Table 6-2, AL6082 has about 50% of its strength in the HAZ (260 Mpa for base metal compared to 138 Mpa for the HAZ). However, this study indicate that the actual reduction in the stiffened panel strength when modeled with the combined properties of base and HAZ, is about 10-25%.

The results of the simplified ONR model indicate very similar pattern in most cases with slightly higher values of ultimate strength.

Looking at the results of models 1 through 8 where the welds are at the stiffener plate junction, the ultimate strength of the panels modeled with properties of base metal is about 3-14 % higher than the panels modeled with combination of base and HAZ properties. If these panels are modeled with the properties of the base metal only, then there is no need to model HAZ and elements used in the analysis can be much larger compared to the elements sizes used in HAZ for the combined model. This will reduce the size of the FEA model and hence reduce the run time significantly. The ultimate strength calculated by this method can then be reduced by about 10% to account for the HAZ softening. Another approach would be to reduce the proof stress by about 10% while developing the stress-strain curve using the Ramberg-Osgood formula and calculate the ultimate strength with this modified stress-strain curve. To test this hypothesis a new stress-strain curve is derived for the base metal with reduced proof stress of 162 Mpa (90% of 180) using the Ramberg-Osgood formula. Models 1 through 8 were reanalyzed with this new stress-strain curve and properties of base metal only. These results are shown in Appendix B and summarized in Figure 7-2. Results indicate that the reduced proof stress model are able to predict ultimate strength values that are very close to those predicted by the combined models. To save time this approach can be used at the early stage of design to develop scantlings for aluminum structure.

For the extruded models, the variation in the ultimate strength when modeled with the properties of base metal ranges from 3-28%. This variation in ultimate strength is quite large and no attempts were made to reanalyze these models with reduced base metal properties. The variation in the ultimate strength when modeled with properties of HAZ is more consistent (20-30%) A new stress-strain curve is developed with the HAZ parameters shown in Table 6-2 but with 25% higher proof stress (184 Mpa). Model 11 was reanalyzed with this approach and results (Figure 7-3) clearly indicate that this approach does not work.

Attempts were also made to see if the reduction in strength could be predicted based on the magnitude of the final average failure stress compared to the proof stress of the weakest HAZ region. The thinking behind such an approach is that the further the average failure stress in the panel exceeds the HAZ proof stress, the more pronounced the material differences between the base and HAZ zones will be, and the larger the impact of the HAZ on the final strength. Such predictions were examined two ways, first by taking the ratio of the average failure stress to the HAZ proof stress (Figure 7-4), and by examining the ratio of the instantaneous tangent modulus of the HAZ and base material at the average failure stress (Figure 7-5). As can be seen from the two figures, no clear pattern emerges, indicating that the failure process is more complex than these simple measures can account for. At failure, the true stress in the HAZ may be significantly different from the average stress in the panel. Thus, it may be necessary to evaluate how the HAZ impacts the plate and stiffener separately, and then calculate how that impacts the overall failure stress. However, it appears that no simple design measure of HAZ impact can be found from these ratios at the current time.

Following conclusions can be made based on the results discussed above:

- In early stages of design, aluminum structure built with AL5083 can be modeled as base metal with reduced proof stress (about 10%). This will avoid time consuming analysis of fine mesh models with small HAZ elements.
- In critical areas, structure should be modeled as combination of base metal and HAZ.

- For extruded structure built with AL6082, full analysis is required to predict the behavior of the structure.

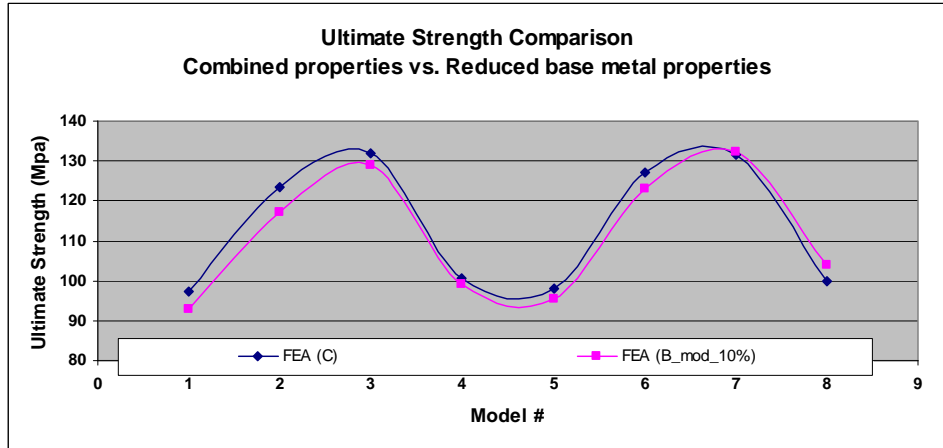


Figure 7-2: Comparison of Ultimate Strength: Combined properties versus reduced base metal properties

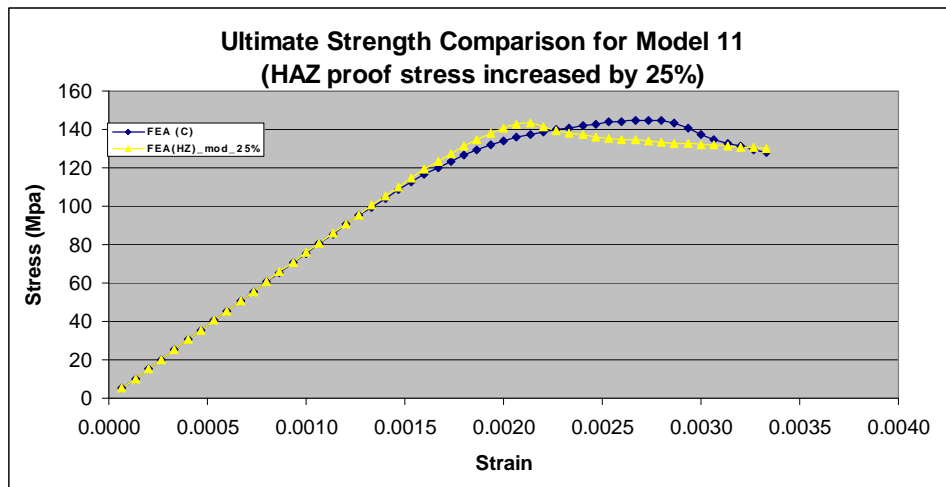


Figure 7-3: Comparison of Ultimate Strength for Model 11: Combined properties versus increased HAZ properties (25% higher proof stress)

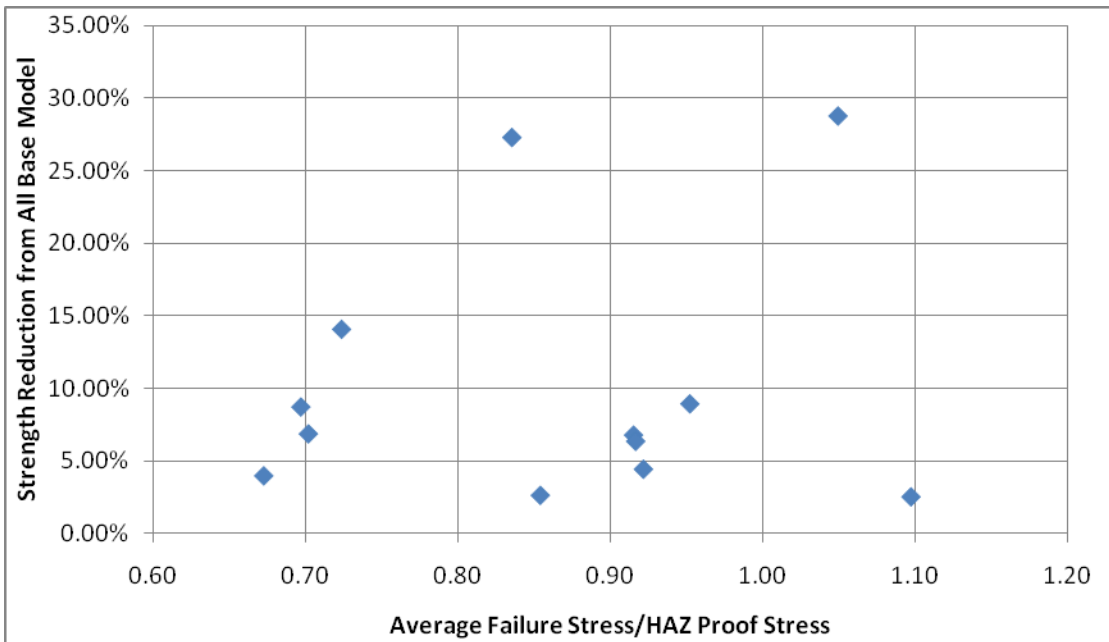


Figure 7-4: Strength Reduction vs. Failure Stress divide by HAZ Proof Stress

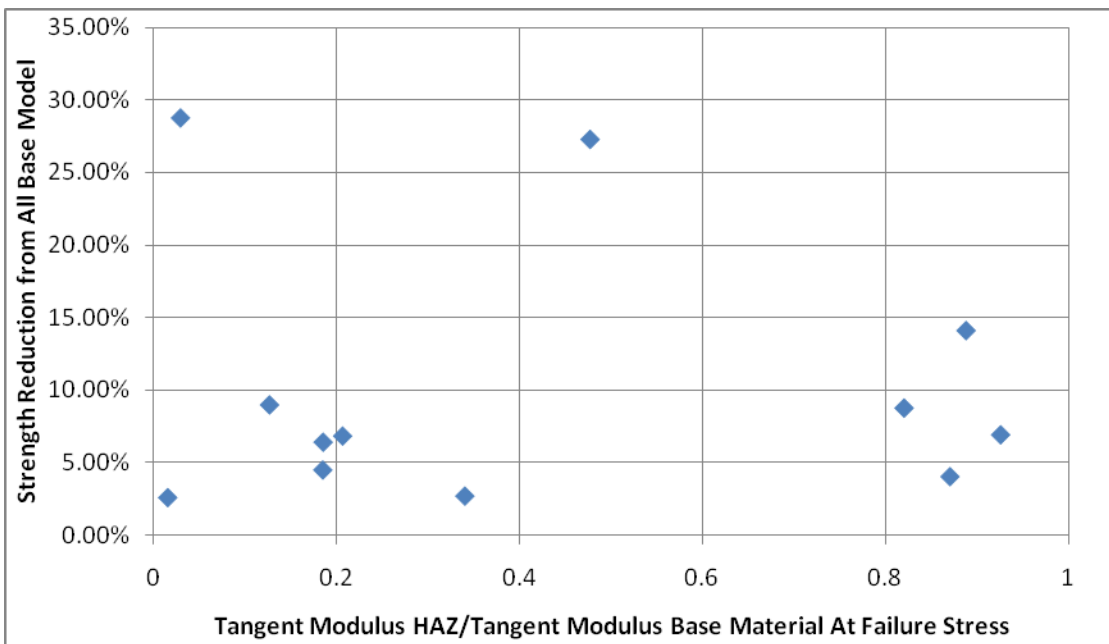


Figure 7-5: Strength Reduction vs. HAZ/Base Ratios of Tangent Modulus at Average Failure Stress

7.2 Tension Load Case

For tension load case, the applied displacements ranged from 10 mm to 15 mm and the step size was 0.2mm. All 36 models were analyzed. The average stress and strain values are calculated and plotted. For each case the strain (and corresponding average stress) value that caused a fixed portion of the local material to reach proof stress was also plotted. These plots are shown in Appendix D. The FEA results are also summarized in the tabular form in Table 7-1 through Table 7-4. Results for models 1, 5, and 9 (2,6, and 10, etc) are clustered in one table as these models have same scantlings but different material and weld locations. As explained in the compression load case, combined model (model with both Base metal and HAZ properties) are designated with 'C', for models with base metal only are designated with 'B', and for models with HAZ properties are designated with 'HZ'.

The yield points of all twelve models are compared in Figure 7-6. This study used the limiting stress as the failure criteria and compared overall tensile forces for each model which cause at least 5% of the base plate or 5% of the HAZ to reach proof stress. These proof stresses are shown in Table 6-2. For the combined case (Base metal + HAZ), the transverse HAZ reaches yield well before the longitudinal HAZ for all twelve models.

As can be seen from the Appendix D that the average stress-strain curve for AL5083 combined models follow the pattern of input stress-strain curves. However, for the AL6082 combined models there are distinct peaks similar to the compressive models. The stiffener webs and flanges yield at these peak values. The transverse HAZ reaches yield well before this peak value as shown in the Appendix D.

For the combined case, models 1 through 4 yield at the average stress value of about 170 Mpa and average strain of 360 μ strain. These average stress values are about 3% less than the models analyzed with base properties and about 17-18% higher than the models analyzed with HAZ property. For models 5 through 8, the average stress values at the yield for the combined models range from 180-200 Mpa, for base models range from 190-210 Mpa, and for the HAZ models range from 136-138 Mpa. These average stress values for the combined models are

about 5% less than the models analyzed with base properties and about 25-30% higher than the models analyzed with HAZ property.

For the extruded stiffened plate panels, yield points for the combined models are around 170 Mpa. The yield points of the combined models are about 50% lower compared to base metal models and about 22% higher compared to HAZ models. These large differences in yield point between various types of models are due to the fact that AL6082 is significantly weaker in the heat affected zone.

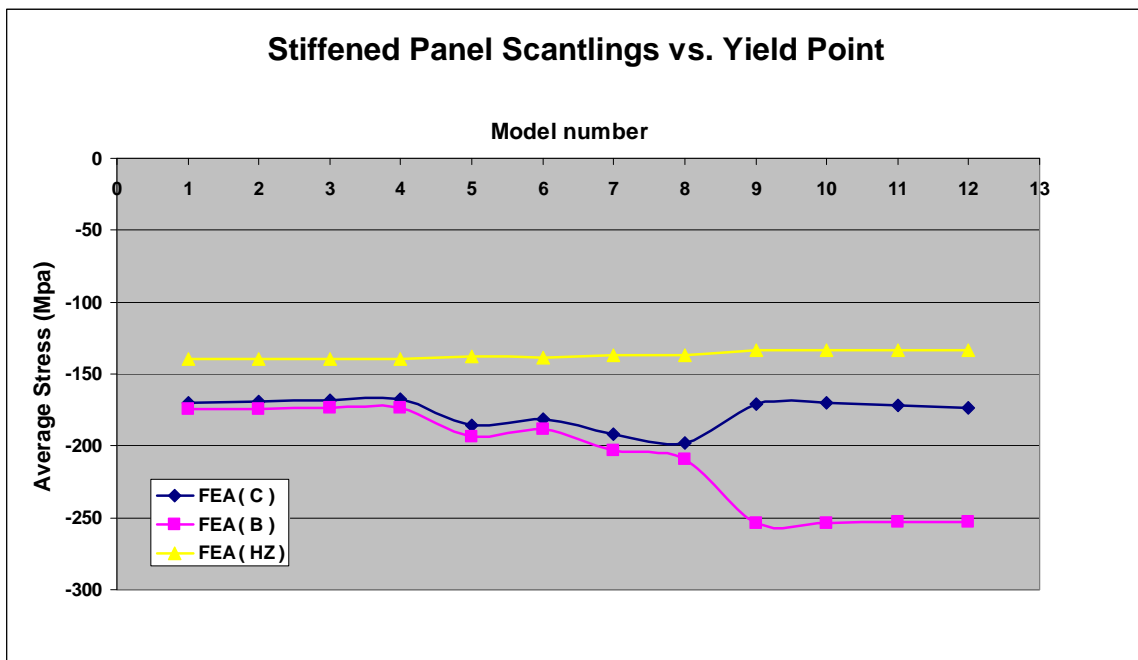


Figure 7-6: Comparison of yield points for tension load case

Following conclusions can be made based on the results discussed above:

- Results for Models 1- 8 show small difference between combined and base model (max 6%).
- Modeling with properties of HAZ is very conservative (17%-30%).
- Results for Models 9 – 12 (AL 6082) indicate large differences depending on the model properties.

- In early stages of design, AL5083 aluminum structure can be modeled as base metal with reduced proof stress (about 10%). This will provide slightly conservative results.

Table 7-5: Yield point comparison of Models 1,5 & 9

Model1			
	Strain	Stress	% difference
Combined	0.003600	-169.7	-
base only	0.003667	-174.0	2.6%
HAZ only	0.003333	-139.5	-17.8%
Model5			
	Strain	Stress	% difference
Combined	0.003533	-185.8	-
base only	0.003733	-193.7	4.3%
HAZ only	0.003333	-138.2	-25.6%
Model9			
	Strain	Stress	% difference
Combined	0.002533	-170.7	-
base only	0.004667	-253.4	48.5%
HAZ only	0.003200	-133.8	-21.6%

Table 7-6: Yield point comparison of Models 2,6 & 10

Model2			
	Strain	Stress	% difference
Combined	0.003600	-169.5	-
base only	0.003667	-174.0	2.7%
HAZ only	0.003333	-139.5	-17.7%
Model6			
	Strain	Stress	% difference
Combined	0.003533	-181.2	-
base only	0.003733	-188.6	4.1%
HAZ only	0.003333	-138.6	-23.5%
Model10			
	Strain	Stress	% difference
Combined	0.002533	-169.7	-
base only	0.004667	-253.5	49.3%
HAZ only	0.003200	-133.8	-21.2%

Table 7-7: Yield point comparison of Models 3,7 & 11

Model3			
	Strain	Stress	% difference
Combined	0.003600	-168.1	-
base only	0.003667	-173.7	3.4%
HAZ only	0.003333	-139.3	-17.1%
Model7			
	Strain	Stress	% difference
Combined	0.003533	-191.6	-
base only	0.003733	-203.0	5.9%
HAZ only	0.003333	-137.2	-28.4%
Model11			
	Strain	Stress	% difference
Combined	0.002533	-172.1	-
base only	0.004667	-253.1	47.1%
HAZ only	0.003200	-133.5	-22.4%

Table 7-8: Yield point comparison of Models 4,8 & 12

Model4			
	Strain	Stress	% difference
Combined	0.003533	-167.8	-
base only	0.003667	-173.6	3.5%
HAZ only	0.003333	-139.2	-17.0%
Model8			
	Strain	Stress	% difference
Combined	0.003533	-197.6	-
base only	0.003733	-209.7	6.2%
HAZ only	0.003333	-136.6	-30.9%
Model12			
	Strain	Stress	% difference
Combined	0.002533	-173.1	-
base only	0.004667	-253.0	46.2%
HAZ only	0.003200	-133.5	-22.9%

7.3 Pressure Load Case

In this study lateral pressure is used to simulate bending of the stiffened plate panels. Applied pressure ranged from 0.1 N/mm^2 (2088 psf) to 0.15 N/mm^2 (3132 psf). All pressure cases are run for 100 iterations. All 36 models were analyzed. For each case the lateral pressure value that caused a fixed portion of the local material to reach proof stress was also plotted in Figure 7-7. The variation in lateral pressure to reach proof stress is shown in Figure 7-8. This plot shows the percentage difference in lateral pressure with respect to the combined case. For all the combined (Base metal +HAZ) cases elements in the transverse HAZ in the center panel of the stiffened plate yield first. These stress plots are shown in Appendix E. This study used the limiting stress as the failure criteria and compared applied pressure for each model which cause at least 5% of the base plate or 5% of the HAZ to reach proof stress. These proof stresses are shown in Table 6-2.

The results indicate that for models 1 through 8, the base metal model over predicts the strength by about 10% compared to the combined model. For models 9 through 12 this difference ranges from 15 to 60% which is expected as the proof stress of AL6082 is higher than that of AL5083 but the proof stress of softened AL6082 is less than that of AL5083. When modeled with properties of HAZ only, models 1 through 4 under estimates the strength by about 10%. For models 5 through 12, this difference is about 25% which is again due to low proof stress of the softened AL6082 material.

Following conclusions can be made based on the results discussed above:

- Results for Models 1- 8 show about 10% difference between combined and base models.
- Modeling with properties of HAZ is very conservative. For AL5083 this difference is about 10% whereas for AL6082 it about 25%.

- In early stages of design, AL5083 aluminum structure can be modeled as base metal with reduced proof stress (about 10%).

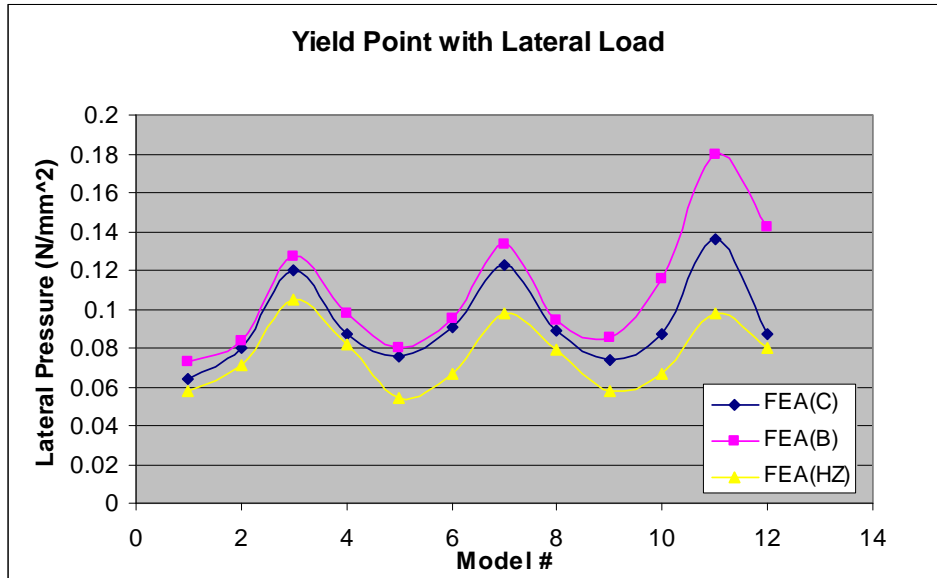


Figure 7-7: Plot of lateral pressure at the yield point

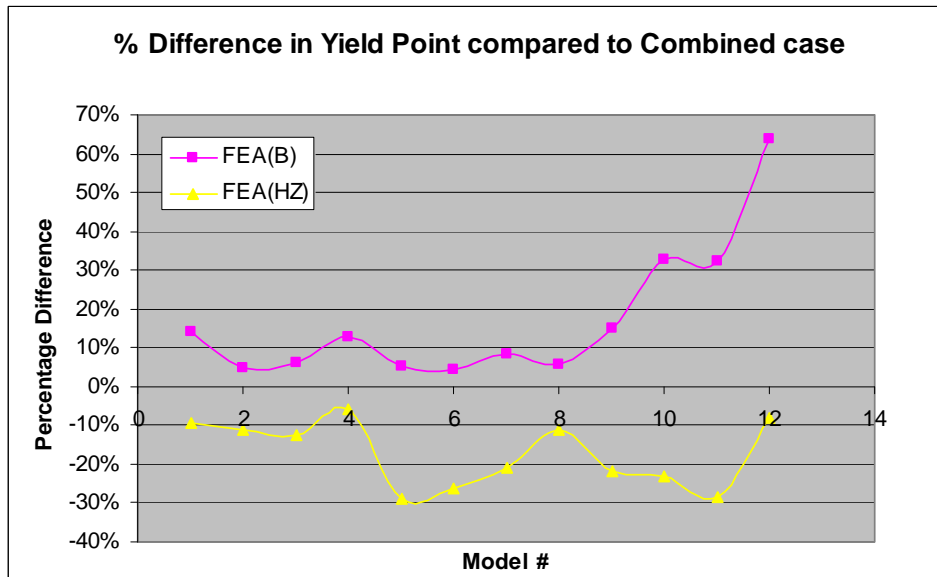


Figure 7-8: Percentage difference in lateral pressure wrt. combined case

7.4 Paik's Closed Form Solution

Paik developed a closed-form design formulations as a first cut estimate of the panel ULS. This kind of formulation is also required to do risk or reliability assessment. The empirical formulae were developed by curve-fitting of the ANSYS computations and available test data (Paik & Duran 2004, Paik et al. 2004b, Paik et al., 2005). The formulae and assumptions from the cited references are reproduced below.

The assumed softening zone is shown in Figure 7-9 and the cross section of the plate stiffener combination is shown in Figure 7-10.

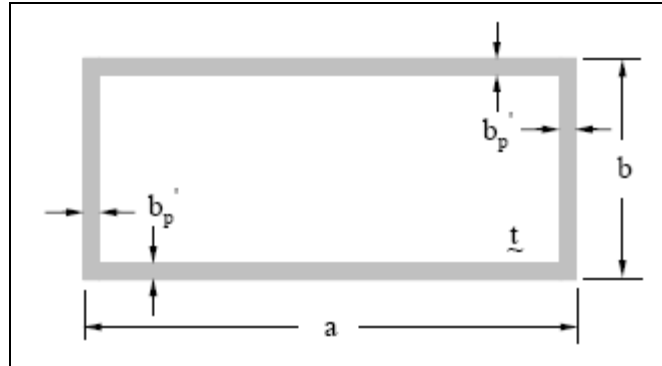


Figure 7-9: Assumed softening zone (Paik 2005)

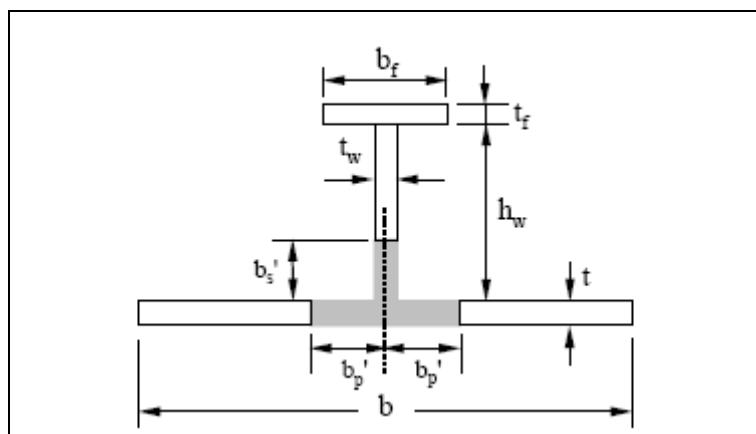


Figure 7-10: Cross section of the plate-stiffener combination with softening zones (Paik 2005)

where

a = plate length,

b = plate breadth,

t = plate thickness,

b_p' = breadth of softening in HAZ (heat affected zone) in plating,

$b_s' = b_{sHAZ}$ = breadths of HAZ softening in stiffener web,

b_f = breadth of stiffener flange,

t_f = thickness of stiffener flange,

h_w = height of stiffener web,

t_w = thickness of stiffener web

For welded aluminum plates simply supported at all (four) edges and under axial compressive loads, the ultimate strength formula developed by Paik et al. is shown below in Equation 7-1. In this equation, β' takes into account the effect of softening in the HAZ in terms of the plate volume or surface. This equation implicitly considers an average level of initial deflection, while the effect of welding residual stress is not accounted for.

$$\frac{\sigma_{xu}}{\sigma_{Yp}'} = \begin{cases} 1.0 & \text{for } \beta' \leq 0.46 \\ -0.215\beta' + 1.1 & \text{for } 0.46 < \beta' \leq 2.2 \\ -0.083\beta' + 0.81 & \text{for } \beta' > 2.2 \end{cases}$$

$$\text{where } \beta' = \frac{b}{t} \sqrt{\frac{\sigma_{Yp}'}{E}}, \quad \sigma_{Yp}' = \frac{P_p}{ab},$$

$$P_p = (a - 2b_p')(b - 2b_p')\sigma_{Yp}' + 2[ab_p' + (b - 2b_p')b_p']\sigma_Y',$$

Equation 7-1

For aluminum stiffened panels simply supported at all (four) edges and under axial compressive loads when they are modeled by a plate-stiffener combination as representing the panel, the following ultimate strength formula (Equation 7-2) was derived by Paik et al. for three levels of initial deflections. This equation also does not account for welding residual stress while the effects of initial deflections and softening in HAZ are taken into account.

$$\sigma_{xu} = \frac{\sigma_{Yseq}'}{\sqrt{C_1 + C_2(\lambda')^2 + C_3(\beta')^2 + C_4(\lambda'\beta')^2 + C_5(\lambda')^4}} \leq \frac{\sigma_{Yseq}'}{(\lambda')^2} \quad (3)$$

$$\text{where, } \lambda' = \frac{a}{\pi r} \sqrt{\frac{\sigma_{Yseq}'}{E}}, \quad \sigma_{Yseq}' = \frac{P_s}{bt + h_w t_w + b_f t_f},$$

$$P_s = (b - 2b_p')t\sigma_{Yp}' + 2b_p't\sigma_{Yp}' + (h_w - b_{sHAZ})t_w\sigma_{Ys} + b_{sHAZ}t_w\sigma_{YsHAZ} + b_f t_f \sigma_{Ys},$$

Equation 7-2

Where

$\sigma_Y' = \sigma_{YHAZ}$ = yield stress in HAZ,

σ_{Ys} = yield stress of stiffener,

σ_{Yp} = yield stress of the plate in base metal.

$r = \sqrt{I / A}$ = radius of gyration,

I = moment of inertia of stiffener with attached plating,

A = cross-sectional area of stiffener with attached plating.

The coefficients C1 – C5 are defined depending on the level of initial deflections of plating and stiffeners, as indicated in Table 7-9.

Table 7-9: Coefficients depending on the levels of initial deflections of plating and stiffeners (Paik 2005)

Coefficient	Slight	Average	Severe
C ₁	0.878	1.038	1.157
C ₂	0.191	1.099	2.297
C ₃	0.106	0.093	0.152
C ₄	-0.017	-0.047	-0.138
C ₅	1.30	1.648	3.684

All twelve models were analyzed using the empirical formula for a stiffened plate panel. These results are compared with the finite element analysis results as shown in Table 7-10 and Figure 7-11. The FEA and ONR study results compare well with the empirical formula and seem to fall between the results for average and severe initial distortions for most cases evaluated in this study.

Table 7-10: Comparison of Ultimate Strengths

Model #	Paik's Formula/Distortion Level			FEA	ONR
	Slight	Average	Severe		
1	127.3	116.0	95.2	97.4	105.0
2	138.7	118.3	94.2	123.3	131.2
3	156.7	144.4	126.0	131.8	140.9
4	134.5	129.2	110.9	100.4	122.4
5	140.1	126.7	103.1	98.0	106.3
6	147.7	125.3	98.9	127.2	139.3
7	182.4	167.1	145.0	131.4	156.2
8	162.2	155.0	132.6	99.9	152.3
9	161.1	147.3	118.6	126.5	142.7
10	173.4	147.0	113.3	151.4	173.9
11	209.6	193.3	165.7	144.8	191.8
12	174.5	169.3	143.6	115.3	172.5

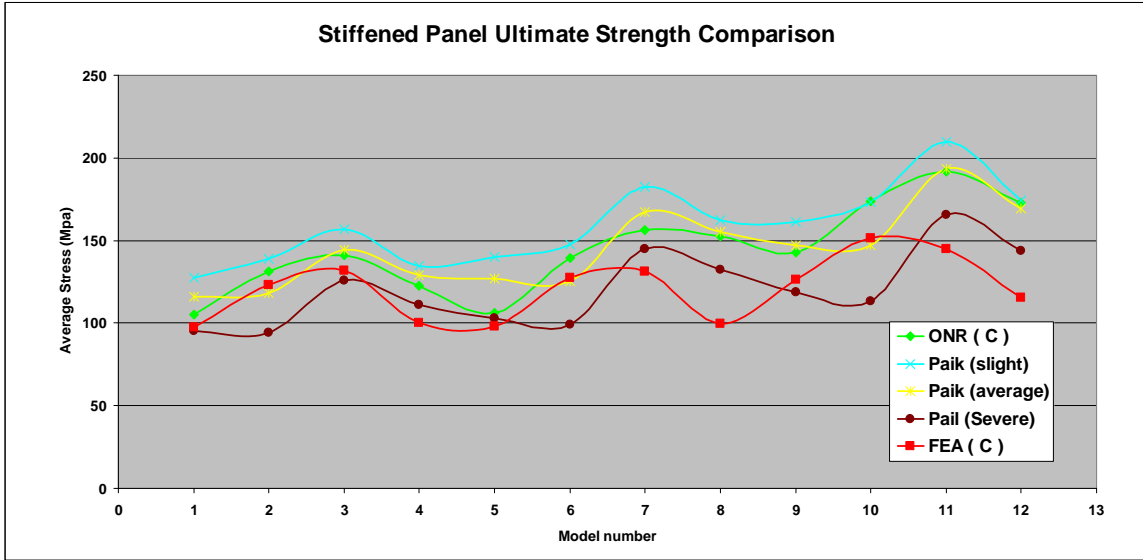


Figure 7-11: Comparison of ultimate strength

8 CONCLUSIONS AND RECOMMENDATIONS

Based on the analysis conducted here for a range of tee-stiffened panels, it appears that there is a significant advantage for modeling aluminum marine stiffened panels by explicitly considering the HAZ extent, location, and strength in place of applying a uniform knock-down factor to the strength of the HAZ material. For the compressive cases studied, the strength penalty for modeling the stiffened panel as all-HAZ material in place of a combined base/HAZ material model ranged from roughly 10% to 30%. The strength reduction was generally higher for the 6xxx-series alloys than the 5xxx-series alloys. This is likely a reflection of the higher strength loss in 6xxx-series HAZ, but it may also be related to the location of the HAZ in the plate component of the panel, for the 6xxx-series panels the HAZ was located at mid-plate, reflecting how 6xxx-extrusions are typically joined together. Efforts to try to correlate the reduction in stiffened panel compressive strength from the all-base material case with ratios of the average failure stress in the panel to the HAZ proof stress, and the relative stiffness in the HAZ, were inconclusive. However, for the 5xxx-series panels, it appears that modeling the structure with a proof stress 90% of the base materials proof stress produces fairly consistent results. This approach did not appear practical or consistent for the 6xxx-series panel. The various simplified methods explored, including the early version of an ONR strength method and Paik's method performed fairly well when compared to the FE results.

The results for tensile and bending under pressure loads were very similar in overall character to the compression load cases. The spread of material yield throughout a fixed portion of the model was used as the condition for determining the strength of the panel. This is not a true collapse limit state related to a plastic hinge forming or ruptures occurring in the HAZ, such models are still a challenge to calibrate and use in conjunction with shell elements. The selected strength point should be conservative with respect to these failure modes. In tension, the penalty for modeling with HAZ-only properties seems higher than for compression, with reductions of 15-30% for 5xxx-series panels, and up to 40% for the all 6xxx-series panels. It is clear that the prevention of rupture in the HAZ is a significant limit state and must be avoided; however, the penalty for an all-HAZ model seems prohibitive. Extensive strain concentration

was not seen in the FE studies, the failure strain in the combined model was often lower than that of the base model. This may be a result of stopping the FE simulation when the proof stress was reached in the HAZ, before significant plastic strains were able to build up. In bending under pressure loads, the conservatism in treating the structure as all-HAZ was smaller, ranging from 10% for the all 5xxx-series panel to 25% for the 6xxx-series panel. This smaller difference is not surprising, in bending, the stiffener flange was placed in tension, while the HAZ regions in the plate and at the plate-stiffener joint were placed in compression. Given the geometry of the stiffened panel, the bending neutral axis is closer to the plate than the stiffener flange. Thus, the stiffener flange will yield well before the plate when the HAZ is not considered. This offset helped reduce the impact of the HAZ in the panels studied. For both tension and bending cases, the approach of reducing the strength of 5xxx-series alloys to 90% of the base metal strength proved fairly accurate.

In summary, based on the literature review and simulations run, the following conclusions and suggestion for future work seem justified:

1. Modeling aluminum structures as all-HAZ material is overly conservative and will result in a substantial weight penalty. Thus, the marine community is advised that developing HAZ-specific strength formulations to remove this penalty is essential.
2. The generally good agreement between the simplified methods studied and the FE results suggests that it is possible to develop reasonable HAZ-specific strength models. Furthermore, reducing the material strength by 10% appears to be a good first step for including conventional HAZ in 5xxx-series alloy structures. On the other hand, simplified methods based on ratios of average failure stresses to HAZ proof stresses as well as associated stiffness were inconclusive.
3. HAZ impacts 6xxx-series are generally larger than that of 5xxx-series alloys.
4. With existing commercial FE codes, it is not straightforward to model extensive strain localization and material failure with the types of shell-element models used in the marine field. This significantly impacts the ability of the structural naval architect to model strain localization for tensile and bending load cases. Given previous literature

on the subject, there is reason to be concerned about decrease in energy absorption and global-strain-to-failure in HAZ-impacted structures. Practical design approaches to quantify these effects are needed.

5. Further analysis of the all-6xxx series panels would be beneficial to separate out the impact of alloy type and HAZ location on the large reductions in strength seen for these panels. Furthermore, in extrusion design, it is possible to locate welds at other locations on the plate. The best location for such welds would be an interesting area of study, including any impact on the extrusions process by having an unbalanced die.

9 REFERENCES

- Aalberg, A., M. Langseth, and P. K. Larsen. 2001. Stiffened aluminium panels subjected to axial compression. *Thin-Walled Structures* 39, no. 10 (October): 861-885. doi:10.1016/S0263-8231(01)00021-0.
- Abildgaard, P.M., P.W. Hansen, and B.C. Simonsen. 2001. Ultimate Strength of Welded Aluminium Structures . In *HIPER 2001*, 4-18. Hamburg, Germany.
- ABS. 2007. Guide for Building and Classing High-Speed Naval Craft. American Bureau of Shipping, January.
- Aluminum Association. 2005. *Aluminum Design Manual*. Arlington, Virginia: The Aluminum Association, June.
- AWS. 2008. *Structural Welding Code - Aluminum*. American Welding Society.
- CEN. 2007. Eurocode 9: *Design of aluminium structures - Part 1-1: General structural rules*. European Committee for Standardization (CEN).
- Chan, T.K., and R.F.D. Porter Goff . 2000. Welded aluminium alloy connections: a simplified plastic model. *Proc. Instn. Civ. Engrs. Structures and Buildings* 140 (May): 161-168.
- Clarke, J.D., and J.W. Swan. 1985. *Interframe Buckling of Aluminium Alloy Stiffened Plating*. Admiralty Research Establishment Dunfermline Report AMTE(S) R85104, October.
- Clarke, J.D. 1987. Buckling of Aluminium Alloy Stiffened Plate Ship Structure. In *Aluminium Structures: Advances, Design, and Construction. Proceedings of International Conference on Steel and Aluminium Structures*. Cardiff: Elsevier Applied Science.
- Collette, M.D. 2007. *Impact of Fusion Welds on the Ultimate Strength of Aluminum Structures*. In PRADS 2007. Houston, Texas, October 30.
- Collette, M.D., X. Wang, J. Li, J. Walters, and T. Yen, 2008. *Ultimate Strength and Optimization of Aluminum Extrusions*. SSC-454. Washington, DC: Ship Structure Committee, October.
- DNV. 2009. *Rules of Classification of High Speed, Light Craft and Naval Surface Craft*. Det Norske Veritas, January. Revision through February 2009 included.
- EAA. 2009. Talat - Home Page. European Aluminium Association. <http://www.eaa.net/eea/education/TALAT/index.htm>. Accessed May 12, 2009

- Edlund, Stefan. 2000. *Buckling of T-section beam-columns in aluminium with or without transverse welds*. PhD, KTH, Department of Structural Engineering.
- European Commission. 2008. Eurocodes: Building the future - The European Commission website on the Eurocodes. <http://eurocodes.jrc.ec.europa.eu/showpage.php?id=332>. Accessed May 12, 2009.
- Faulkner, D. J. Adamchak, G. Snyder, and M. Vetter. 1973. "Synthesis of Welded Grillages to Withstand Compression and Normal Loads," *Computers & Structures*, 3, pp. 221-246.
- Gordo, J. and C. Guedes Soares, C. 1993. "Approximate Load Shortening Curves for Stiffened Plate Under Uni-axial Compression". *Proceedings of the 5th International Conference on the Structural Integrity of Offshore Structures*. Glasgow, UK: pp. 189-211.
- Faulkner, D. 1975. A. Review of Effective Plating for Use in the Analysis of Stiffened Plating in Bending and Compression. *Journal of Ship Research* 19, no. 1 (March): 1-17.
- Hill, H.N., J.W. Clark, and A.M. Brungraber. 1960. Design of Welded Aluminum Structures. *Journal of the Structural Division, Proceedings of the ASCE* 86, no. ST6 (June): 101-124.
- Höglund, Torsten. 2008. Strength and stability of aluminium members according to EN 1999-1-1 – Eurocode 9 presented at the Eurocodes: Background and applications workshop, February, Brussels.
http://eurocodes.jrc.ec.europa.eu/doc/WS2008/EN1999_5_Hoglund.pdf.
- Hopperstad, O. S., M. Langseth, and L. Hanssen. 1997. Ultimate compressive strength of plate elements in aluminium: Correlation of finite element analyses and tests. *Thin-Walled Structures* 29, no. 1-4: 31-46. doi:10.1016/S0263-8231(97)00013-X.
- Hopperstad, O.S., M. Langseth, and T. Tryland. 1999. Ultimate Strength of Aluminum Alloy Outstands in Compression: Experiments and Simplified Analysis. *Thin-Walled Structures*, 43, pp. 279-295.
- Hval, M., R.H. Johnsen, and C. Thaulow. 1995. Strength and Deformation Properties of Welded Aluminium Structures With Reference to Local Design and Material Properties. In *Proceedings of the 6th International Conference on Aluminum Welding (INALCO)*, 167-182.
- IACS. 2005. *Unified Requirement W26: Requirements for Welding Consumables for Aluminium Alloys Rev. 1*. IACS, June.
- IACS. 2006. *Unified Requirement W25: Aluminium Alloys for Hull Construction and Marine Structure Rev. 3*. IACS, May.

- Kissell, J, and R. Ferry. 2002. *Aluminum structures: a guide to their specifications and design*. 2nd ed. New York: Wiley.
- Kristensen, Odd. 2001. *Ultimate Capacity of Aluminium Plates under Multiple Loads, Considering HAZ Properties*. PhD, Norwegian University of Science and Technology.
- Matusiak, M., and P. K. Larsen. 1998. Strength and Ductility of Welded Connections in Aluminium Alloys. In *Joints in Aluminium - INALCO 98*, 299-310. Cambridge.
- Matusiak, M. 1999. *Strength and Ductility of Welded Structures in Aluminium Alloys*. PhD Thesis, Norwegian University of Science and Technology.
- Mazzolani, Federico. 1995. *Aluminium alloy structures*. 2nd ed. London New York: E & FN Spon.
- Moen, L.A., O. S. Hopperstad, and M. Langseth. 1999. Rotational Capacity of Aluminum Beams under Moment Gradient. I: Experiments. *Journal of Structural Engineering* 125, no. 8 (August): 910-920.
- Mofflin, David. 1983. *Plate Buckling in Steel and Aluminium*. PhD Thesis, Trinity College, University of Cambridge, August.
- Nelson, F.G., and F.M. Howell. 1952. The Strength and Ductility of Welds in Aluminum Alloy Plate. *Welding Journal Research Supplement* (September): 397s-402s.
- Övreas, L, C. Thaulow, and M. Hval. 1992. Effect of Geometry and Size on the Mechanical Properties of AlMgSi1 Weldments. In *Proceedings of the 5th International Conference on Aluminum Welding (INALCO)*, 10.1.1-10.1.8.
- Paik, Jeom Kee, and Alexandre Duran. 2004. Ultimate Strength of Aluminum Plates and Stiffened Panels for Marine Applications. *Marine Technology* 41, no. 3 (July): 108-121.
- Paik, J. K., Hughes, O. F., Hess, P. E. , and Renaud, C., 2005 “ Ultimate Limit State Design Technology for Aluminum Multi-Hull Ship Structures”, SNAME Transactions, 2005.
- Paik, Jeom Kee, Anil Kumar Thayamballi, J.K. Ryu, J.H. Jang, J.K. Seo, S.W. Park, S.K. Soe, C. Renaud, and N.I. Kim. 2008. *Mechanical Collapse Testing on Aluminum Stiffened Panels for Marine Applications*. SSC-451. Washington, DC: Ship Structure Committee, February.
- Paik, Jeom Kee. 2009. *Buckling Collapse Testing of Friction Stir Welded Aluminum Stiffened Plate Structures*. Working Final Draft SR-1454. Washington, DC: Ship Structure Committee, February 3.
- Rigo, P., R. Sarghiuta, S. Estefen, E. Lehmann, S. C. Otelea, I. Pasqualino, B. C. Simonsen, Z. Wan, and T. Yao. 2003. Sensitivity analysis on ultimate strength of aluminium stiffened

panels. *Marine Structures* 16, no. 6 (August): 437-468.
doi:10.1016/j.marstruc.2003.09.002.

- Rigo, P., R. Sarghiuta, S. C. Otelea, I. Pasqualino, Z. Wan, T. Yao, C. Toderan, and T. Richir. 2004. Ultimate Strength of Aluminium Stiffened Panels: Sensitivity Analysis. In *PRADS 2004*. October.
- Satoh, K. and Toyoda, M. 1970. Static Strength of Welded Plates Including Soft Interlayer under Tension across a Weld Line. *Transactions of the Japan Welding Society*, 1, No. 2: 10-17.
- Scott, M.H., and M.F. Gittos. 1983. Tensile and Toughness Properties of Arc-Welded 5083 and 6082 Aluminum Alloys. *Welding Journal Research Supplement*, September: 243s-252s.
- Sielski, R. 2008. *Aluminum Marine Structure Design and Fabrication Guide*. Washington, DC: Ship Structure Committee, February.
- Stowell, E.Z. 1948. *A Unified Theory of Plastic Buckling of Columns and Plates*. NACA Technical Note 1556.
- Wang, Xiaozhi, Haihong Sun, Akira Akiyama, and Aiping Du. 2005. Buckling and Ultimate Strength of Aluminum Plates and Stiffened Panels in Marine Structures. In *The Fifth International Forum on Aluminum Ships*. Tokyo, Japan, October.
- Wang, Ting. 2006. Modelling of Welded Thin-Walled Aluminium Structures. PhD, Norwegian University of Science and Technology.
- Wang, T., O.S. Hopperstad, P.K. Larsen, and O.-G. Lademo. 2006. Evaluation of a finite element modelling approach for welded aluminium structures. *Computers & Structures* 84, no. 29-30 (November): 2016-2032. doi:10.1016/j.compstruc.2006.08.011.
- Wang, T., O.S. Hopperstad, O.-G. Lademo, and P.K. Larsen. 2007a. Finite element modelling of welded aluminium members subjected to four-point bending. *Thin-Walled Structures* 45, no. 3 (March): 307-320. doi:10.1016/j.tws.2007.02.009.
- Wang, T., O.S. Hopperstad, O.-G. Lademo, and P.K. Larsen. 2007b. Finite element analysis of welded beam-to-column joints in aluminium alloy EN AW 6082 T6. *Finite Elements in Analysis and Design* 44, no. 1-2 (December): 1-16. doi:10.1016/j.finel.2007.08.010.
- Xiao, Yugang, and Craig Menzemer. 2003. Ultimate Compressive Strength of Aluminum Plate Elements. *Journal of Structural Engineering* 129, no. 11 (November): 1441-1447.
- Zha, Yufeng, and Torgeir Moan. 2001. Ultimate strength of stiffened aluminium panels with predominantly torsional failure modes. *Thin-Walled Structures* 39, no. 8 (August): 631-648. doi:10.1016/S0263-8231(01)00027-1.

- Zhang, Z. L., J. Odegard, O.R. Mhyr, and H. Fjaer. 2001. From microstructure to deformation and fracture behaviour of aluminium welded joints - a holistic modelling approach. *Computational Materials Science* 21: 429-435.
- Zheng, L., D. Petry, H. Rapp, and T. Wierzbicki. 2009. Characterization of material and fracture of AA6061 butt weld. *Thin-Walled Structures* 47, no. 4 (April): 431-441. doi:10.1016/j.tws.2008.08.008.
- Zhu, Ji-Hua, and Ben Young. 2006a. Aluminum alloy tubular columns--Part I: Finite element modeling and test verification. *Thin-Walled Structures* 44, no. 9 (September): 961-968. doi:10.1016/j.tws.2006.08.011.
- Zhu, Ji-Hua, and Ben Young. 2006b. Aluminum alloy tubular columns--Part II: Parametric study and design using direct strength method. *Thin-Walled Structures* 44, no. 9 (September): 969-985. doi:10.1016/j.tws.2006.08.012.
- Zhu, Ji-Hua, and Ben Young. 2007. Effects of transverse welds on aluminum alloy columns. *Thin-Walled Structures* 45, no. 3 (March): 321-329. doi:10.1016/j.tws.2007.02.008.

APPENDIX A

Panel Geometry Selection for FEA

1: Introduction

This sheet performs a parameter study to decide potential panel designs for the SR-1460 finite element study. It is divided into the following sections:

1: Introduction

2: Target Slenderness Ranges

3: Panel Formulas

4: Proposed Panels

2: Target Slenderness Ranges

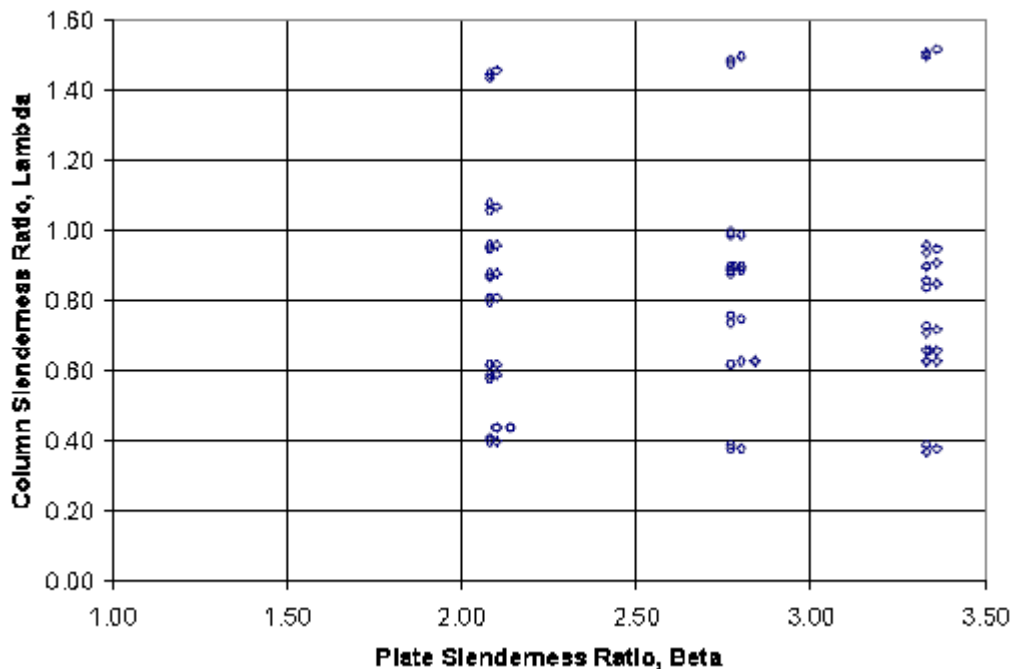
The panel slenderness will be rated in terms of both the plate and column slenderness ratios, and λ respectively.

$$\beta(b, t, \sigma_{0.2}, E) := \frac{b}{t} \cdot \sqrt{\frac{\sigma_{0.2}}{E}}$$

$$\lambda(\text{len}, r, \sigma_{0.2}, E) := \frac{\text{len}}{\pi \cdot r} \cdot \sqrt{\frac{\sigma_{0.2}}{E}}$$

Where r is the radius of gyration

From Paik's SSC-451 panel test, his panels, chosen to be roughly for 80m long aluminum HSV represented the following slender ratios



It appears that plate slenderness ratios of roughly 2-3.2 and column slenderness ratios between 0.4 and 1.5 should be expected.

Panel lengths for these vessels are typically 500mm-1500mm, with stiffener spacing between 150mm and 400mm.

3: Panel Formulations

The panel gyradius can be found by:

$$r_{yy}(b, t_p, h_w, t_w, t_f, b_f) := \left\{ \begin{array}{l} \text{Area} \leftarrow b \cdot t_p + h_w \cdot t_w + t_f \cdot b_f \\ \text{Fmom} \leftarrow b \cdot t_p \cdot \frac{t_p}{2} + h_w \cdot t_w \cdot \left(t_p + \frac{h_w}{2} \right) + t_f \cdot b_f \cdot \left(t_p + h_w + \frac{t_f}{2} \right) \\ \text{NA} \leftarrow \frac{\text{Fmom}}{\text{Area}} \\ \text{Iy} \leftarrow \frac{1}{12} \cdot b \cdot t_p^3 + b \cdot t_p \cdot \left(\text{NA} - \frac{t_p}{2} \right)^2 + \frac{1}{12} \cdot h_w^3 \cdot t_w + h_w \cdot t_w \cdot \left[\text{NA} - \left(t_p + \frac{h_w}{2} \right) \right]^2 \dots \\ \quad + \frac{1}{12} \cdot t_f^3 \cdot b_f + t_f \cdot b_f \cdot \left[\text{NA} - \left(t_p + h_w + \frac{t_f}{2} \right) \right]^2 \\ r \leftarrow \sqrt{\frac{\text{Iy}}{\text{Area}}} \\ r \end{array} \right.$$

Paik and Duran's 2003 aluminum panel strength paper gave the following formula for the strength of panels, implicitly assuming "normal" aluminum welds, where the strength is the % of the base material proof stress

$$\sigma_{\text{Fail}}(\lambda, \beta) := \left\{ \begin{array}{l} \sigma_{\text{temp}} \leftarrow \frac{1}{\sqrt{1.148 + 1.180\lambda^2 + 0.096\beta^2 - 0.052\lambda^2 \cdot \beta^2 + 1.651\lambda^4}} \\ \sigma_{\text{elastic_limit}} \leftarrow \frac{1}{\lambda^2} \\ \sigma_{\text{temp}} \leftarrow \sigma_{\text{elastic_limit}} \quad \text{if } \sigma_{\text{temp}} > \sigma_{\text{elastic_limit}} \\ \sigma_{\text{temp}} \end{array} \right.$$

The webs and flanges of stiffeners also need to be checked to prevent local buckling, this will be done with the ABS recommendations:

$$\min_{t_w}(h, \sigma_{0.2}, E) := \frac{h}{1.5 \cdot \sqrt{\frac{E}{\sigma_{0.2}}}} \qquad \min_{t_f}(b_f, \sigma_{0.2}, E) := \frac{b_f}{0.5 \cdot \sqrt{\frac{E}{\sigma_{0.2}}}}$$

4: Proposed Panels

During the project kick-off pre-meeting, it was decided to look at 5083 and 6082 material, which have typical compressive strengths of:

$$\sigma_{0.2_6082} := 260 \cdot \text{MPa}$$

$$\sigma_{0.2_5083} := 180 \cdot \text{MPa}$$

$$E := 70000 \cdot \text{MPa}$$

Plating

Two plate thicknesses were to be examined, 4mm and 6mm. The stiffener spacing will be selected first to give a good range of β values:

$$b := 225 \cdot \text{mm}$$

For the 5083 Plates

$$\beta_{5083_4} := \beta(b, 4 \cdot \text{mm}, \sigma_{0.2_5083}, E)$$

$$\beta_{5083_4} = 2.852$$

$$\beta_{5083_6} := \beta(b, 6 \cdot \text{mm}, \sigma_{0.2_5083}, E)$$

$$\beta_{5083_6} = 1.902$$

For the 6082 Plates

$$\beta_{6082_4} := \beta(b, 4 \cdot \text{mm}, \sigma_{0.2_6082}, E)$$

$$\beta_{6082_4} = 3.428$$

$$\beta_{6082_6} := \beta(b, 6 \cdot \text{mm}, \sigma_{0.2_6082}, E)$$

$$\beta_{6082_6} = 2.285$$

A breadth of 225mm looks to cover a good range of β

Now selecting the stiffener, both a light and heavy stiffener will be selected, choosing an overall panel length of 1000mm

$$\text{len} := 1000 \cdot \text{mm}$$

Light Stiffener

$$h_w := 60 \cdot \text{mm} \quad t_f := 6 \cdot \text{mm}$$

$$t_w := 3.0 \cdot \text{mm} \quad b_f := 30 \cdot \text{mm}$$

For the two plate thickness, we get a

$$r_{4_L} := r_{yy}(b, 4 \cdot \text{mm}, h_w, t_w, t_f, b_f)$$

$$r_{4_L} = 24.537 \text{ mm}$$

$$r_{6_L} := r_{yy}(b, 6 \cdot \text{mm}, h_w, t_w, t_f, b_f)$$

$$r_{6_L} = 22.334 \text{ mm}$$

$$\lambda_{5083_4_L} := \lambda(\text{len}, r_{4_L}, \sigma_{0.2_5083}, E)$$

$$\lambda_{5083_6_L} := \lambda(\text{len}, r_{6_L}, \sigma_{0.2_5083}, E)$$

$$\lambda_{5083_4_L} = 0.658$$

$$\lambda_{5083_6_L} = 0.723$$

Heavy Stiffener

$$\tilde{h}_w := 100 \cdot \text{mm} \quad \tilde{t}_f := 10 \cdot \text{mm}$$

$$\tilde{t}_w := 6 \cdot \text{mm} \quad \tilde{b}_f := 40 \cdot \text{mm}$$

For the two plate thickness, we get a

$$r_{4_H} := r_{yy}(b, 4 \cdot \text{mm}, \tilde{h}_w, \tilde{t}_w, \tilde{t}_f, \tilde{b}_f)$$

$$r_{4_H} = 44.865 \text{ mm}$$

$$r_{6_H} := r_{yy}(b, 6 \cdot \text{mm}, \tilde{h}_w, \tilde{t}_w, \tilde{t}_f, \tilde{b}_f)$$

Checking the required web and flange
Thickness: 6082 is the most limiting

$$\min_{t_w}(h_w, \sigma_{0.2_6082}, E) = 2.438 \text{ mm}$$

$$\min_{t_f}\left(\frac{b_f}{2}, \sigma_{0.2_6082}, E\right) = 1.828 \text{ mm}$$

All ok

$$\lambda_{6082_4_L} := \lambda(\text{len}, r_{4_L}, \sigma_{0.2_6082}, E)$$

$$\lambda_{6082_6_L} := \lambda(\text{len}, r_{6_L}, \sigma_{0.2_6082}, E)$$

$$\lambda_{6082_4_L} = 0.791$$

$$\lambda_{6082_6_L} = 0.869$$

Checking the required web and flange thickness:
6082 is the most limiting

$$\min_{t_w}(h_w, \sigma_{0.2_6082}, E) = 4.063 \text{ mm}$$

$$\min_{t_f}\left(\frac{b_f}{2}, \sigma_{0.2_6082}, E\right) = 2.438 \text{ mm}$$

All ok

$$r_{6_H} = 43.588 \text{ mm}$$

$$\lambda_{5083_4_H} := \lambda(\text{len}, r_{4_H}, \sigma_{0.2_5083}, E)$$

$$\lambda_{6082_4_H} := \lambda(\text{len}, r_{4_H}, \sigma_{0.2_6082}, E)$$

$$\lambda_{5083_6_H} := \lambda(\text{len}, r_{6_H}, \sigma_{0.2_5083}, E)$$

$$\lambda_{6082_6_H} := \lambda(\text{len}, r_{6_H}, \sigma_{0.2_6082}, E)$$

$$\lambda_{5083_4_H} = 0.36$$

$$\lambda_{6082_4_H} = 0.432$$

$$\lambda_{5083_6_H} = 0.37$$

$$\lambda_{6082_6_H} = 0.445$$

Checking the strength as a proportion of the base metal proof strength - we want the majority of the panels above 0.6 so the average stress at failure will cause yielding in the HAZ

$$\sigma_{\text{Fail}}(\lambda_{5083_4_L}, \beta_{5083_4}) = 0.624$$

$$\sigma_{\text{Fail}}(\lambda_{6082_4_L}, \beta_{6082_4}) = 0.552$$

$$\sigma_{\text{Fail}}(\lambda_{5083_4_H}, \beta_{5083_4}) = 0.698$$

$$\sigma_{\text{Fail}}(\lambda_{5083_4_H}, \beta_{6082_4}) = 0.649$$

$$\sigma_{\text{Fail}}(\lambda_{5083_6_L}, \beta_{5083_6}) = 0.637$$

$$\sigma_{\text{Fail}}(\lambda_{6082_6_L}, \beta_{6082_6}) = 0.553$$

$$\sigma_{\text{Fail}}(\lambda_{5083_6_H}, \beta_{5083_6}) = 0.776$$

$$\sigma_{\text{Fail}}(\lambda_{6082_6_H}, \beta_{6082_6}) = 0.727$$

This range looks very good. Note that the difference in strength between the light and heavy stiffeners is much more for the heavy panel than for the light panel. This may mean that the panels with 4mm plate will fail primarily in plate buckling, while those with 6mm will fail in column buckling.

Appendix B

Ultimate Strength for Compressive Lad Case

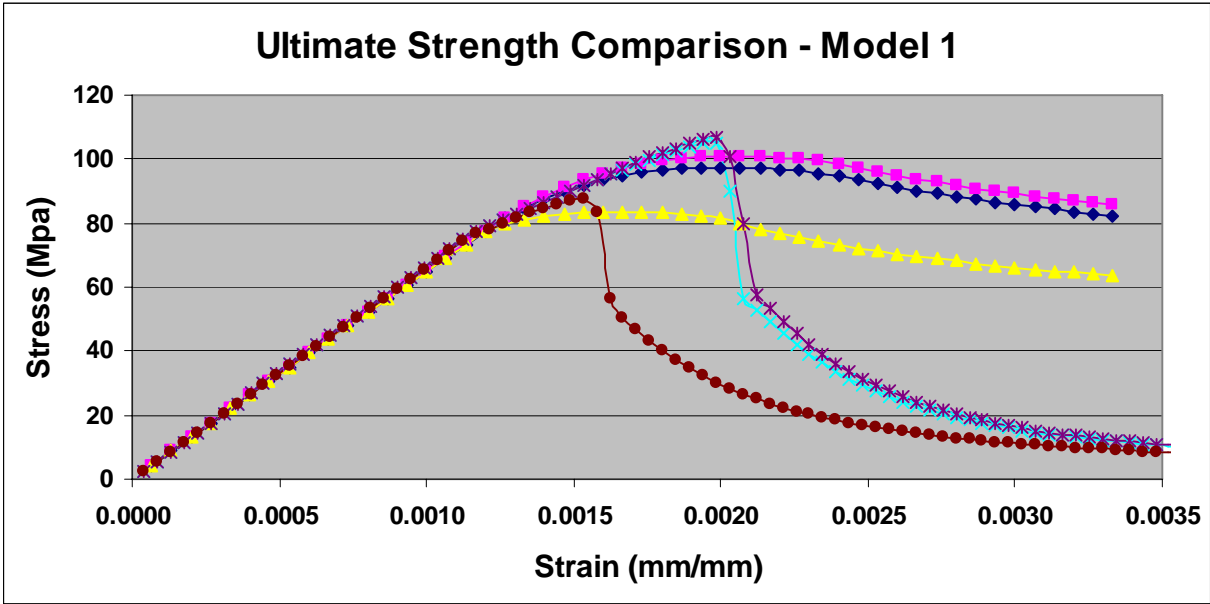


Figure B-1: Ultimate strength comparison (Model 1)

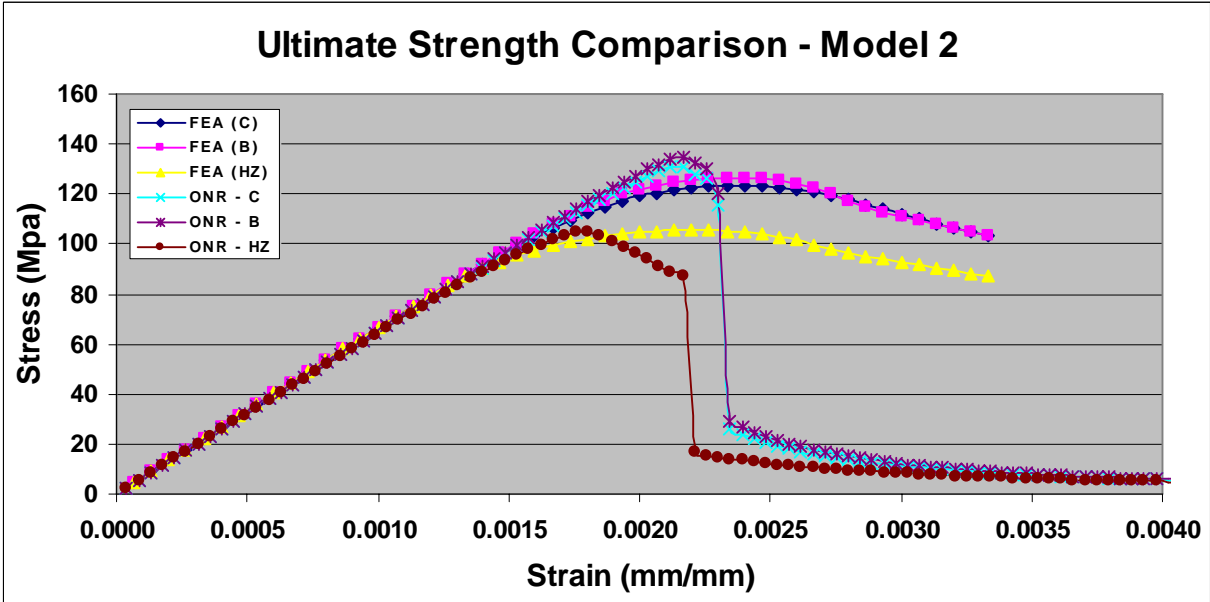


Figure B-2: Ultimate strength comparison (Model 2)

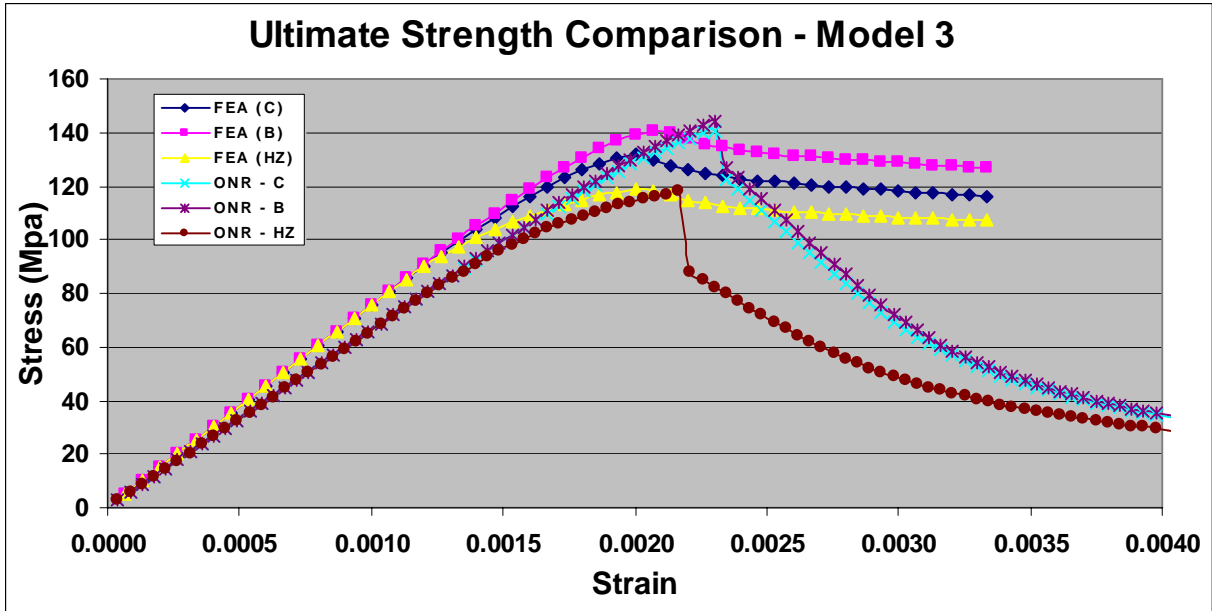


Figure B-3: Ultimate strength comparison (Model 3)

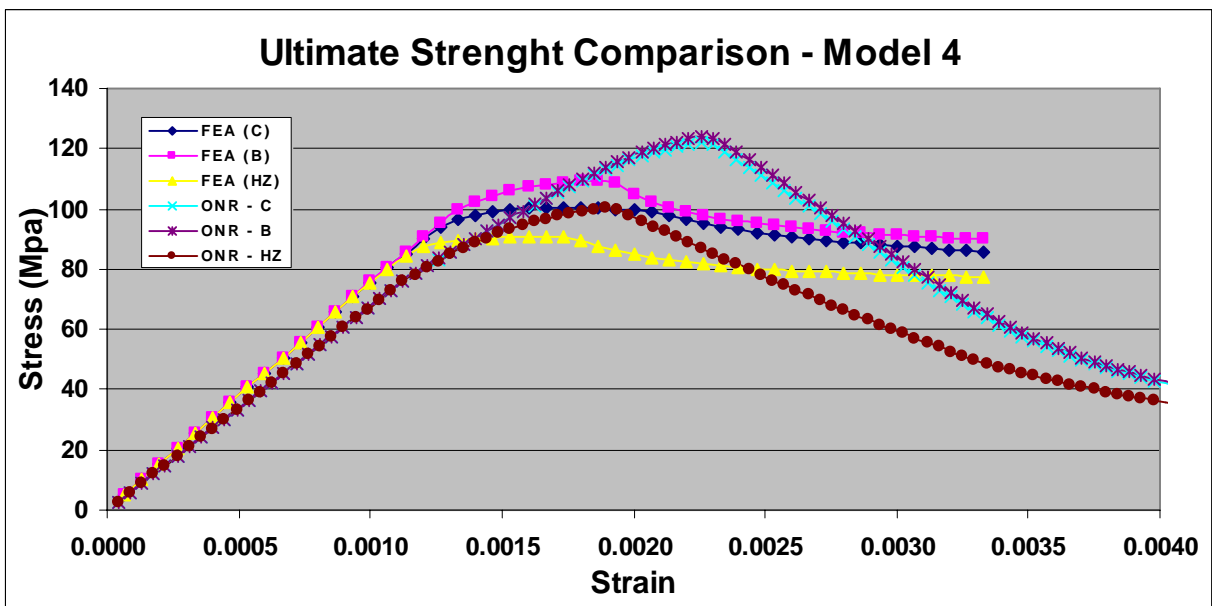


Figure B-4: Ultimate strength comparison (Model 4)

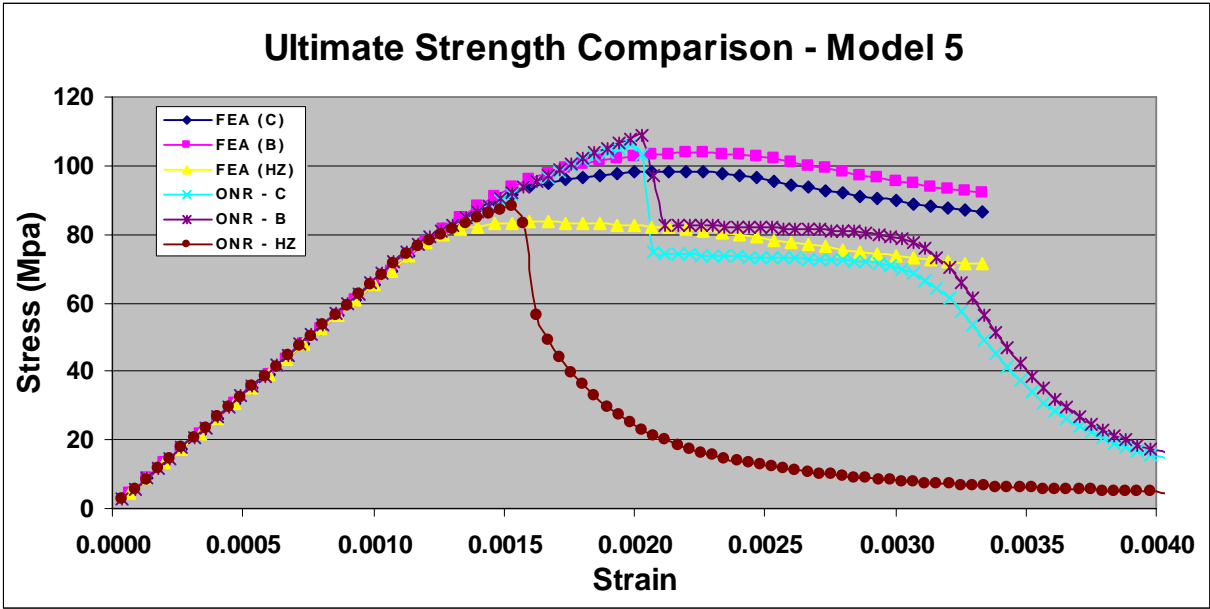


Figure B-5: Ultimate strength comparison (Model 5)

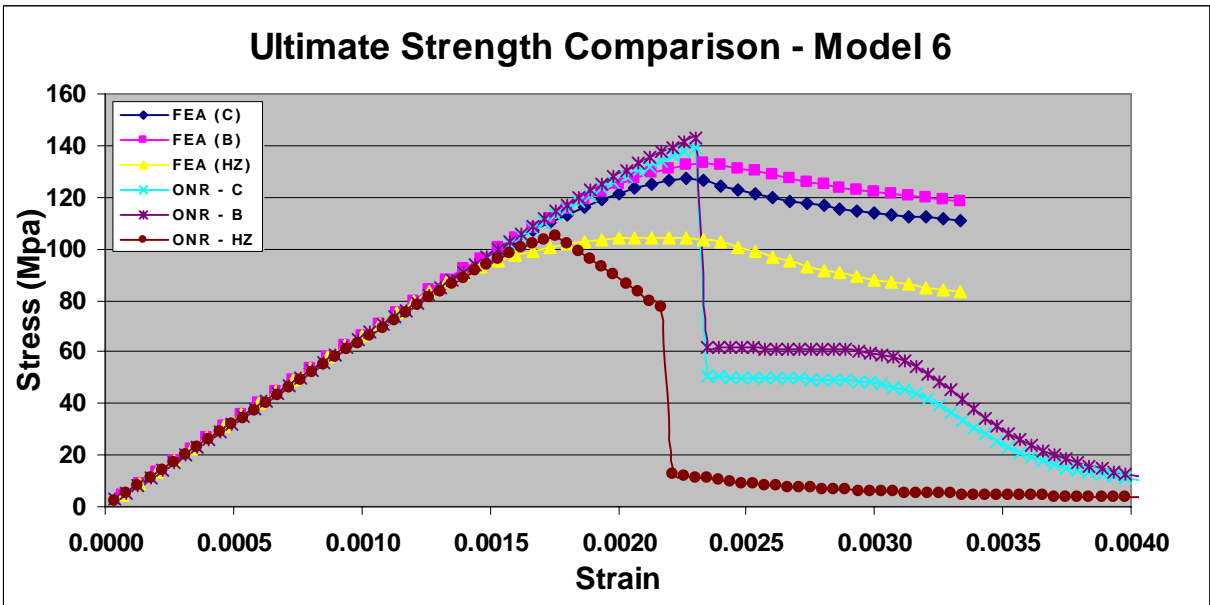


Figure B-6: Ultimate strength comparison (Model 6)

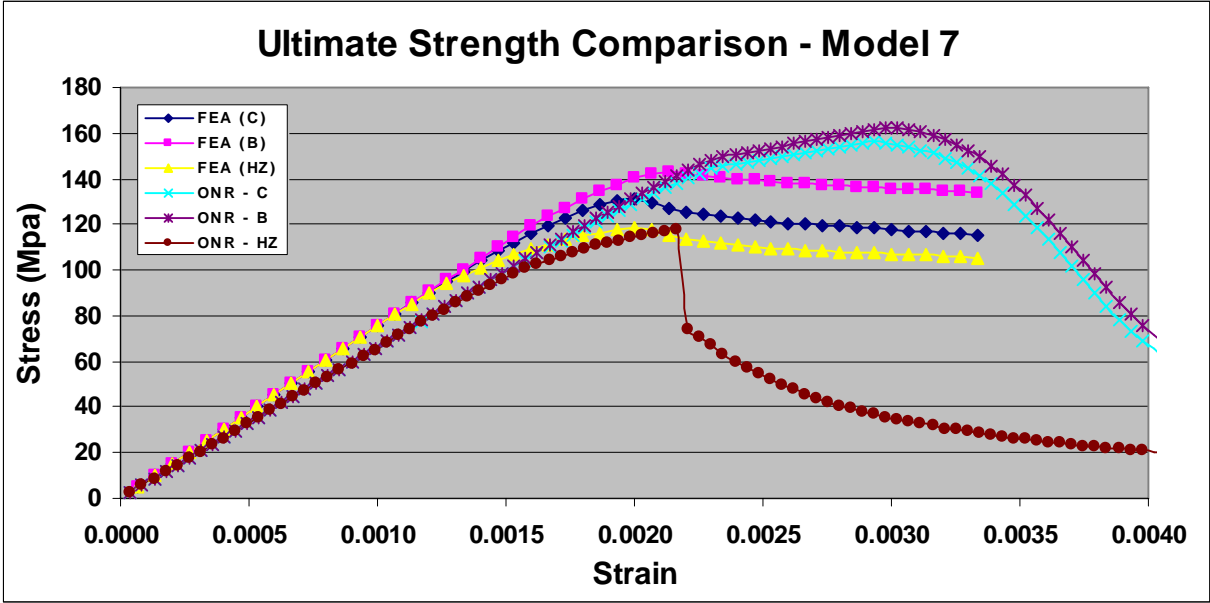


Figure B-7: Ultimate strength comparison (Model 7)

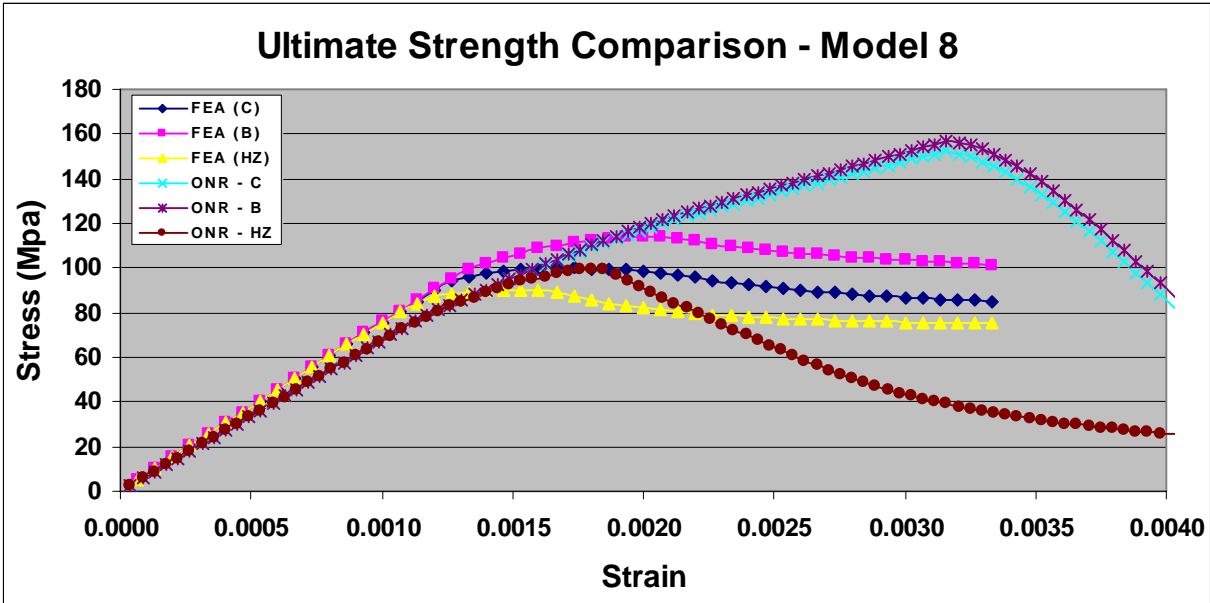


Figure B-8: Ultimate strength comparison (Model 8)

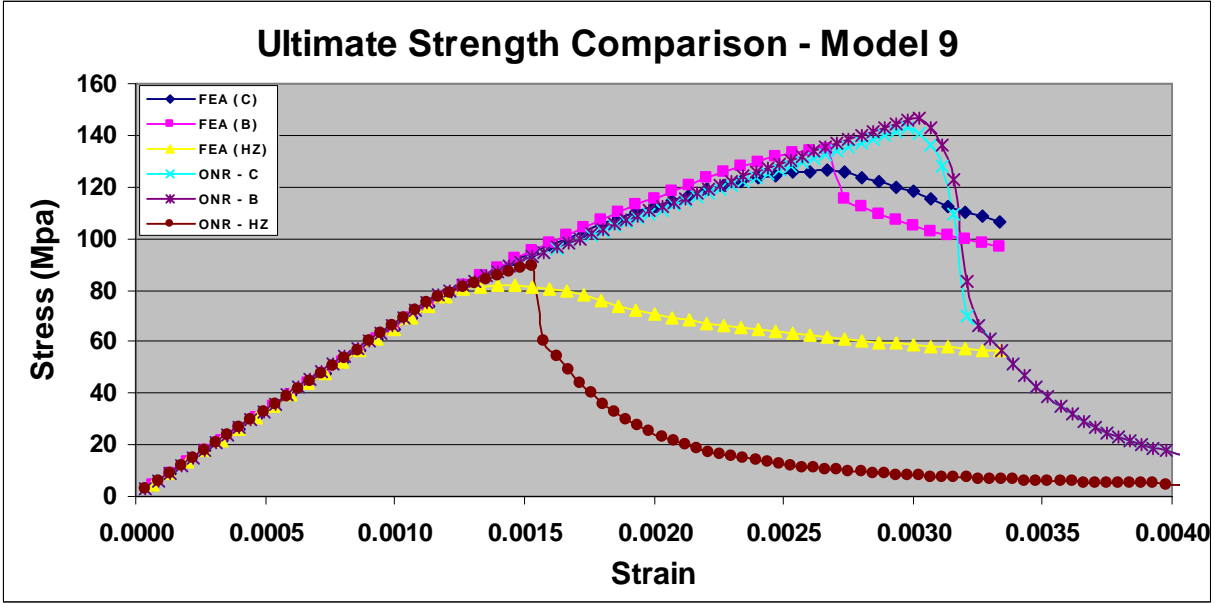


Figure B-9: Ultimate strength comparison (Model 9)

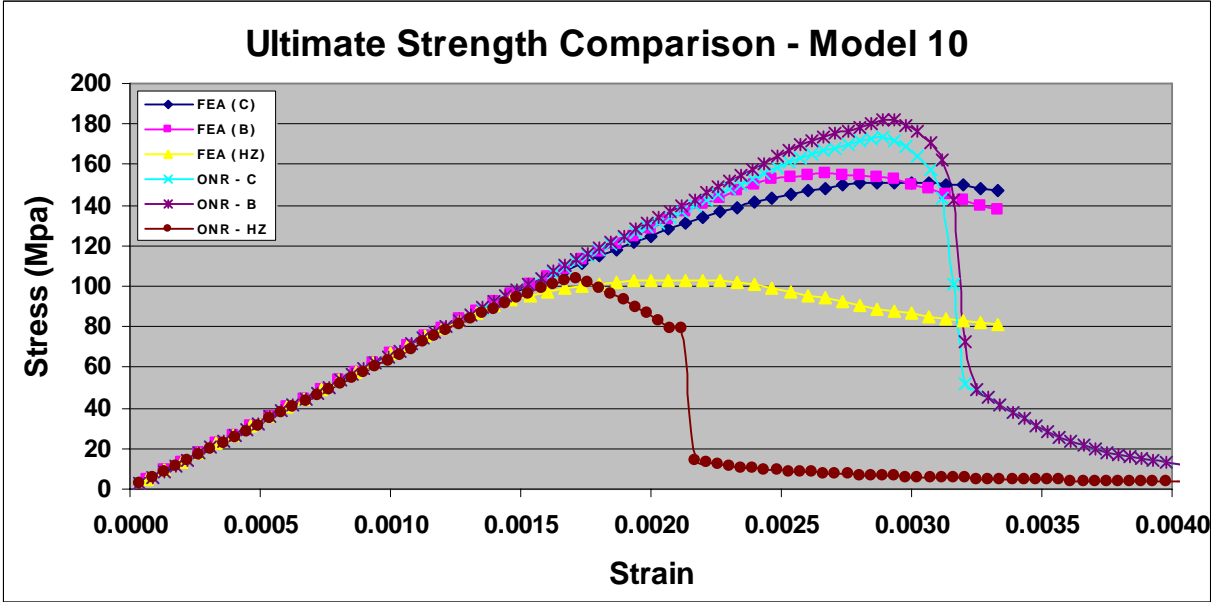


Figure B-10: Ultimate strength comparison (Model 10)

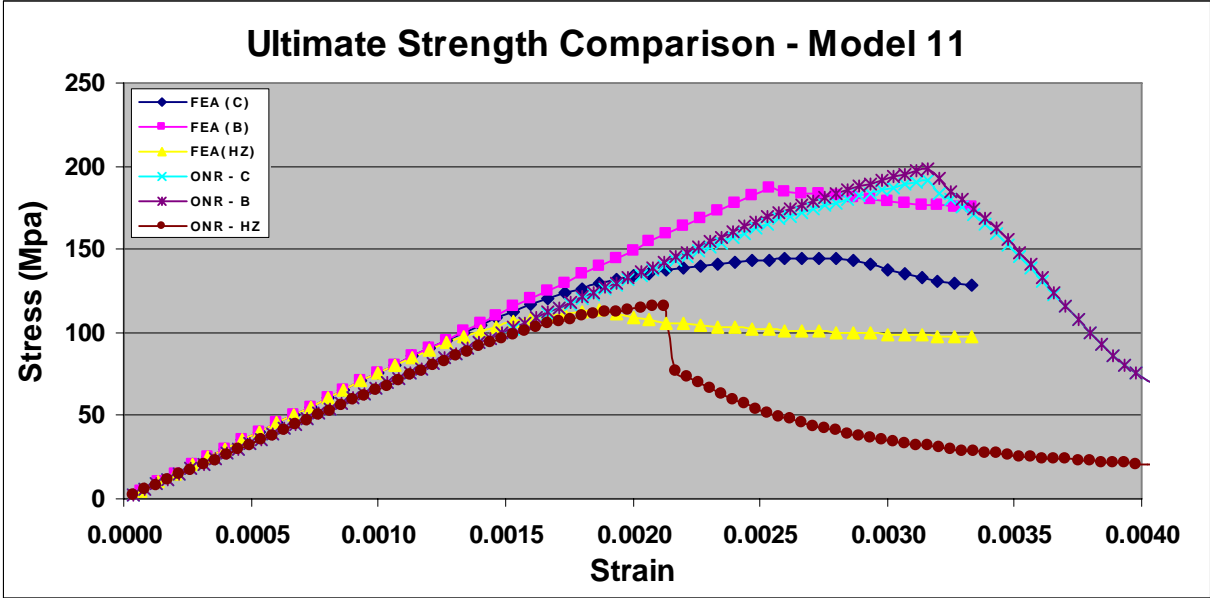


Figure B-11: Ultimate strength comparison (Model 11)

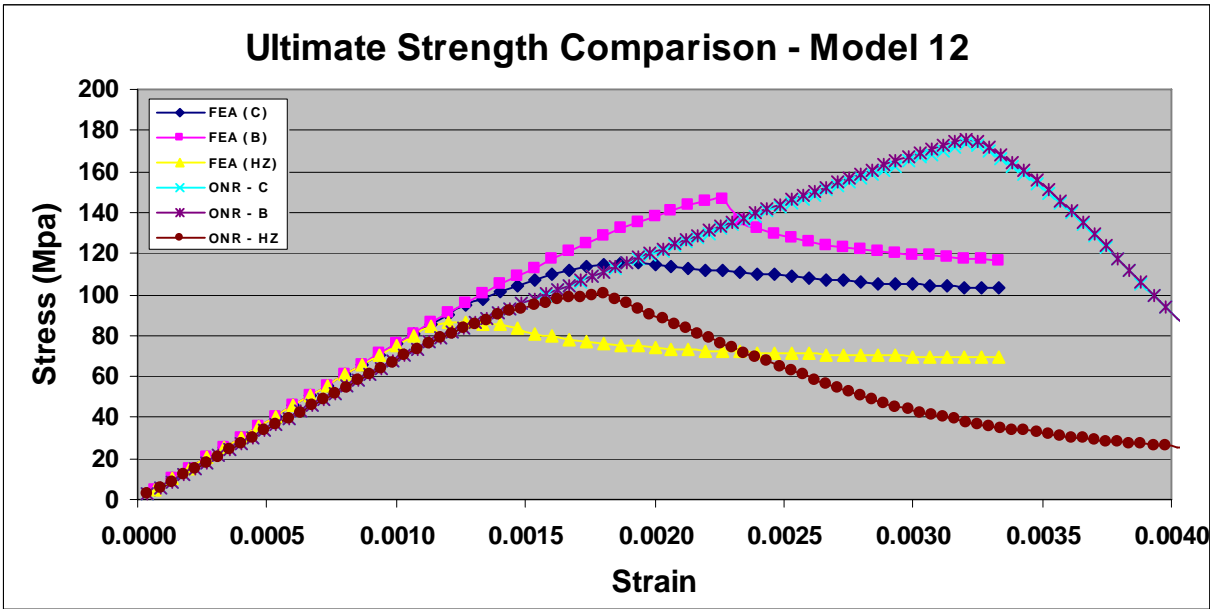


Figure B-12: Ultimate strength comparison (Model 12)

Appendix B2:

Ultimate Strength Comparisons between models with combined properties (base + HAZ) and models with only base metal properties with base metal proof stress reduced by 10%.

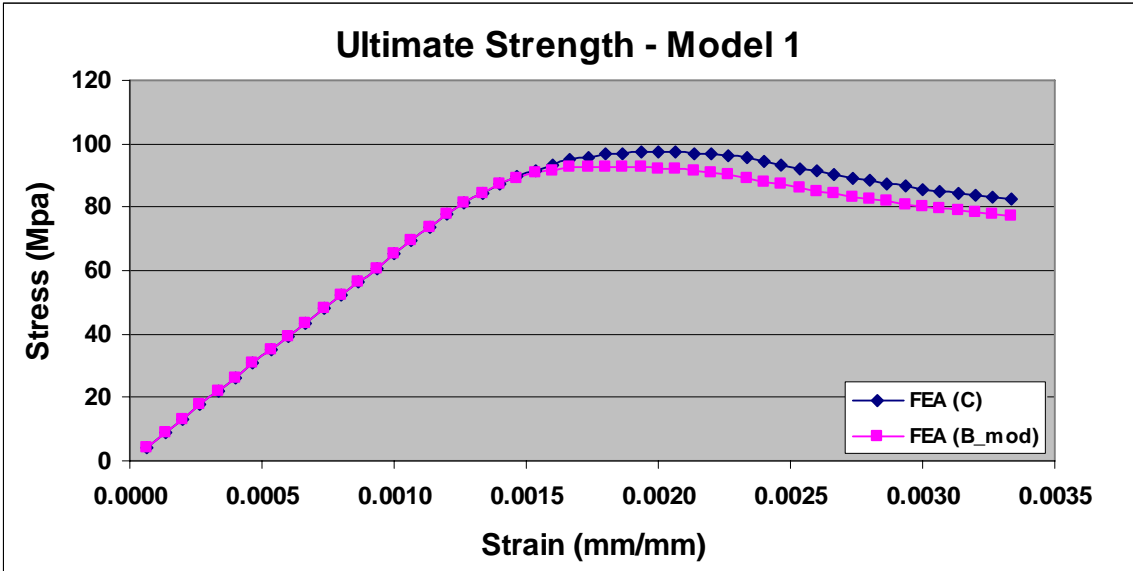


Figure B-13: Modified ultimate strength (Model 1)

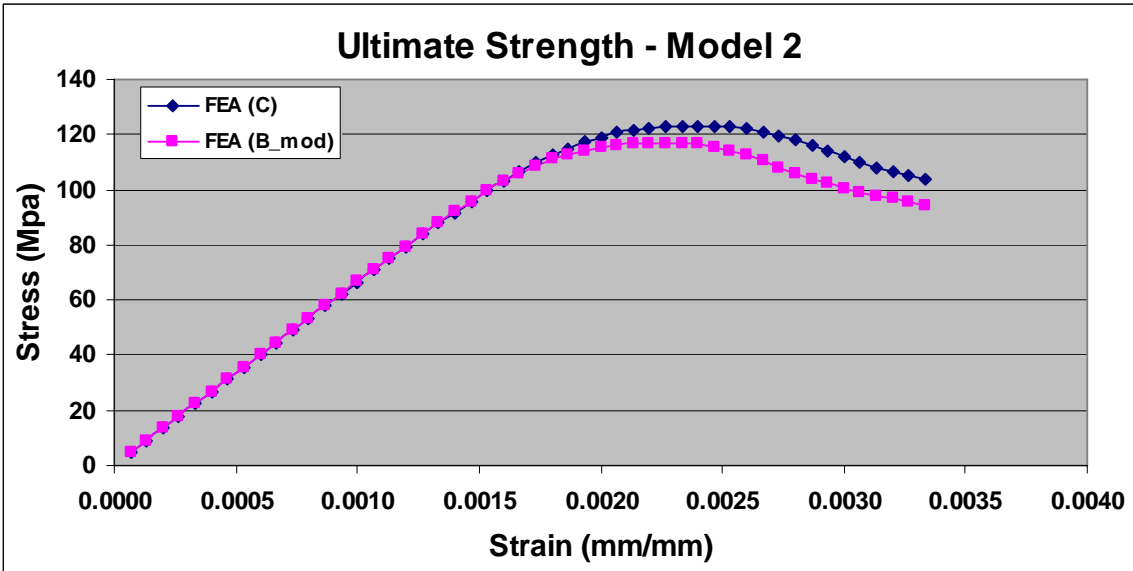


Figure B-14: Modified ultimate strength (Model 2)

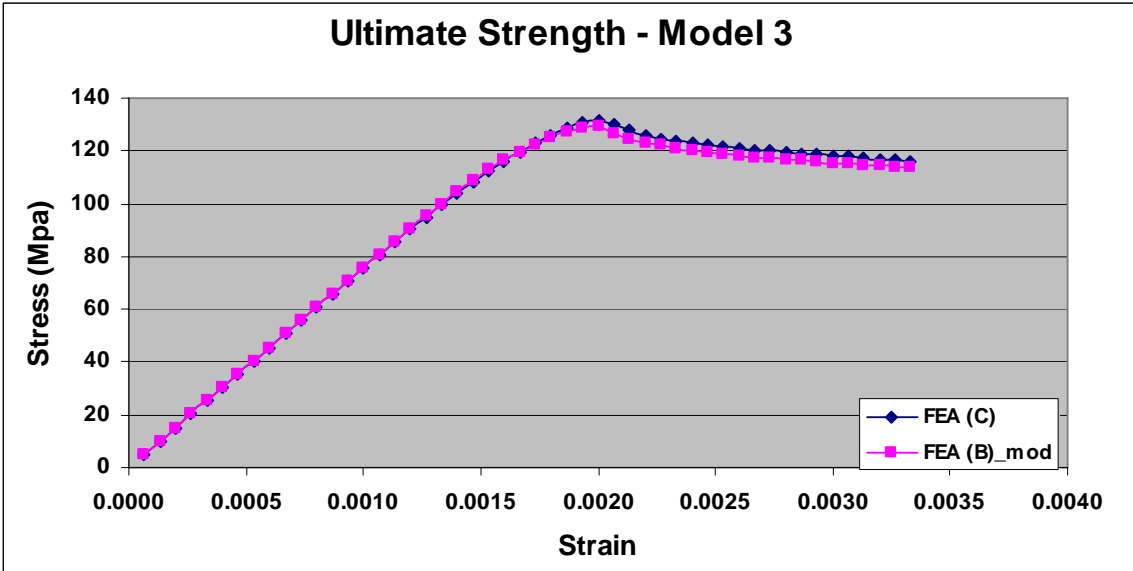


Figure B-15: Modified ultimate strength (Model 3)

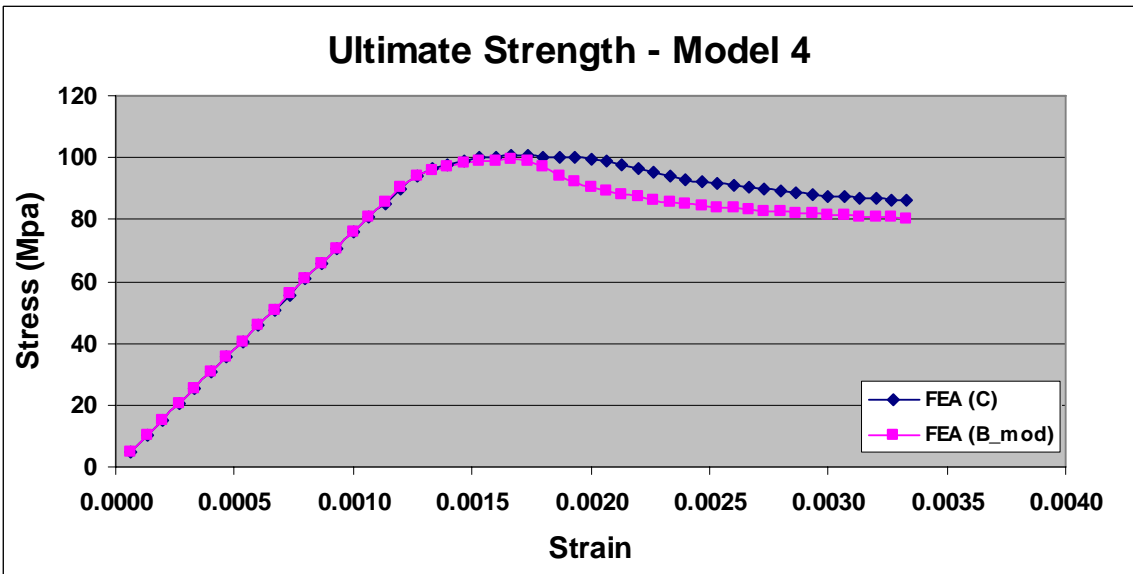


Figure B-16: Modified ultimate strength (Model 4)

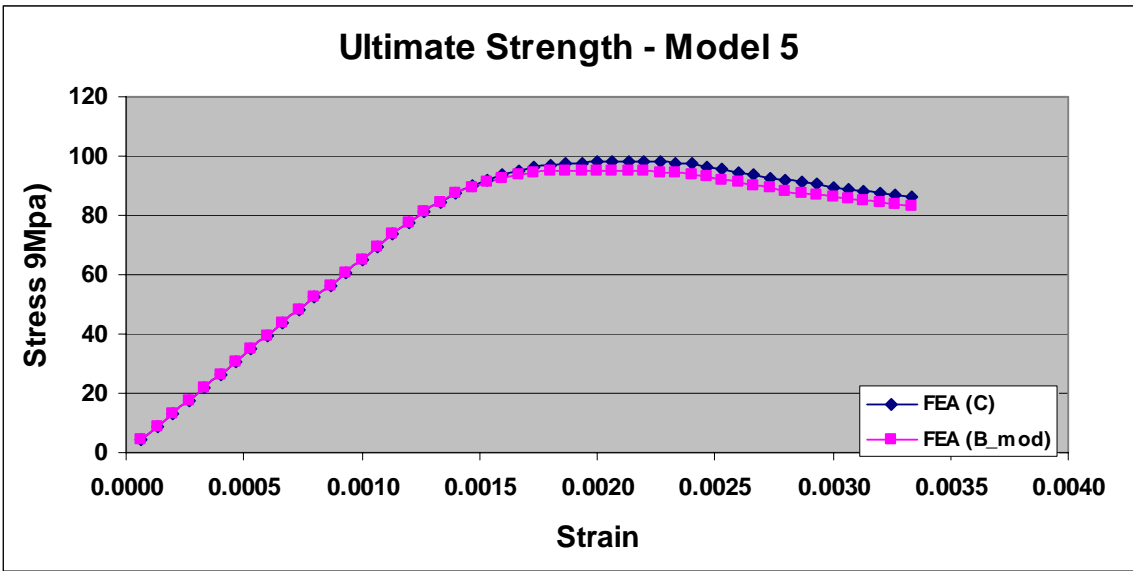


Figure B-17: Modified ultimate strength (Model 5)

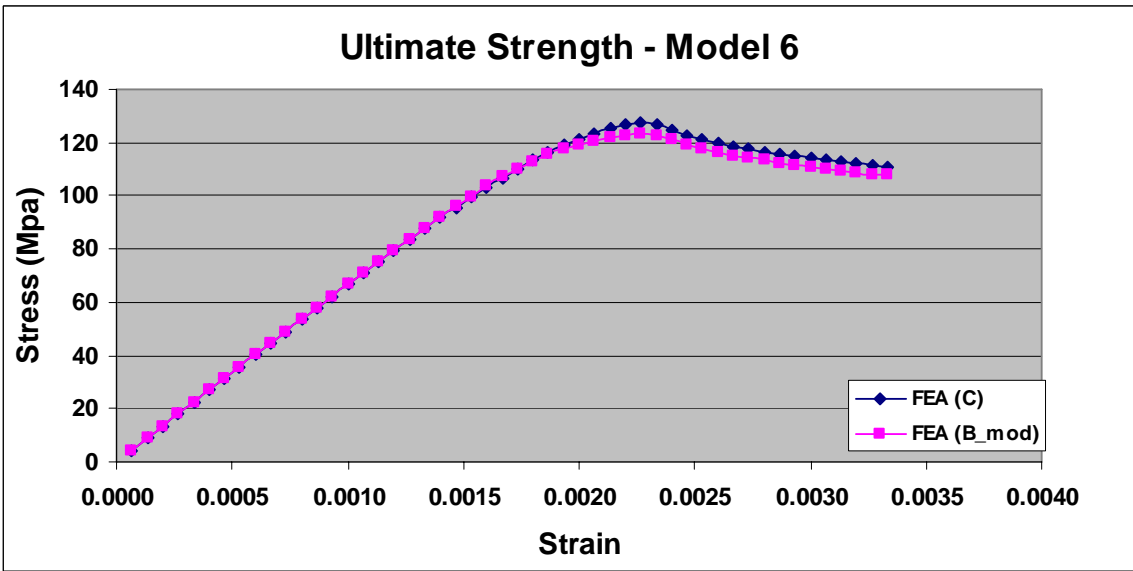


Figure B-18: Modified ultimate strength (Model 6)

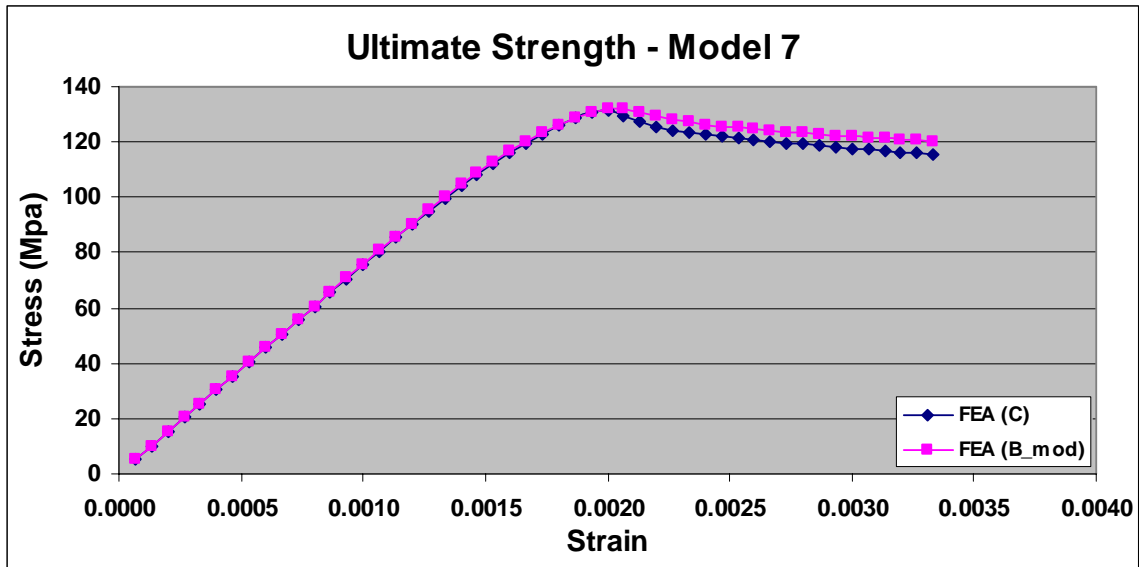


Figure B-19: Modified ultimate strength (Model 7)

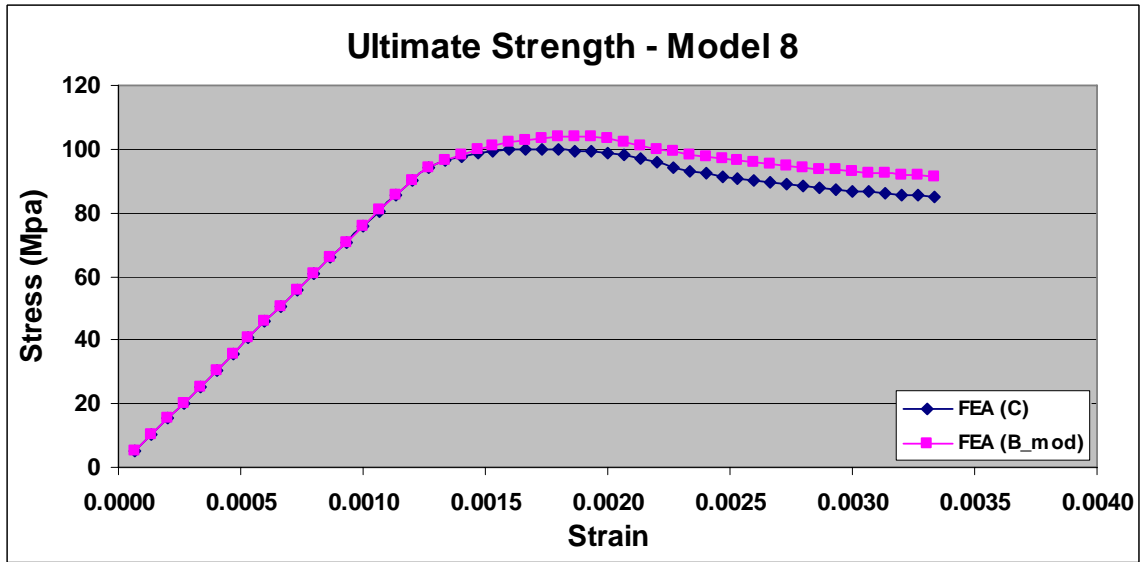


Figure B-20: Modified ultimate strength (Model 8)

APPENDIX C

Compression Load Case - FEA Stress & Deflection Plots

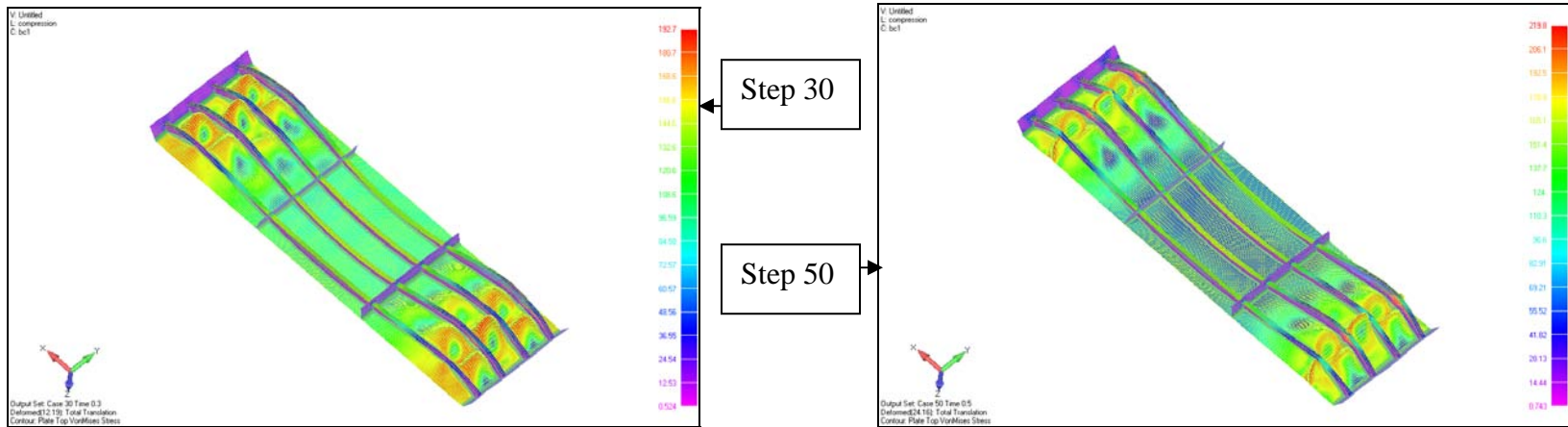


Figure C-1: Stress and Deflection Plot - Model 1- Combined (Base + HAZ)(step 30 - At Ultimate Strength)

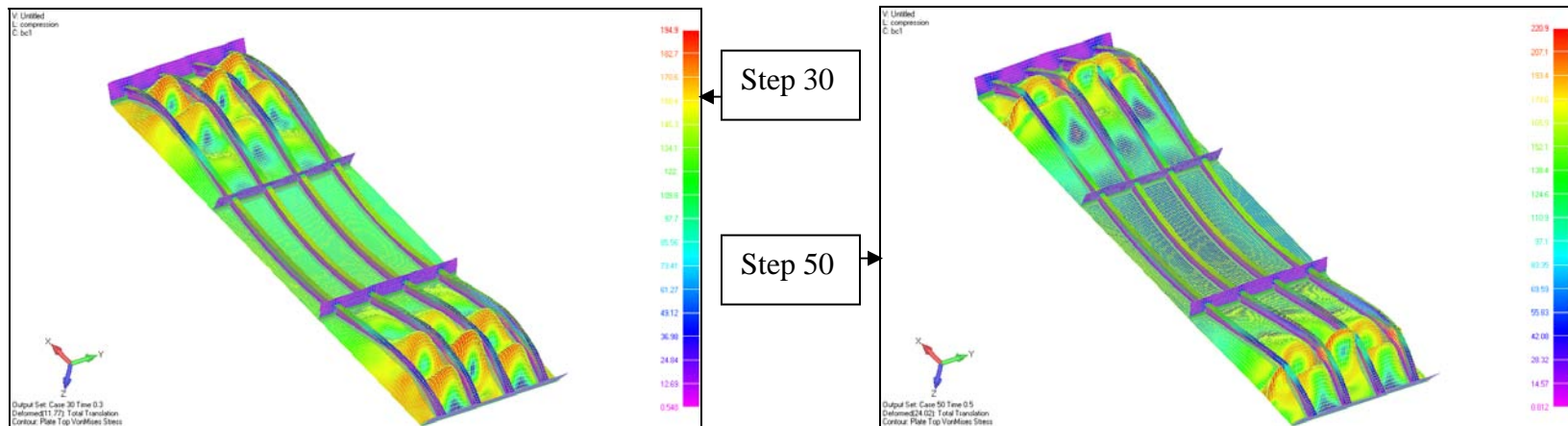


Figure C-2: Stress and Deflection Plot - Model 1- Base Metal Properties (step 30 - At Ultimate Strength)

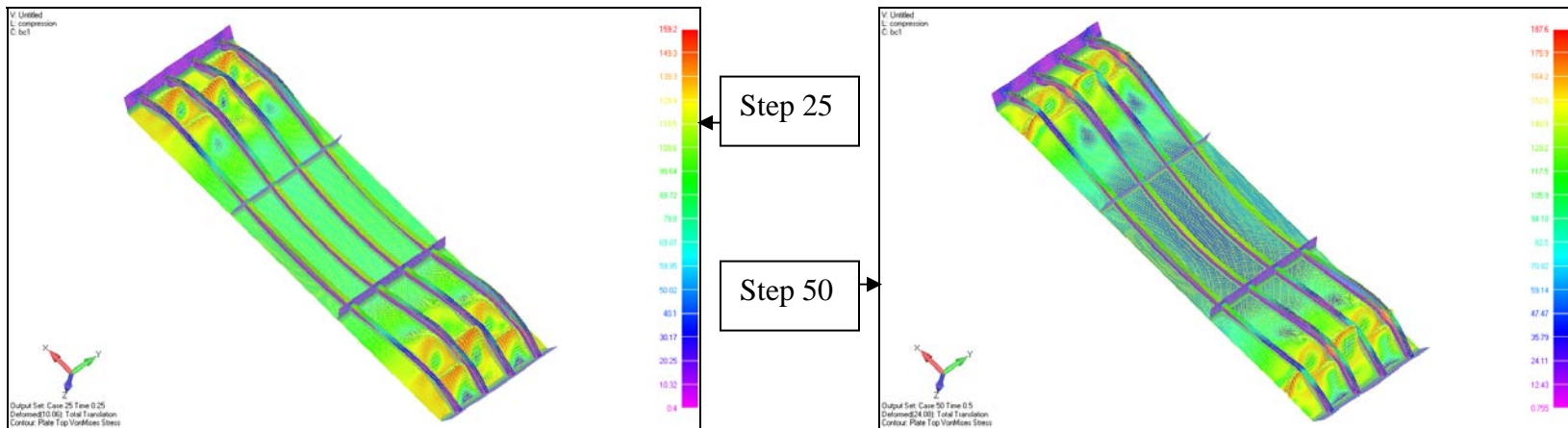


Figure C-3: Stress and Deflection Plot - Model 1- HAZ Properties (step 25 - At Ultimate Strength)

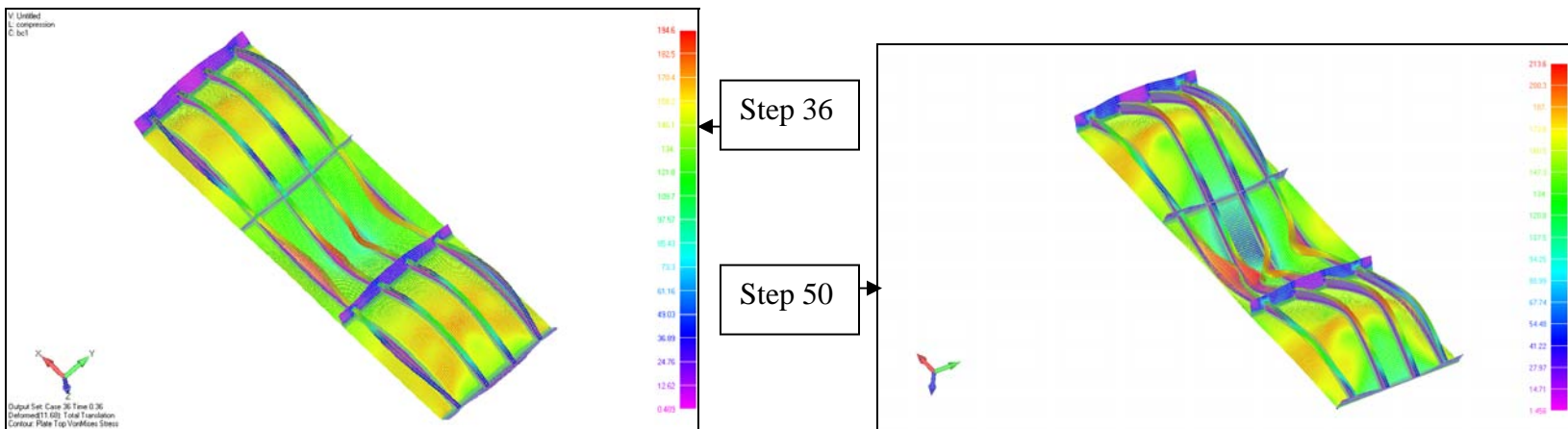


Figure C-4: Stress and Deflection Plot - Model 2- Combined (Base + HAZ)(step 36 - At Ultimate Strength)

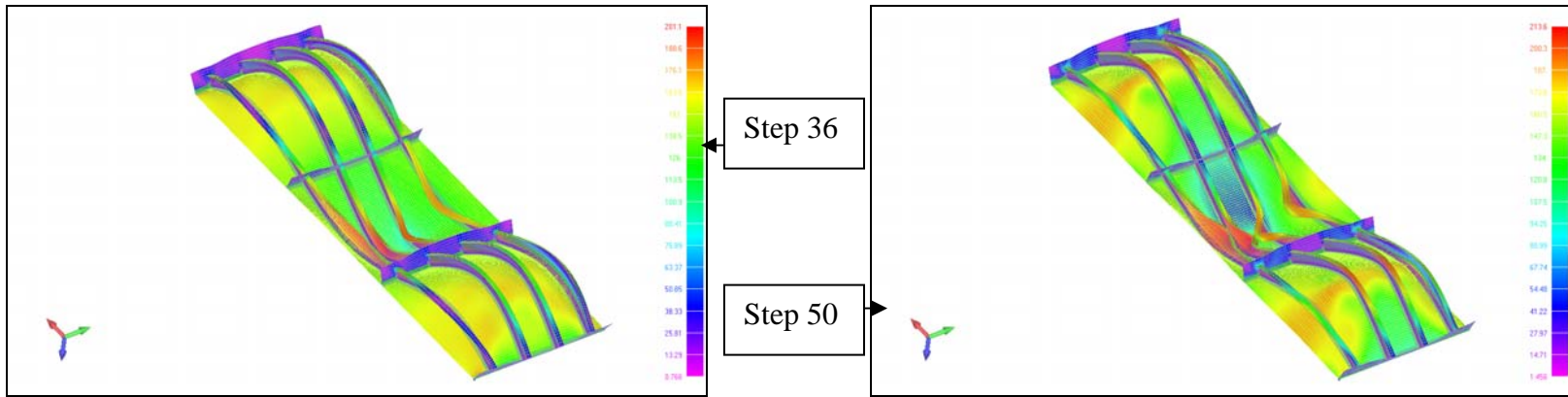


Figure C-5: Stress and Deflection Plot - Model 2- Base Metal Properties (step 36 - At Ultimate Strength)

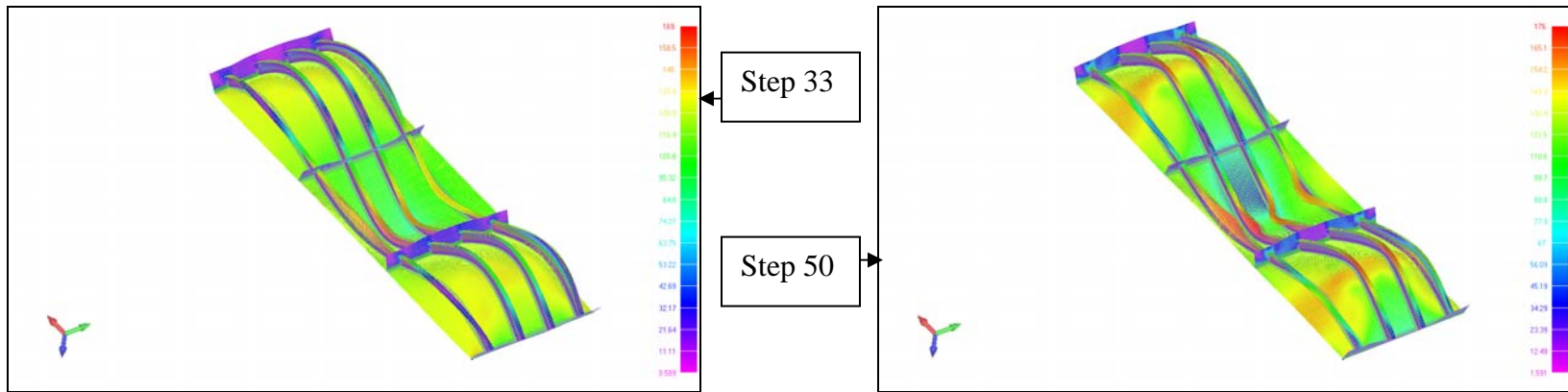


Figure C-6: Stress and Deflection Plot - Model 2- HAZ Properties (step 33 - At Ultimate Strength)

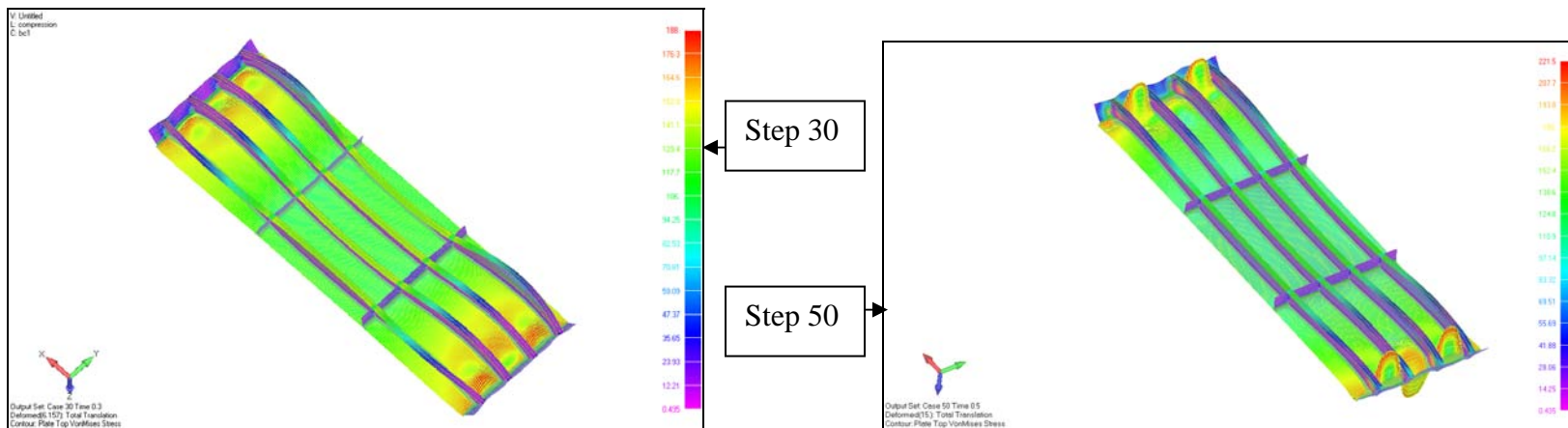


Figure C-7: Stress and Deflection Plot - Model 3- Combined (Base + HAZ)(step 30 - At Ultimate Strength)

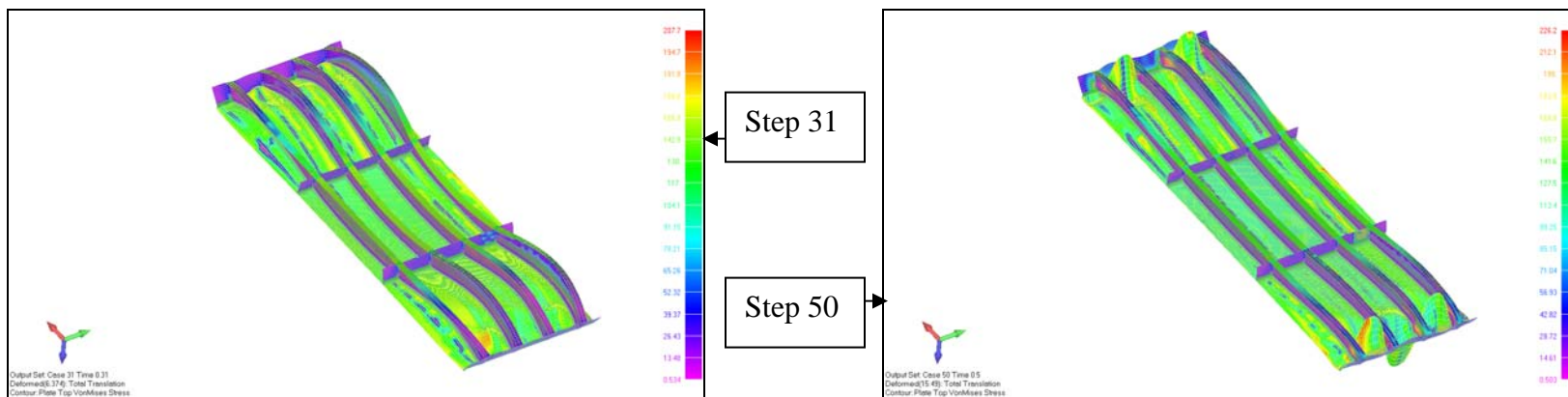


Figure C-8: Stress and Deflection Plot - Model 3- Base Metal Properties (step 31 - At Ultimate Strength)

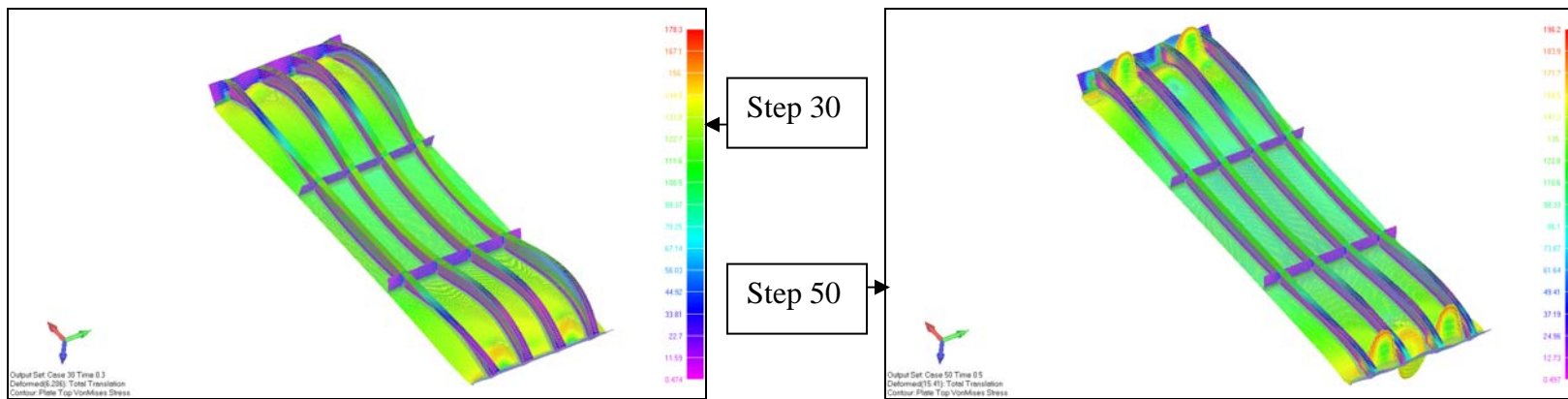


Figure C-9: Stress and Deflection Plot - Model 3- HAZ Properties (step 30 - At Ultimate Strength)

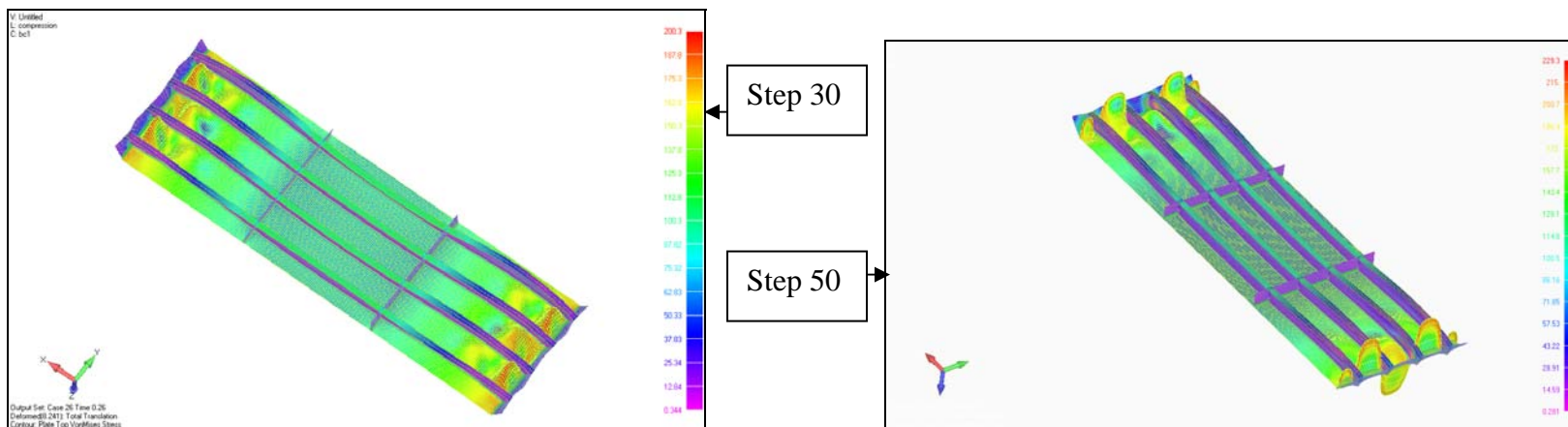


Figure C-10: Stress and Deflection Plot - Model 4- Combined (Base + HAZ)(step 30 - At Ultimate Strength)

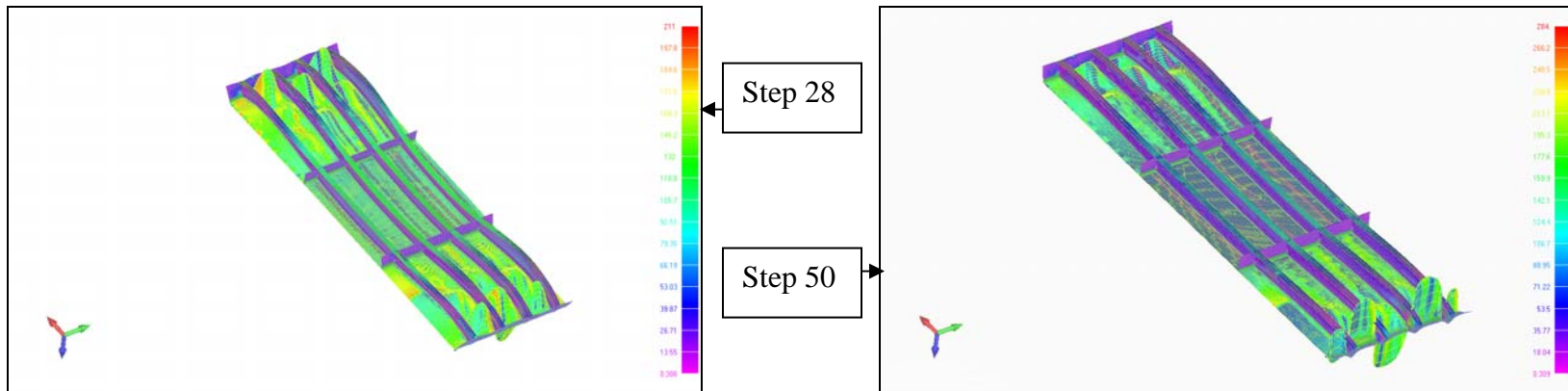


Figure C-11: Stress and Deflection Plot - Model 4- Base Metal Properties (step 28 - At Ultimate Strength)

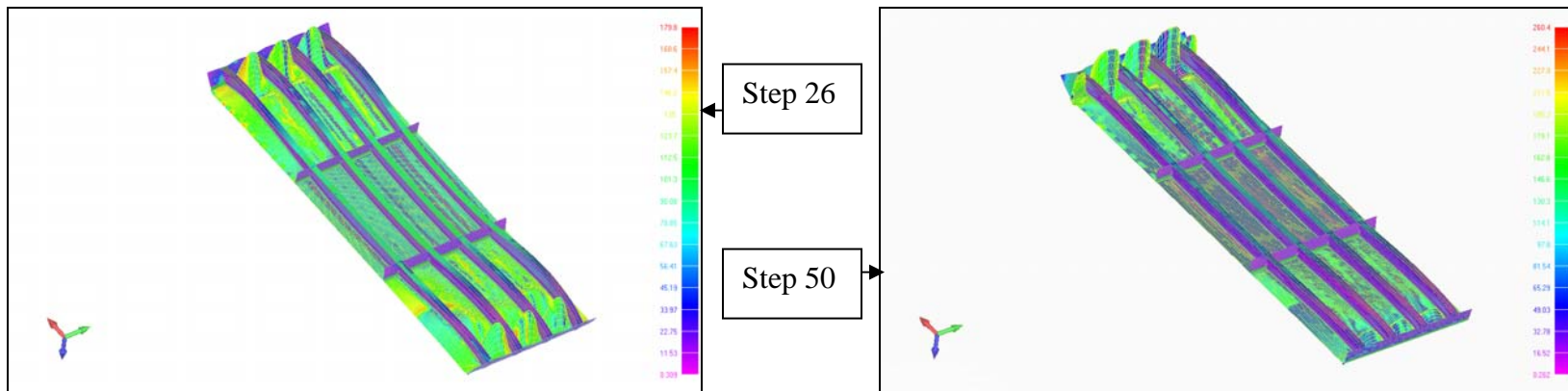


Figure C-12: Stress and Deflection Plot - Model 4- HAZ Properties (step 26 - At Ultimate Strength)

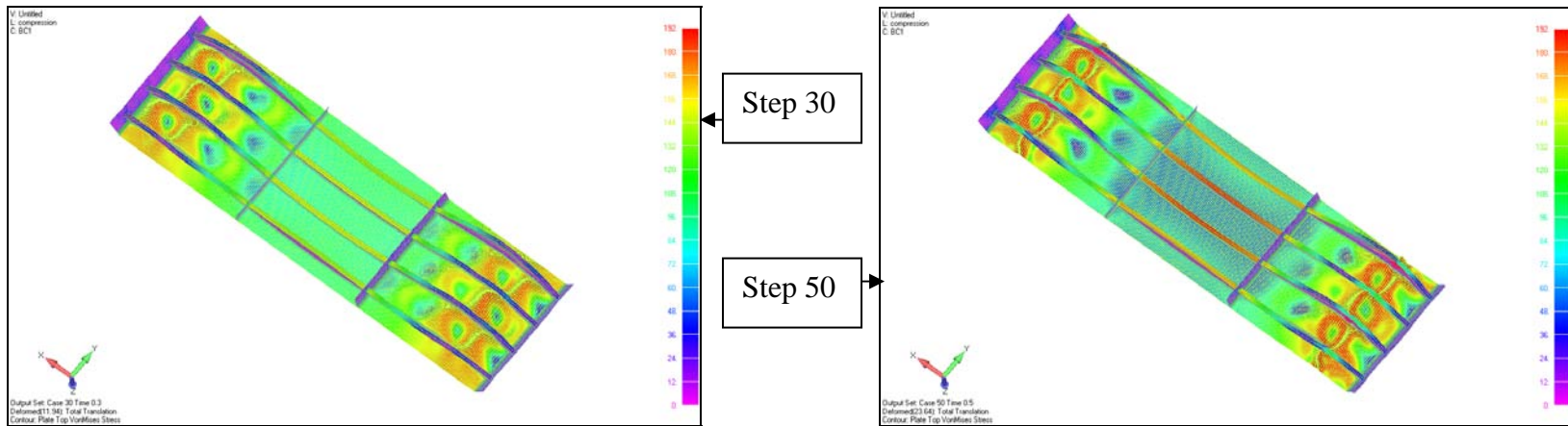


Figure C-1: Stress and Deflection Plot - Model 5- Combined (Base + HAZ)(step 30 - At Ultimate Strength)

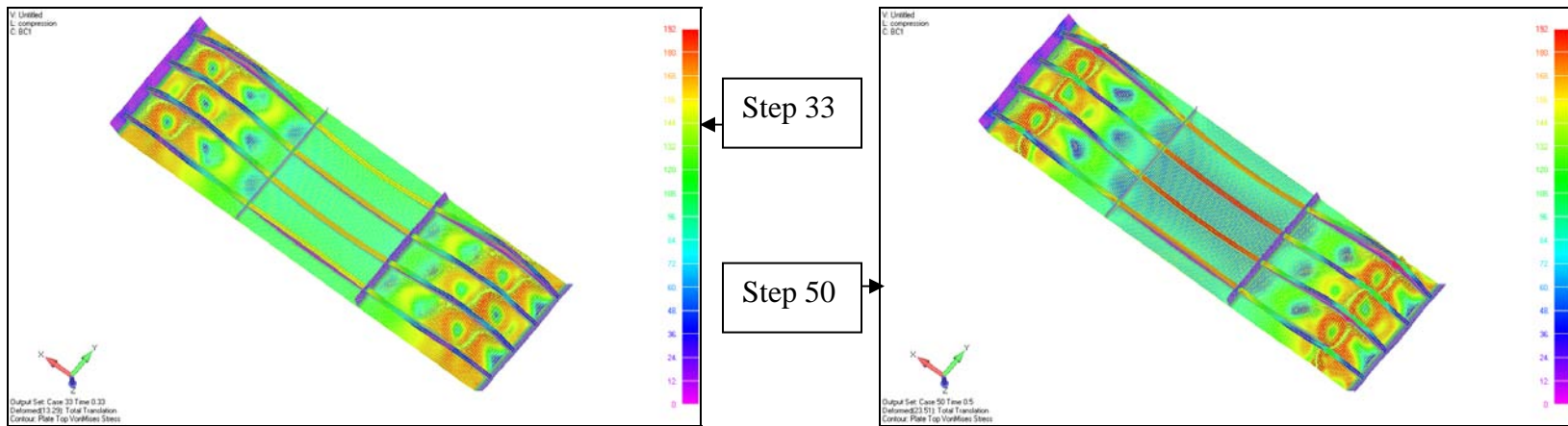


Figure C-2: Stress and Deflection Plot - Model 5- Base Metal Properties (step 33 - At Ultimate Strength)

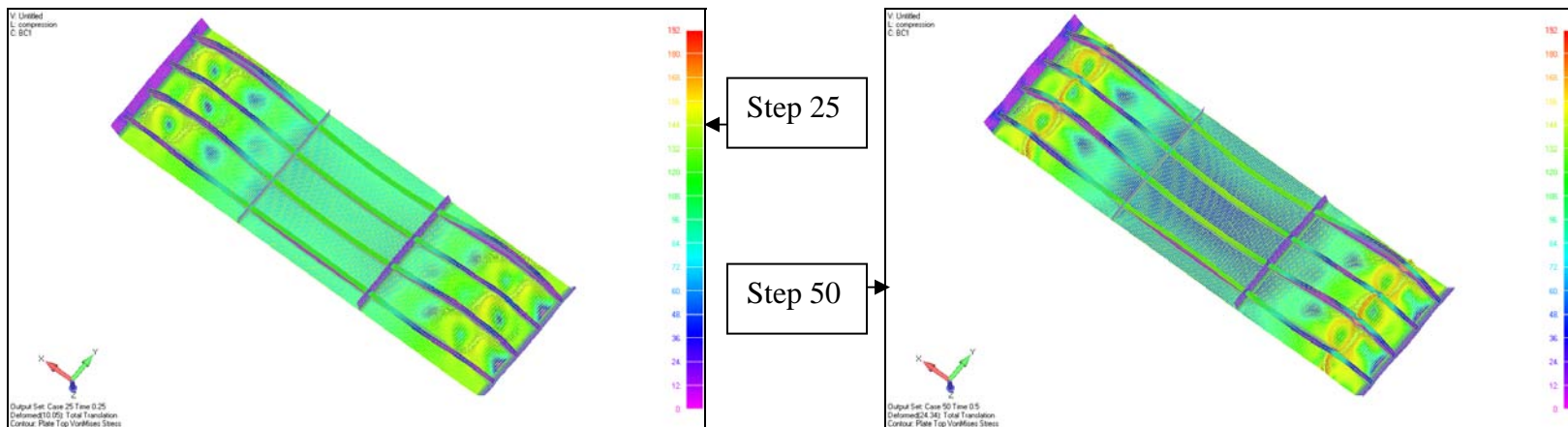


Figure C-3: Stress and Deflection Plot - Model 5- HAZ Properties (step 25 - At Ultimate Strength)

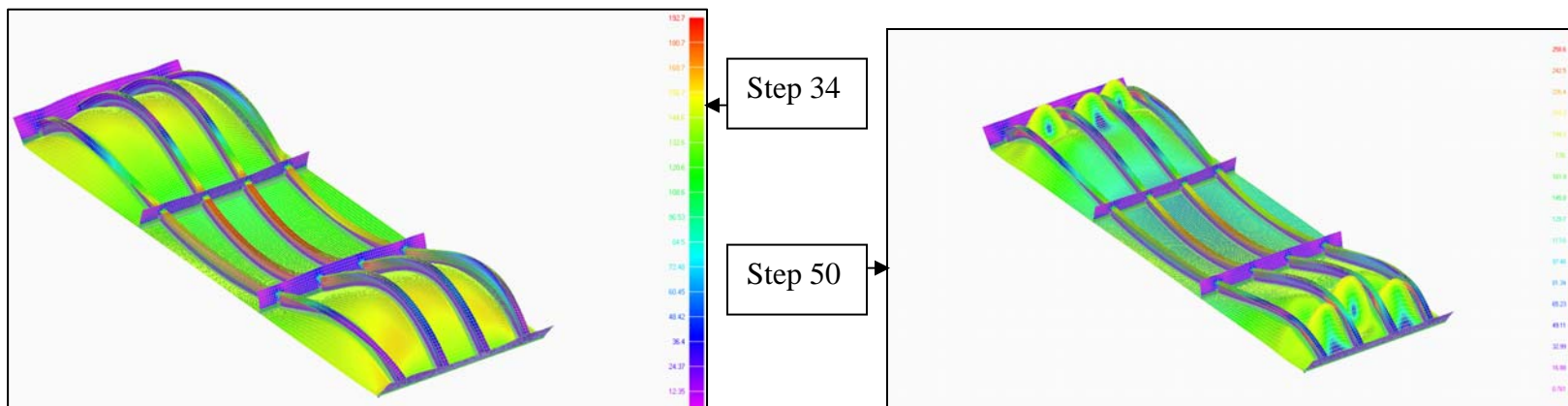


Figure C-4: Stress and Deflection Plot - Model 6- Combined (Base + HAZ)(step 34 - At Ultimate Strength)

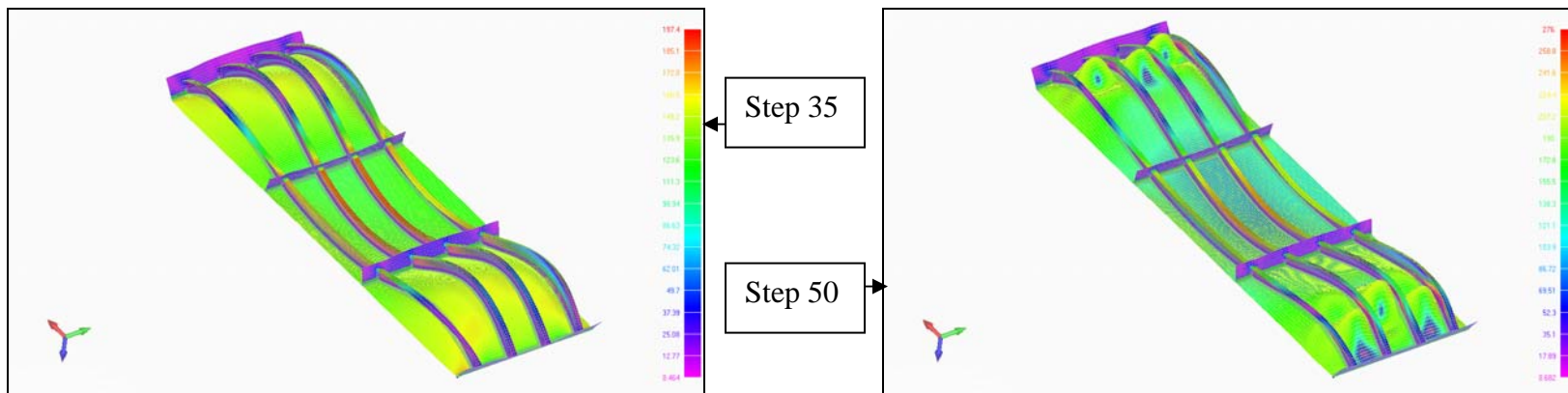


Figure C-5: Stress and Deflection Plot - Model 6- Base Metal Properties (step 35 - At Ultimate Strength)

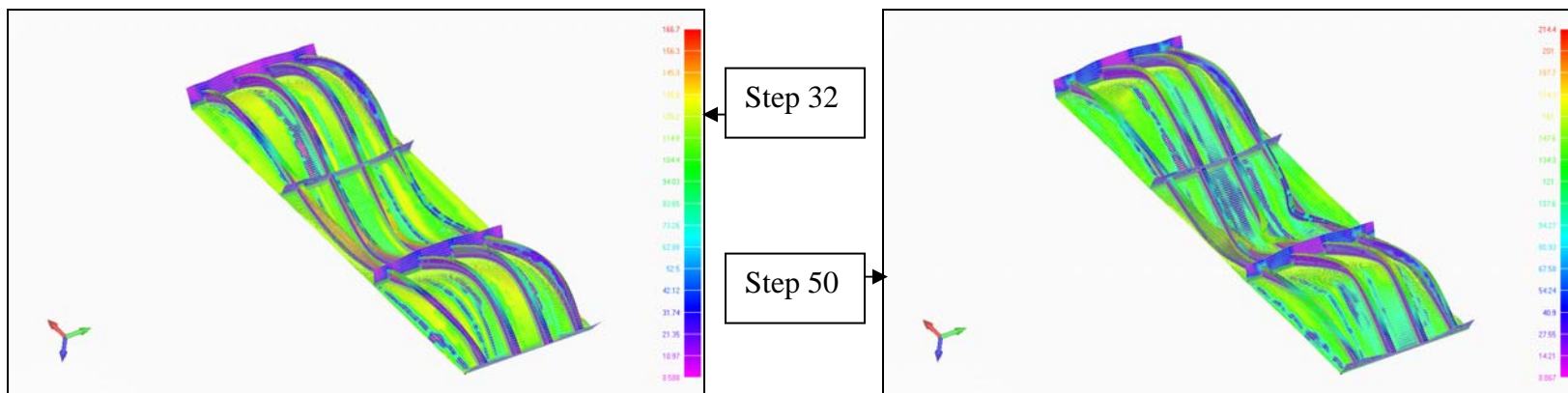


Figure C-6: Stress and Deflection Plot - Model 6- HAZ Properties (step 32 - At Ultimate Strength)

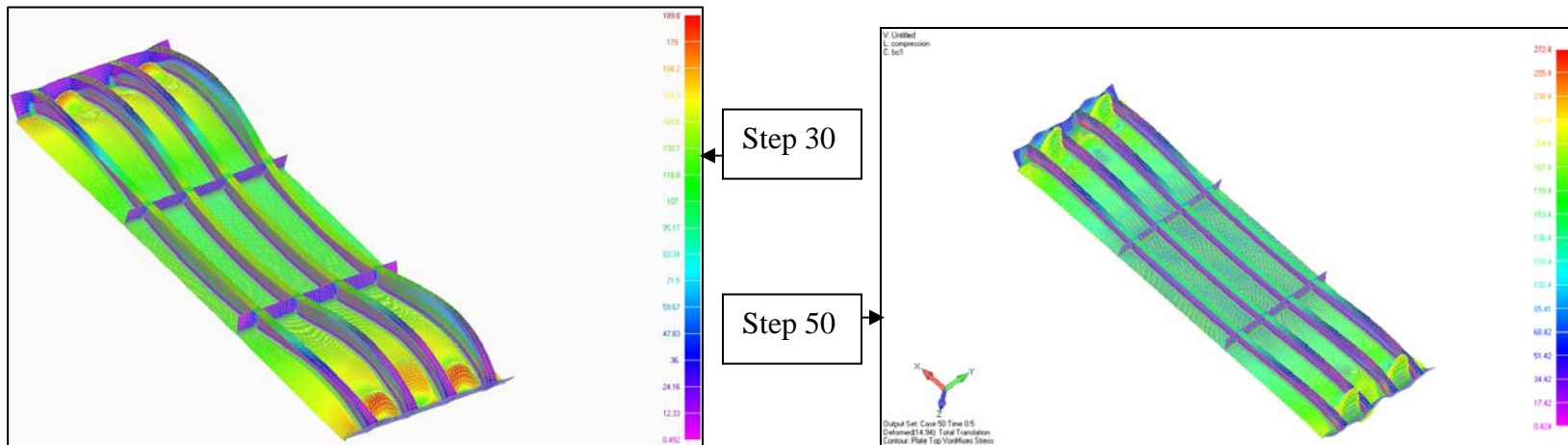


Figure C-7: Stress and Deflection Plot - Model 7- Combined (Base + HAZ)(step 30 - At Ultimate Strength)

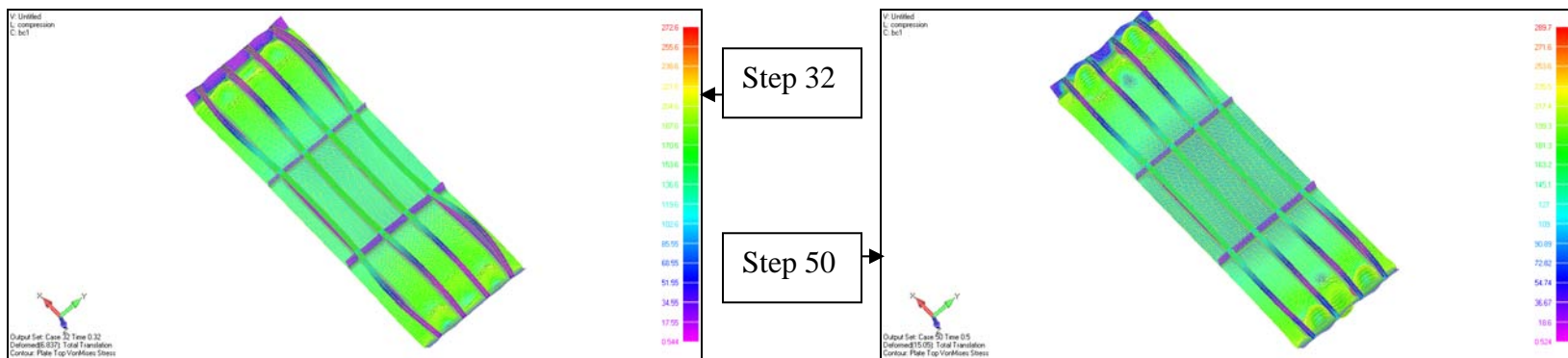


Figure C-8: Stress and Deflection Plot - Model 7- Base Metal Properties (step 32 - At Ultimate Strength)

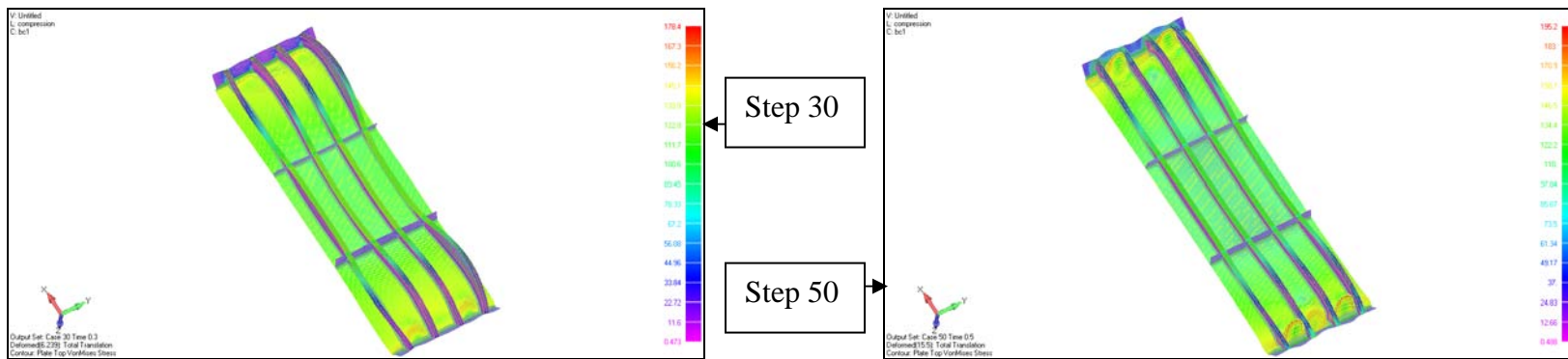


Figure C-9: Stress and Deflection Plot - Model 7- HAZ Properties (step 30 - At Ultimate Strength)

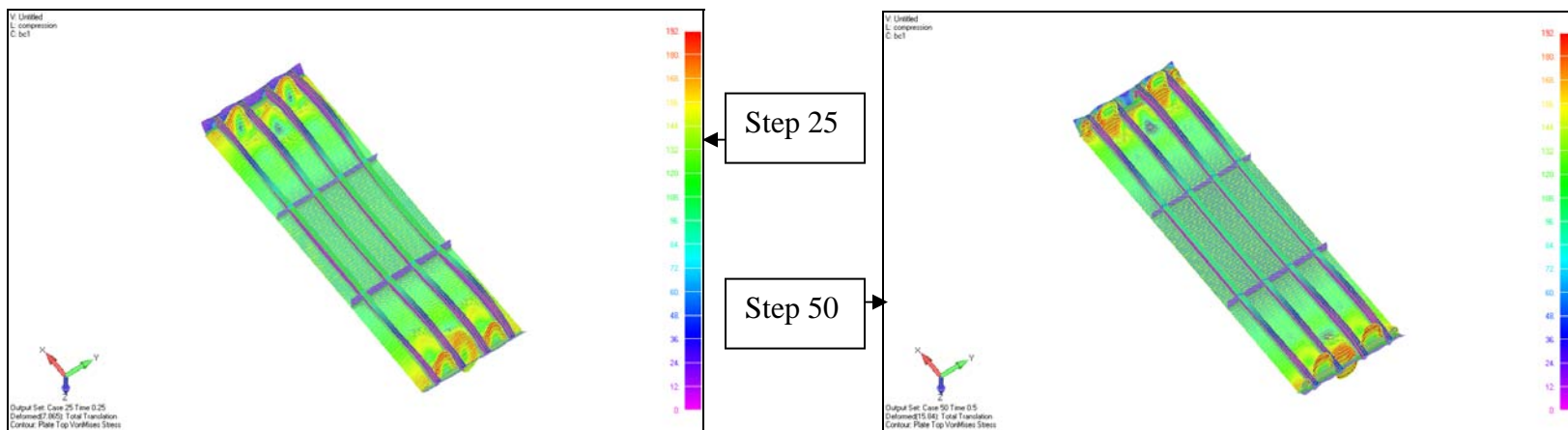


Figure C-10: Stress and Deflection Plot - Model 8- Combined (Base + HAZ)(step 25 - At Ultimate Strength)

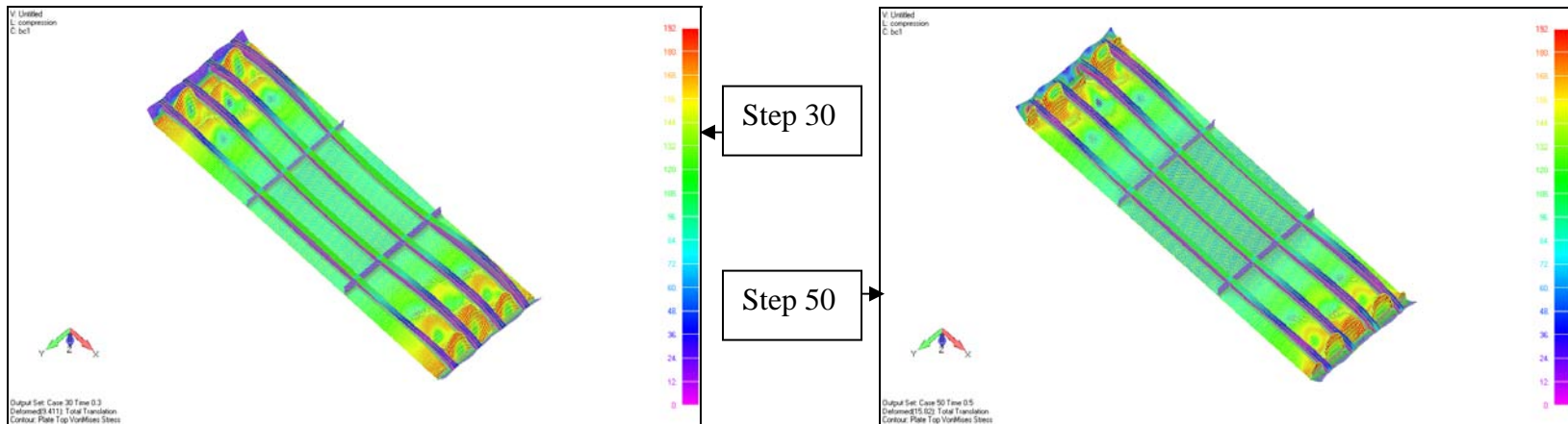


Figure C-11: Stress and Deflection Plot - Model 8- Base Metal Properties (step 30 - At Ultimate Strength)

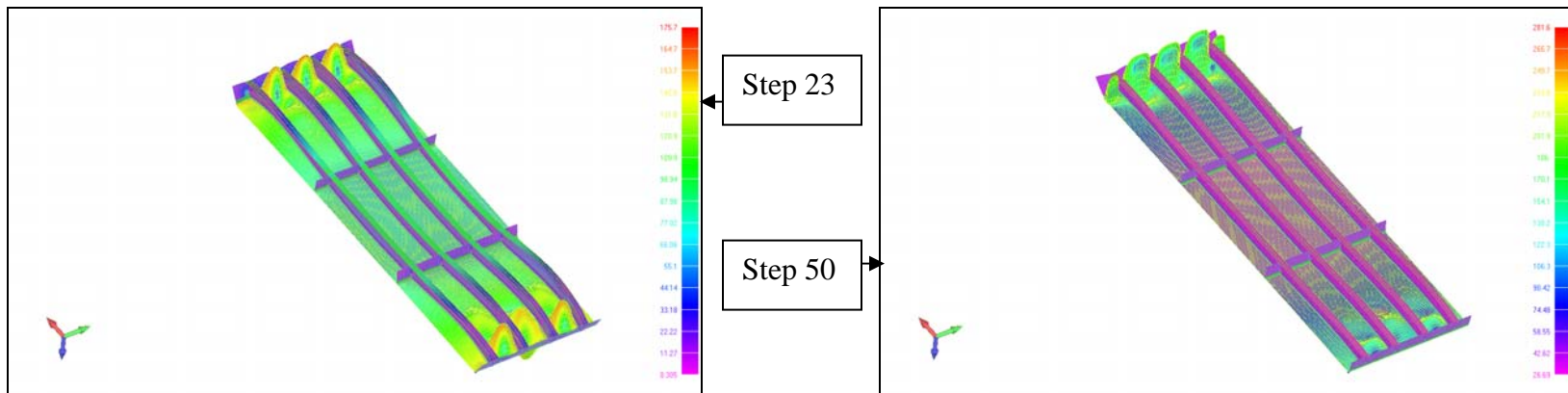


Figure C-12: Stress and Deflection Plot - Model 8- HAZ Properties (step 23 - At Ultimate Strength)

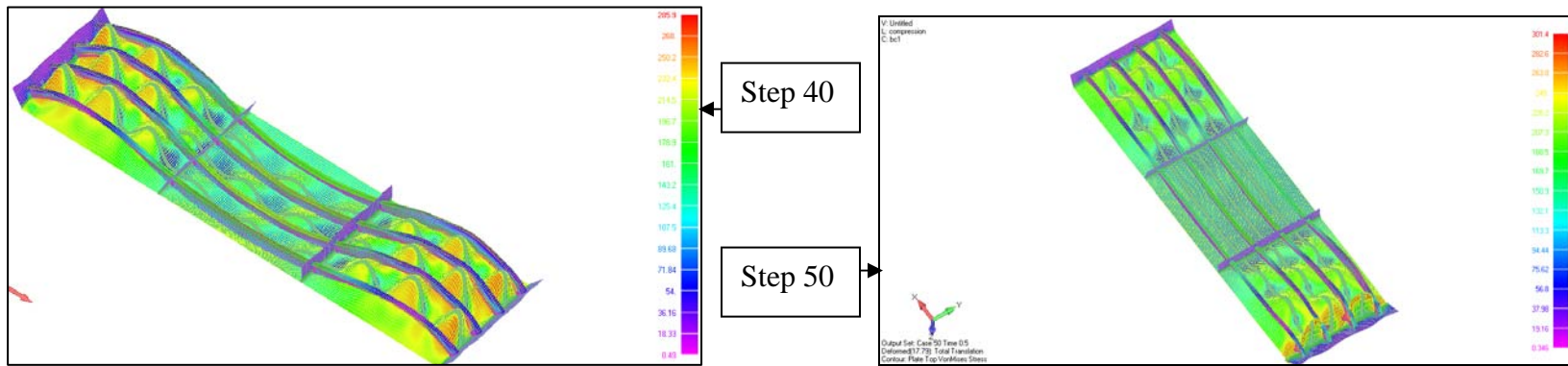


Figure C-13: Stress and Deflection Plot - Model 9- Combined (Base + HAZ)(step 40 - At Ultimate Strength)

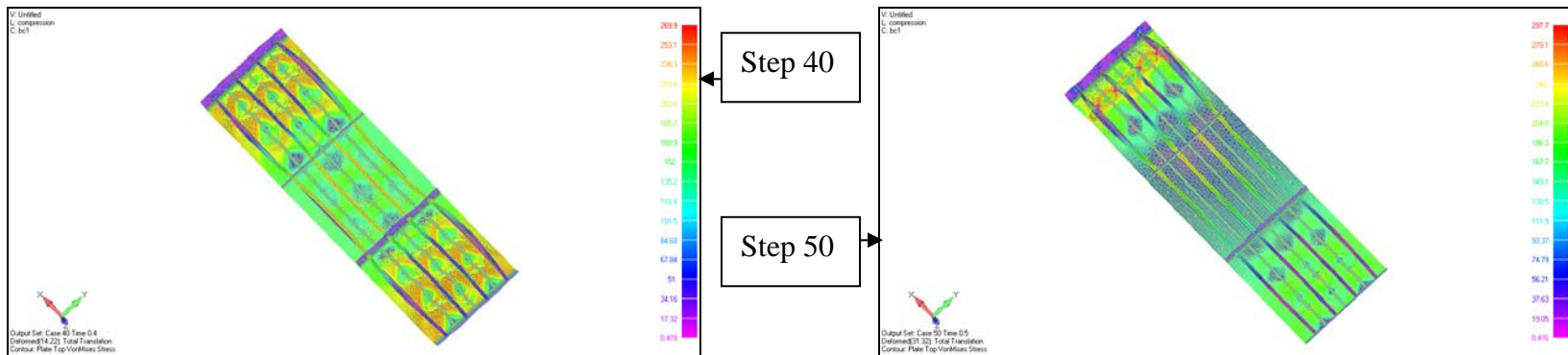


Figure C-14: Stress and Deflection Plot - Model 9- Base Metal Properties (step 40 - At Ultimate Strength)

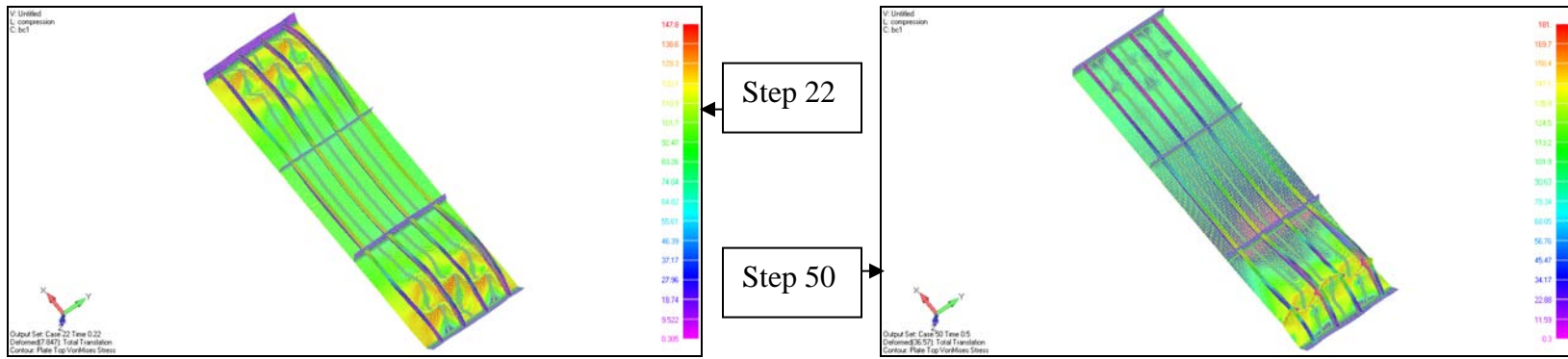


Figure C-15: Stress and Deflection Plot - Model 9- HAZ Properties (step 22 - At Ultimate Strength)

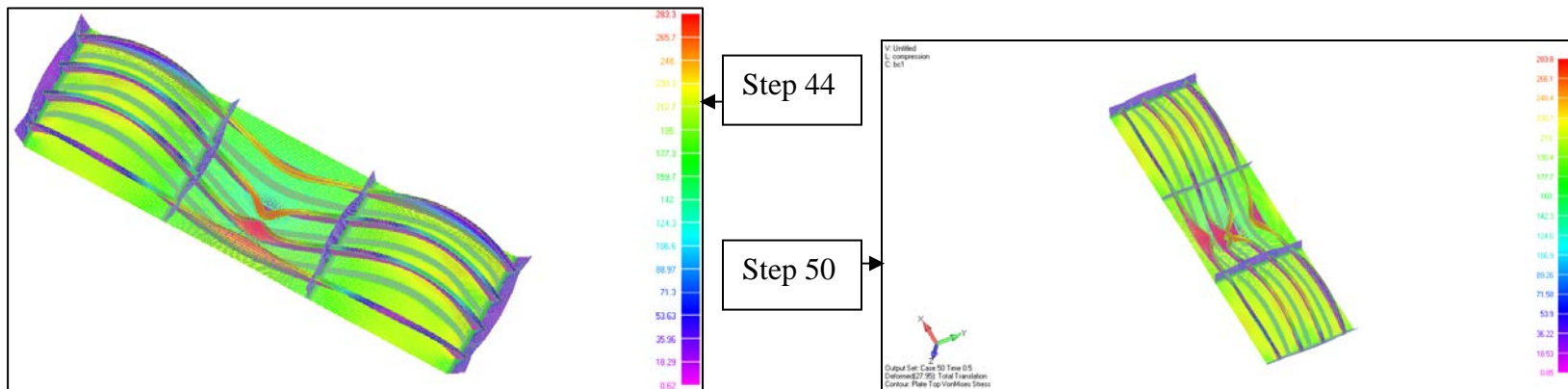


Figure C-16: Stress and Deflection Plot - Model 10- Combined (Base + HAZ)(step 44 - At Ultimate Strength)

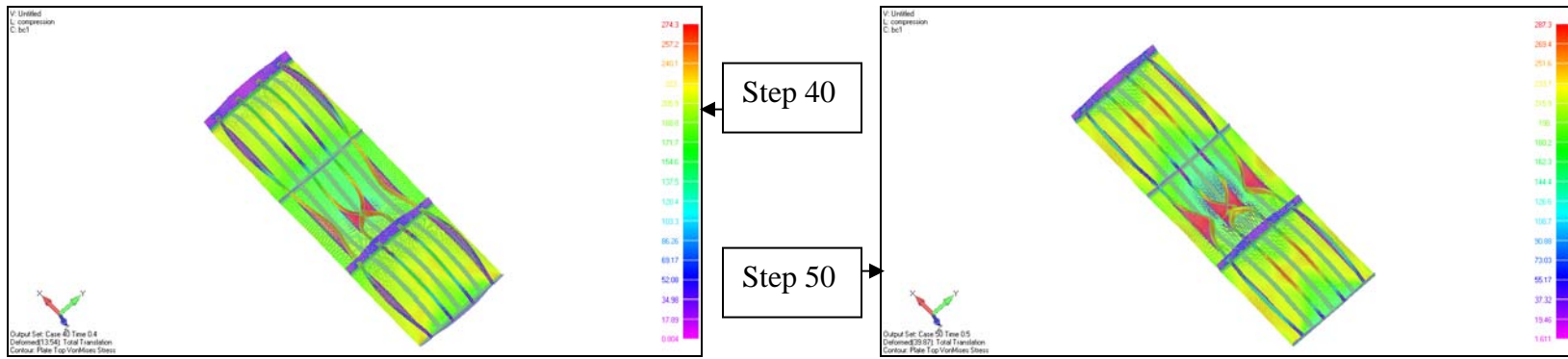


Figure C-17: Stress and Deflection Plot - Model 10- Base Metal Properties (step 40 - At Ultimate Strength)

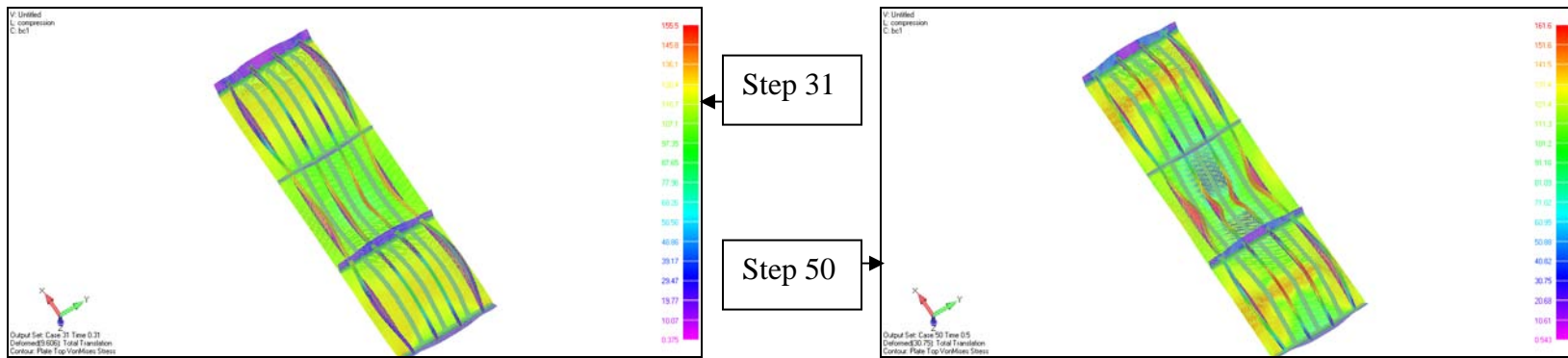


Figure C-18: Stress and Deflection Plot - Model 10- HAZ Properties (step 31 - At Ultimate Strength)

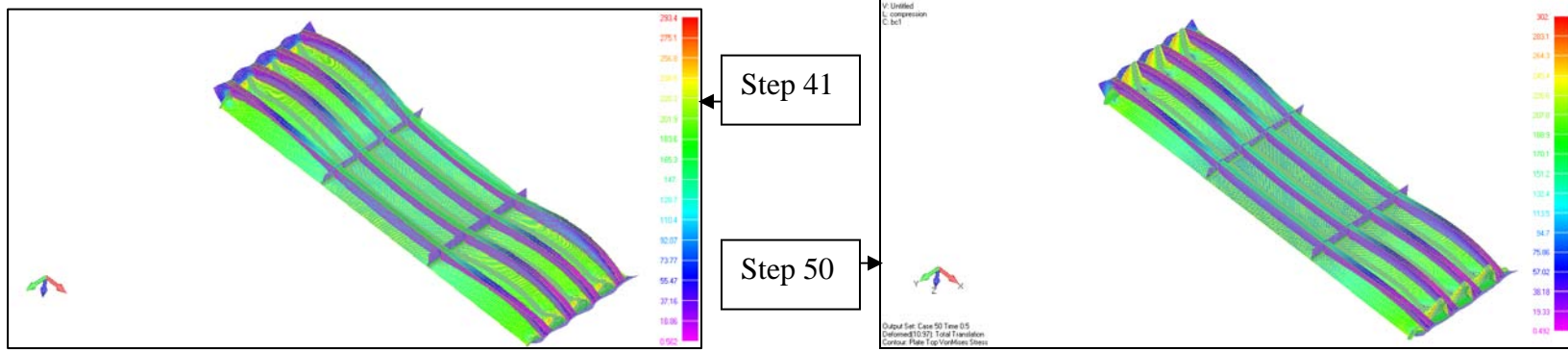


Figure C-19: Stress and Deflection Plot - Model 11- Combined (Base + HAZ)(step 41 - At Ultimate Strength)

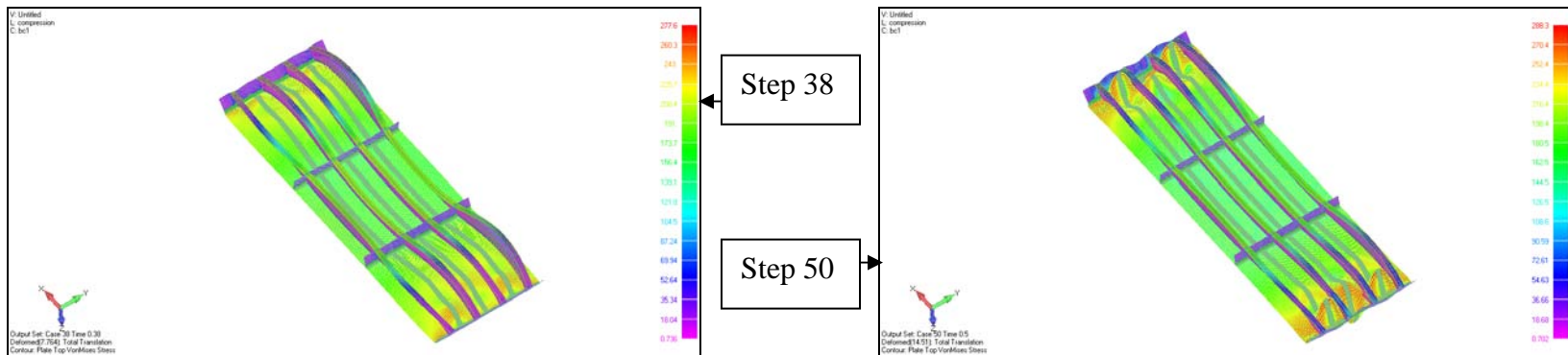


Figure C-20: Stress and Deflection Plot - Model 11- Base Metal Properties (step 38 - At Ultimate Strength)

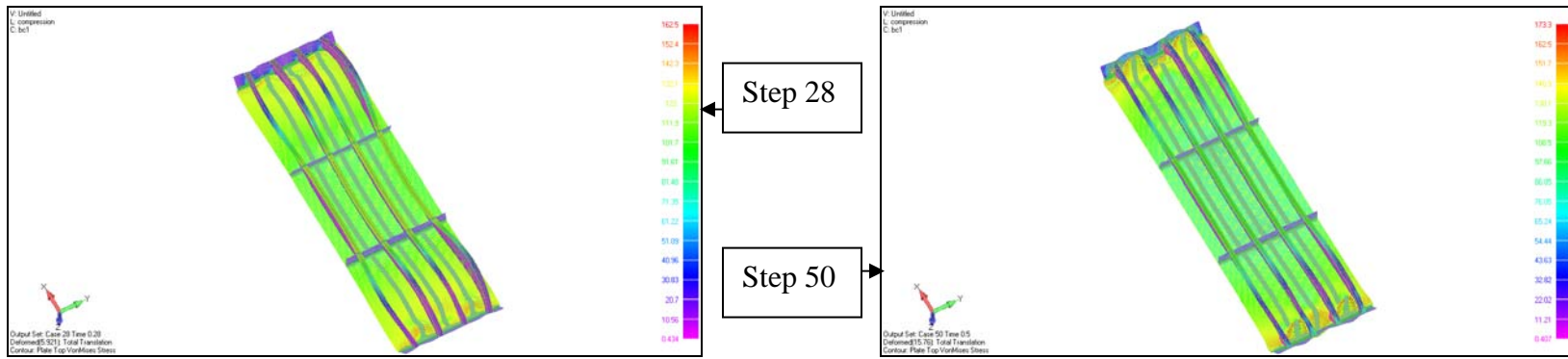


Figure C-21: Stress and Deflection Plot - Model 11- HAZ Properties (step 28 - At Ultimate Strength)

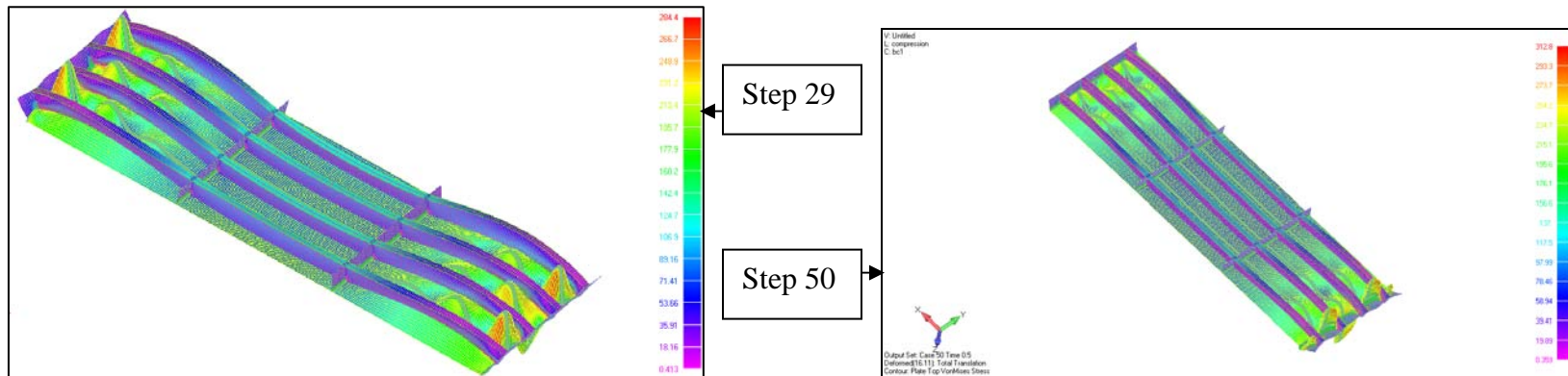


Figure C-22: Stress and Deflection Plot - Model 12- Combined (Base + HAZ)(step 29 - At Ultimate Strength)

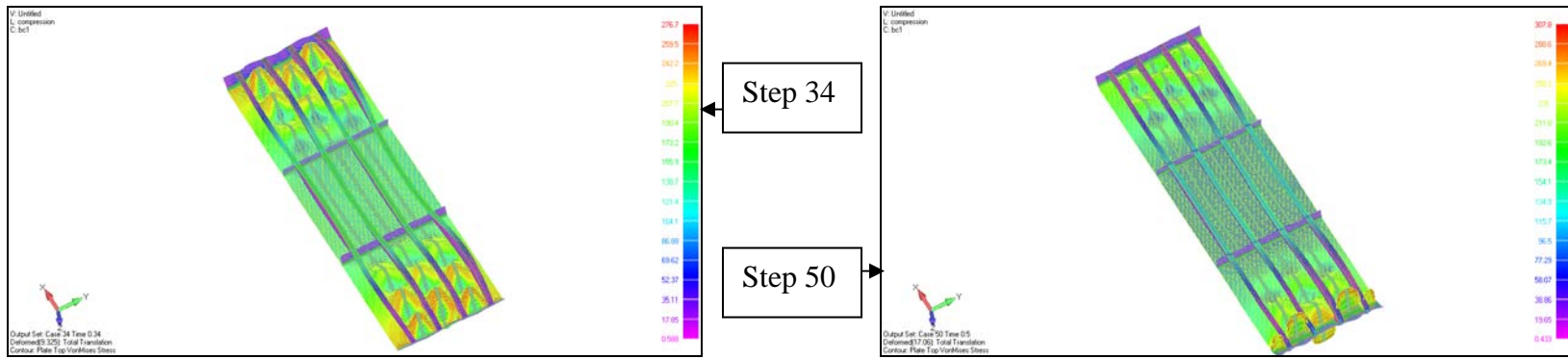


Figure C-23: Stress and Deflection Plot - Model 12- Base Metal Properties (step 34 - At Ultimate Strength)

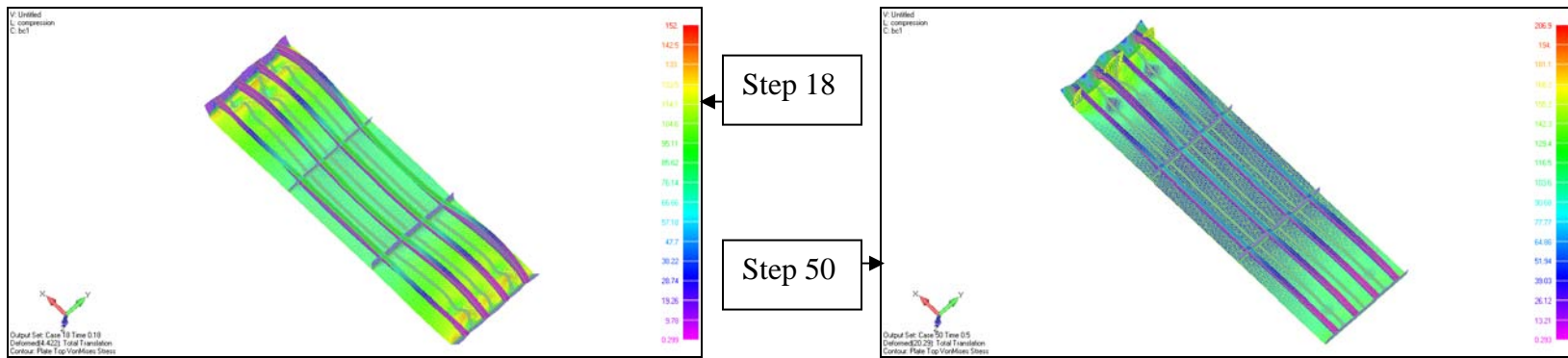


Figure C-24: Stress and Deflection Plot - Model 12- HAZ Properties (step 18 - At Ultimate Strength)

Appendix D

Tension Load Case: Yield Point and Stress Plots

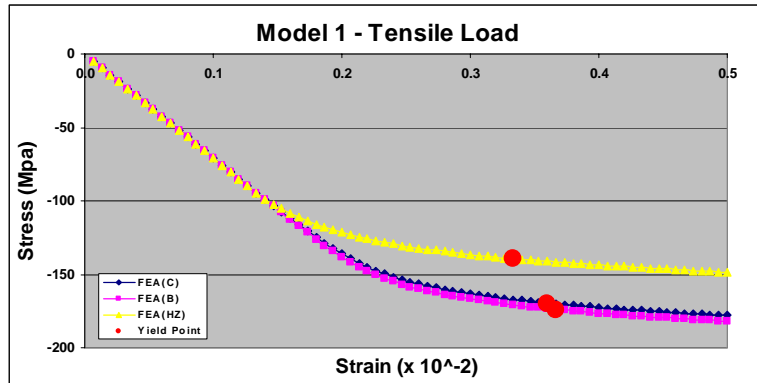


Figure D-1: Tension Yield Points for Model 1

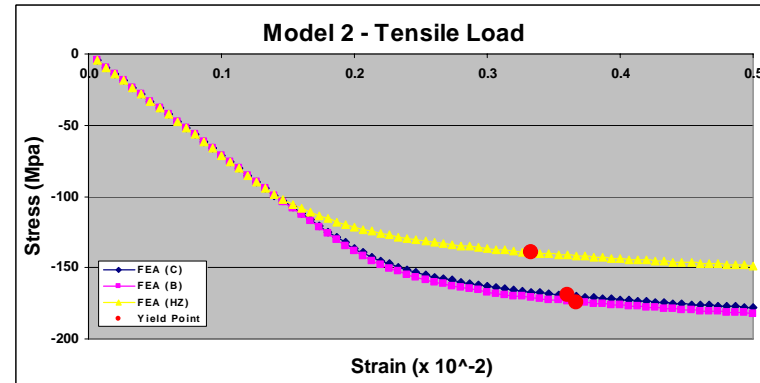


Figure D-2: Tension Yield Points for Model 2

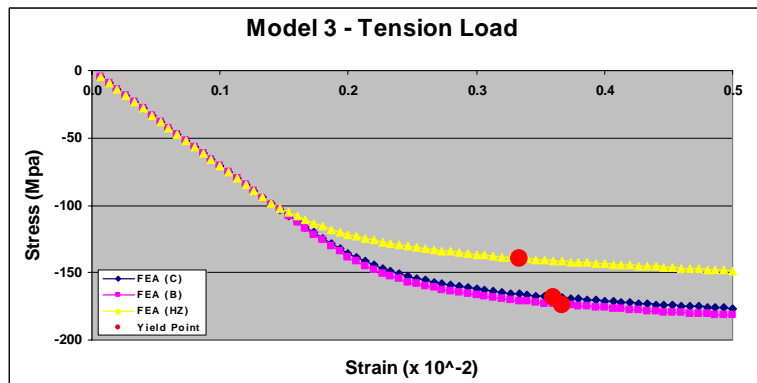


Figure D-3: Tension Yield Points for Model 3

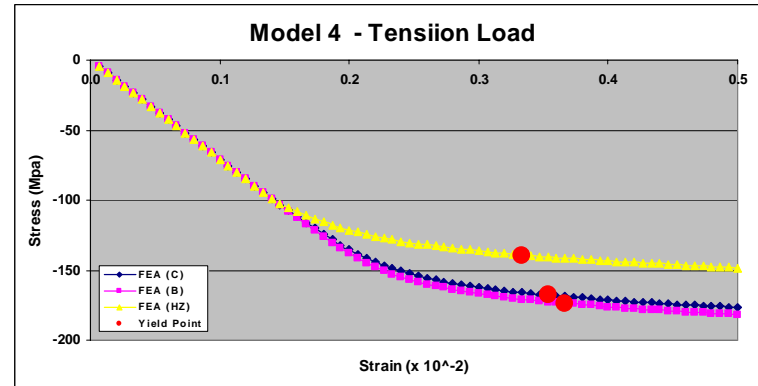


Figure D-4: Tension Yield Points for Model 4

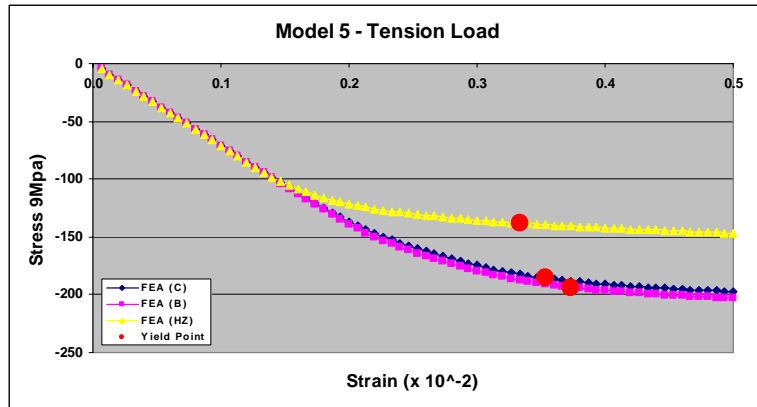


Figure D-5: Tension Yield Points for Model 5

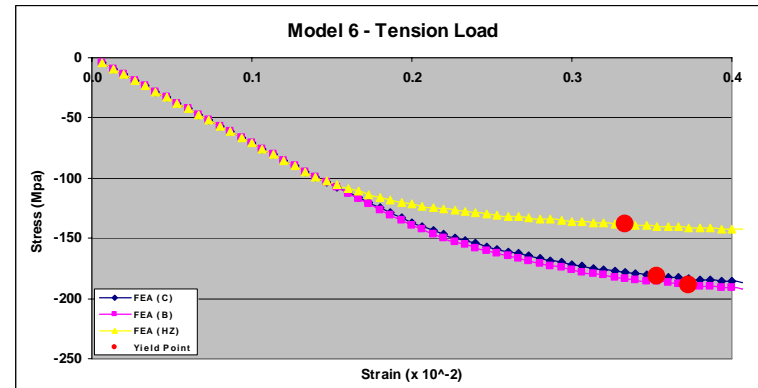


Figure D-6: Tension Yield Points for Model 6

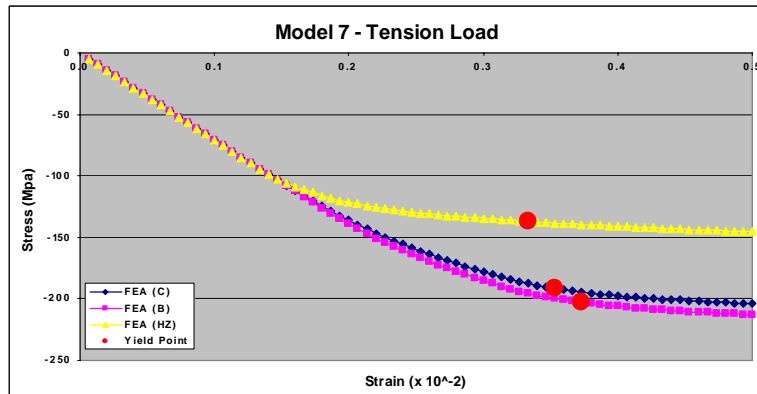


Figure D-7: Tension Yield Points for Model 7

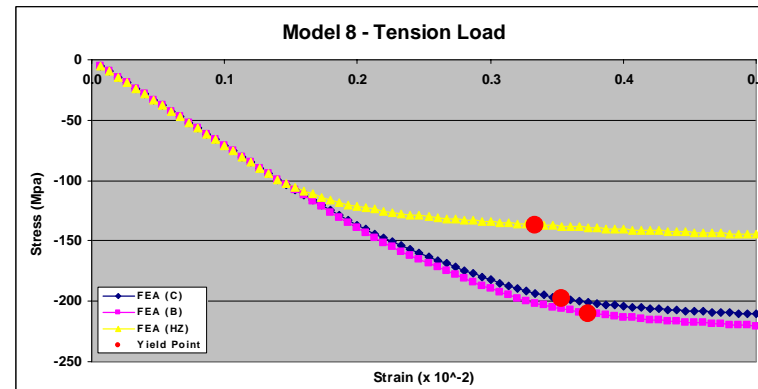


Figure D-8: Tension Yield Points for Model 8

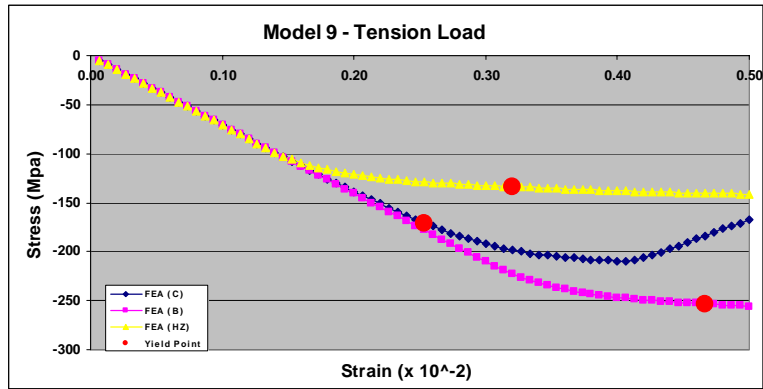


Figure D-9: Tension Yield Points for Model 9

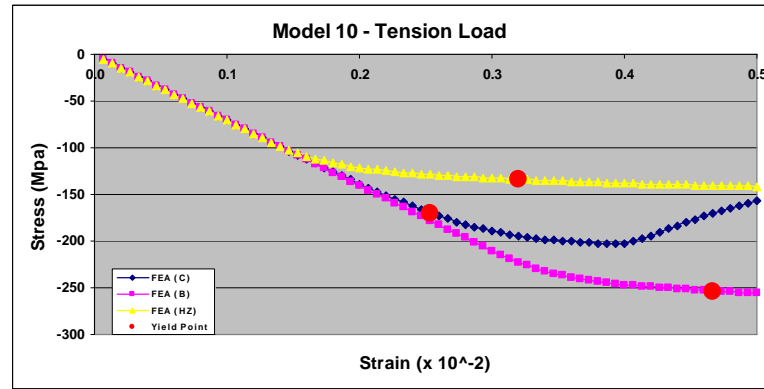


Figure D-10: Tension Yield Points for Model 10

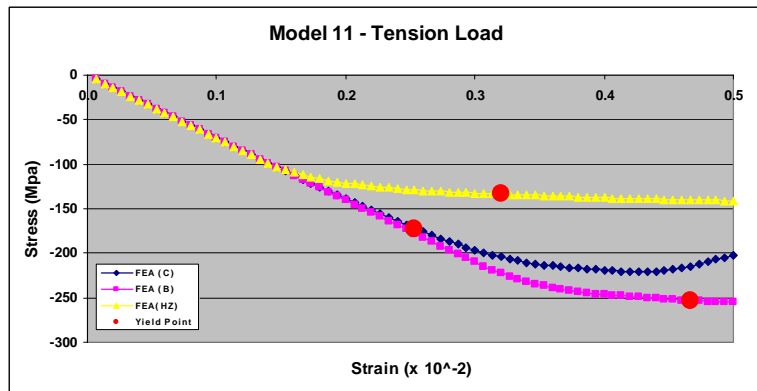


Figure D-11: Tension Yield Points for Model 11

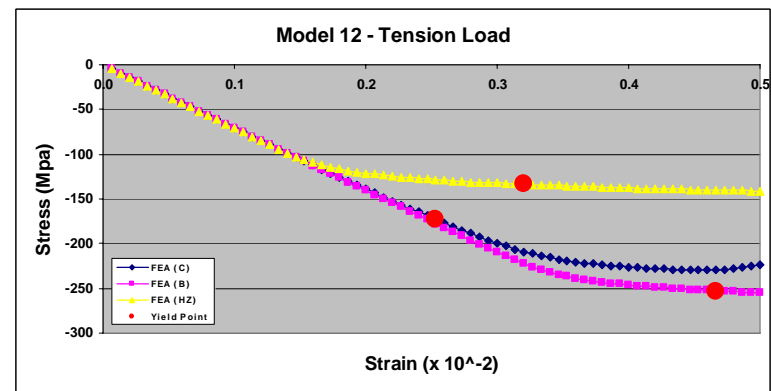


Figure D-12: Tension Yield Points for Model 12

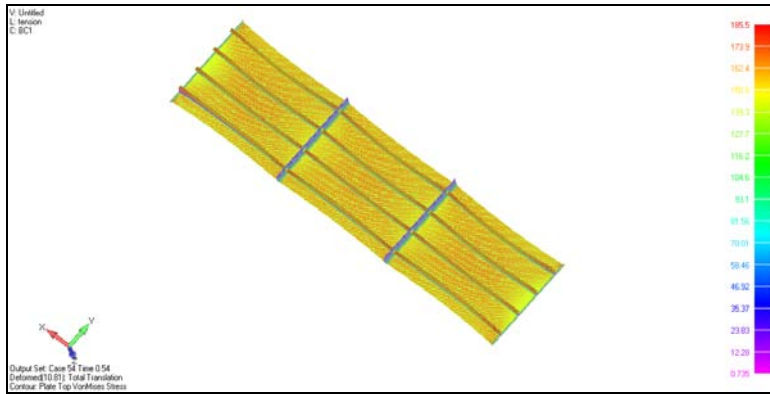


Figure D-13: Stress & Deflection plot for Model 1

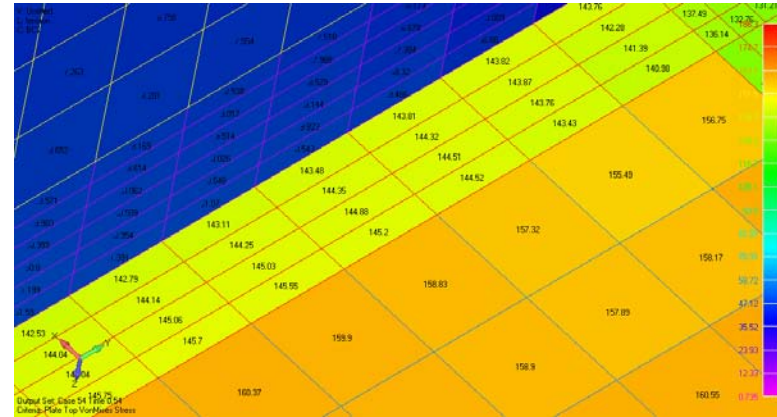


Figure D-14: Tension Yield Points (HAZ) for Model 1

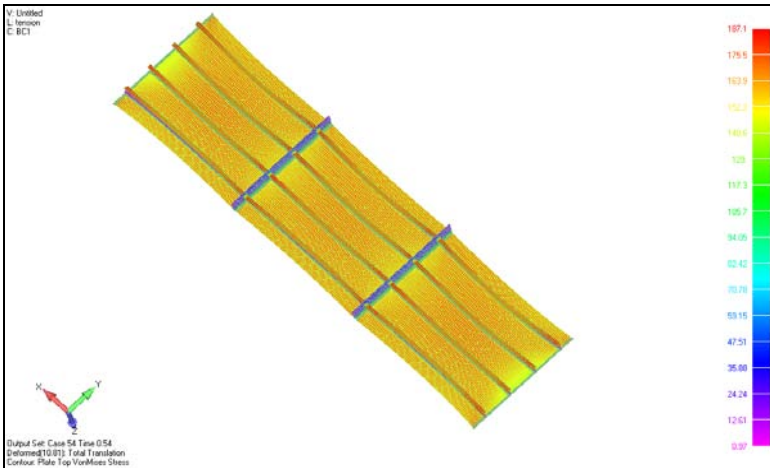


Figure D-15: Stress & Deflection plot for Model 2

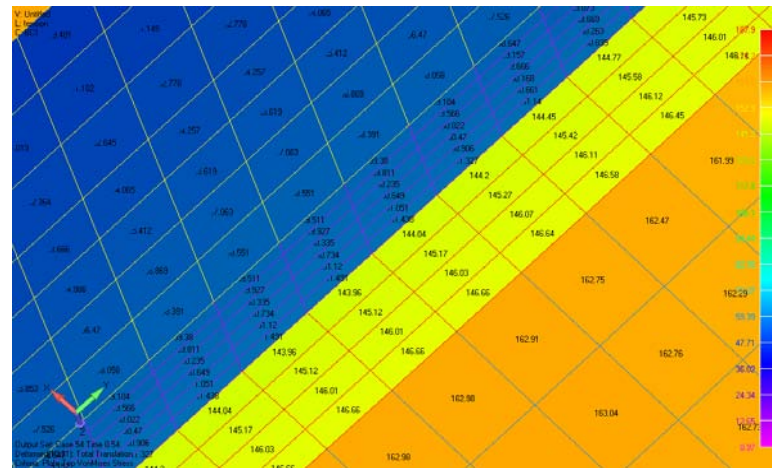


Figure D-16: Tension Yield Points (HAZ) for Model 2

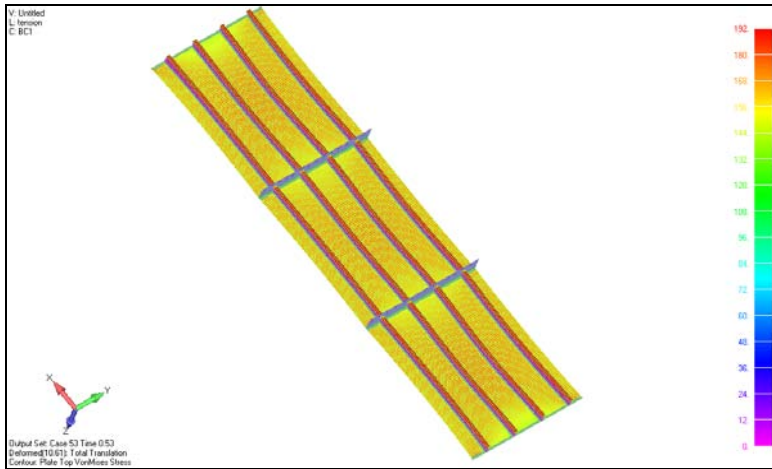


Figure D-17: Stress & Deflection plot for Model 3

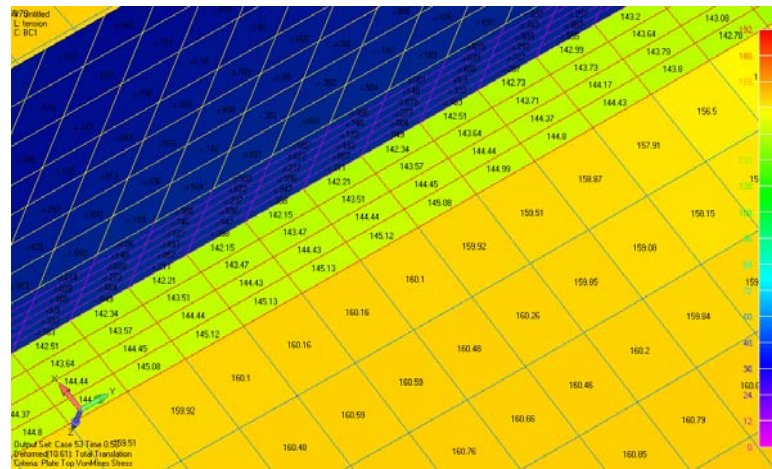


Figure D-18: Tension Yield Points (HAZ) for Model 3

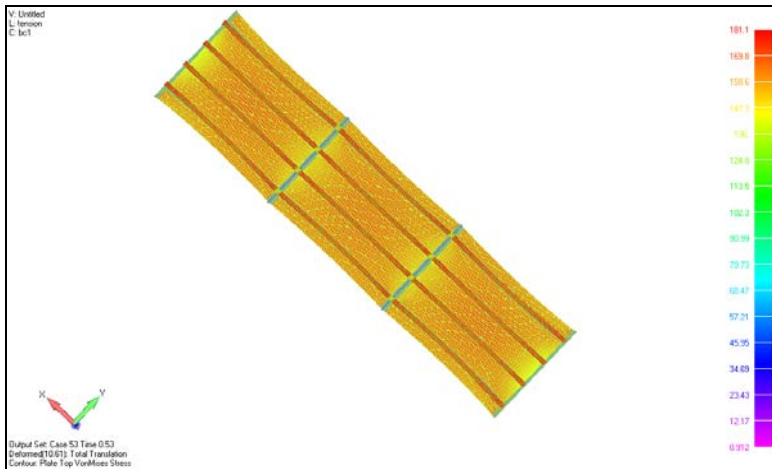


Figure D-19: Stress & Deflection plot for Model 4

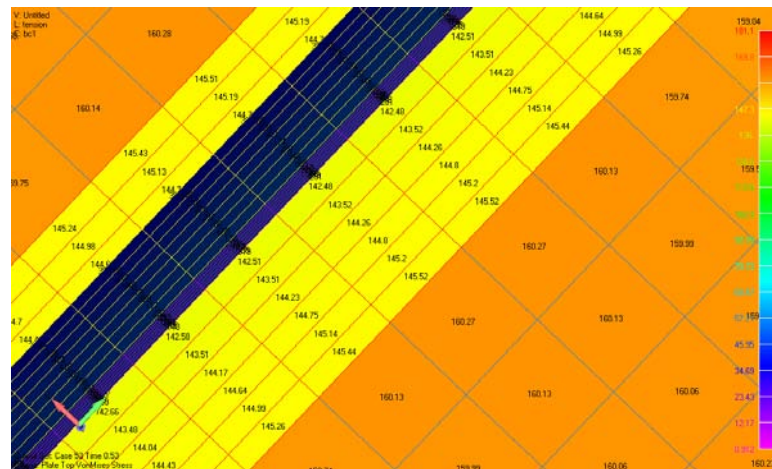


Figure D-20: Tension Yield Points (HAZ) for Model 4

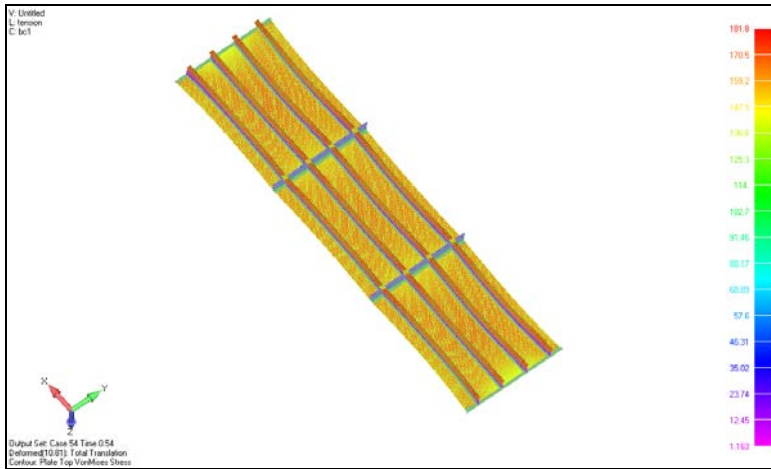


Figure D-21: Stress & Deflection plot for Model 5

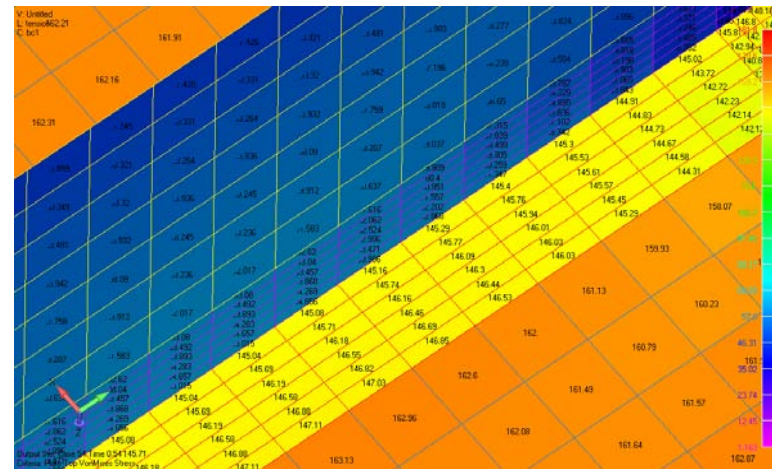


Figure D-22: Tension Yield Points (HAZ) for Model 5

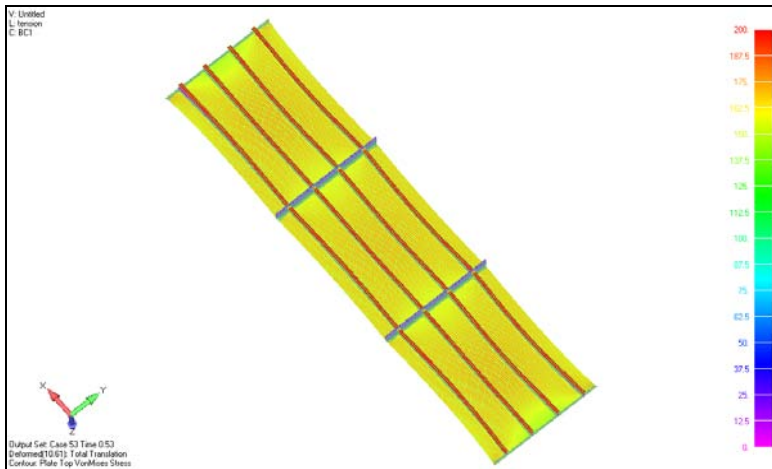


Figure D-23: Stress & Deflection plot for Model 6

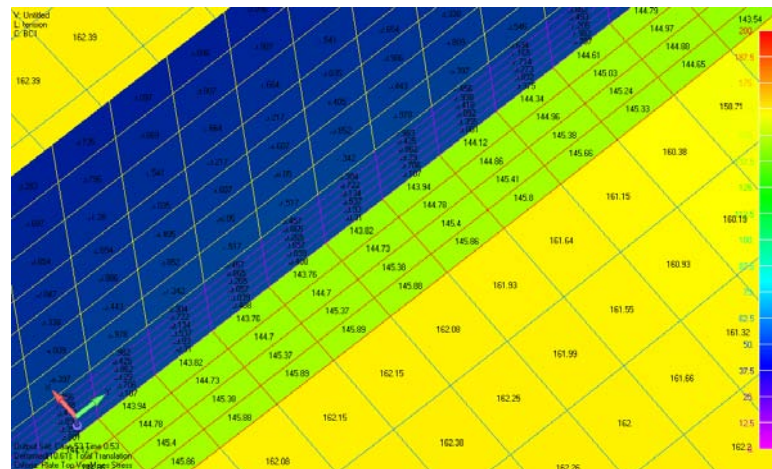


Figure D-24: Tension Yield Points (HAZ) for Model 6

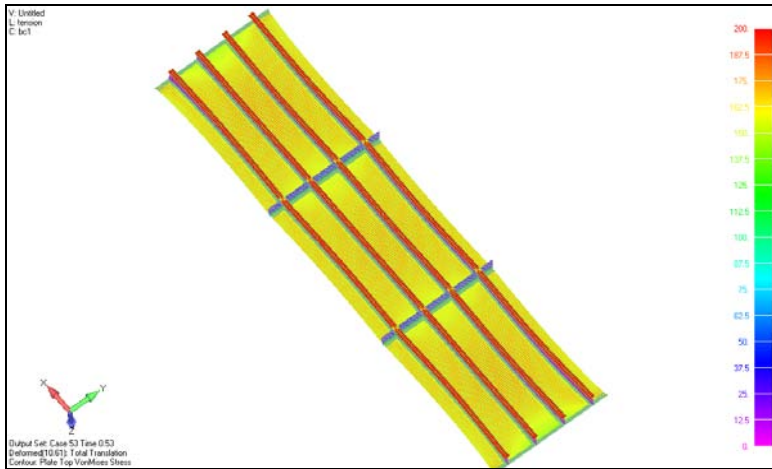


Figure D-25: Stress & Deflection plot for Model 7

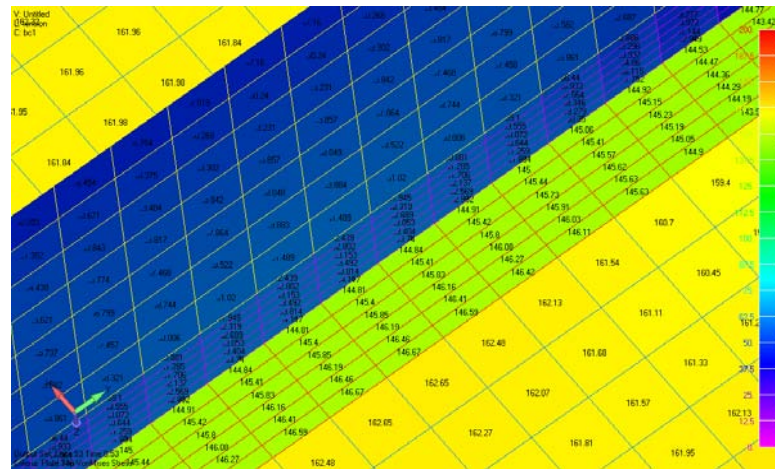


Figure D-26: Tension Yield Points (HAZ) for Model 7

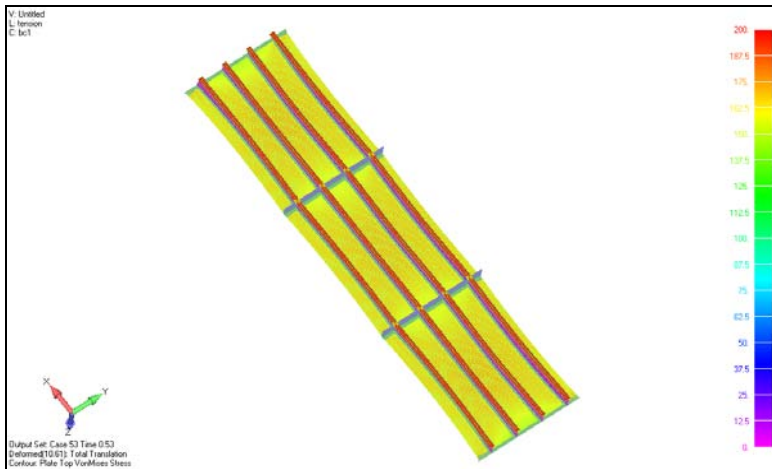


Figure D-27: Stress & Deflection plot for Model 8

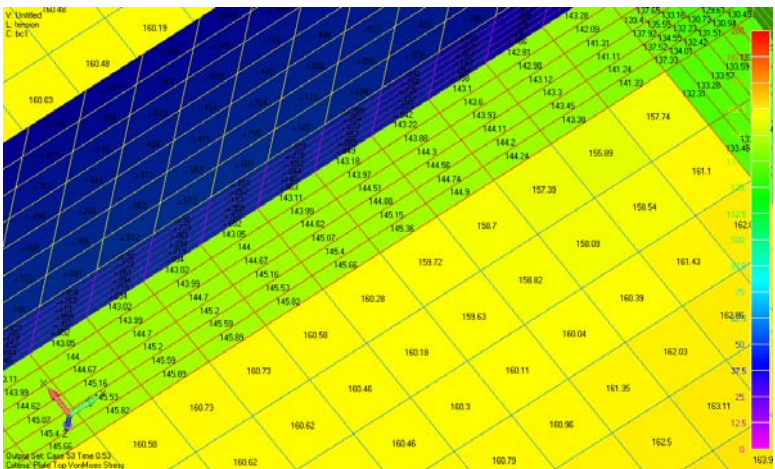


Figure D-28: Tension Yield Points (HAZ) for Model 8

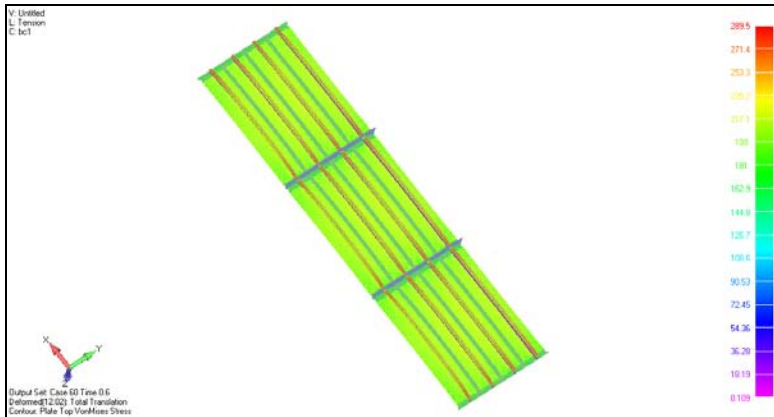


Figure D-29: Stress & Deflection plot for Model 9

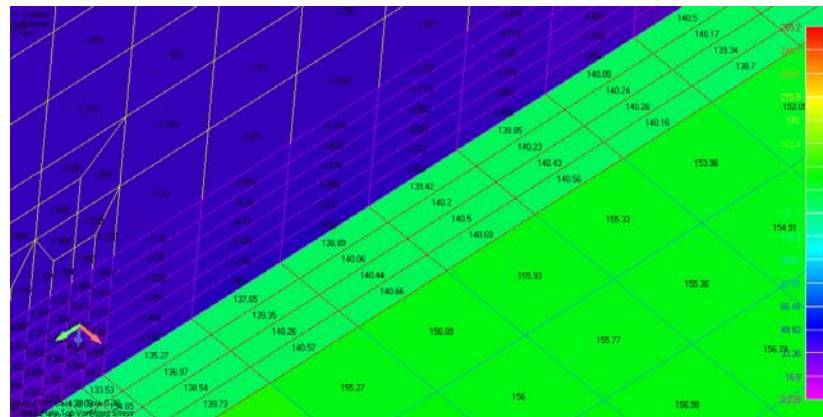


Figure D-30: Tension Yield Points (stiffener) for Model 9

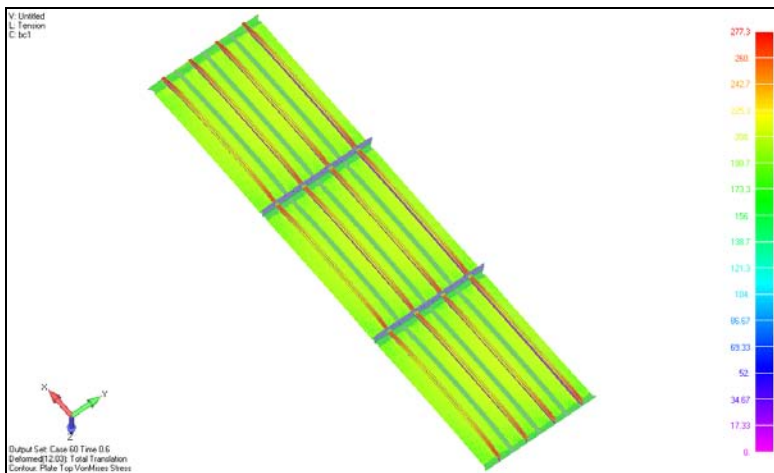


Figure D-31: Stress & Deflection plot for Model 10

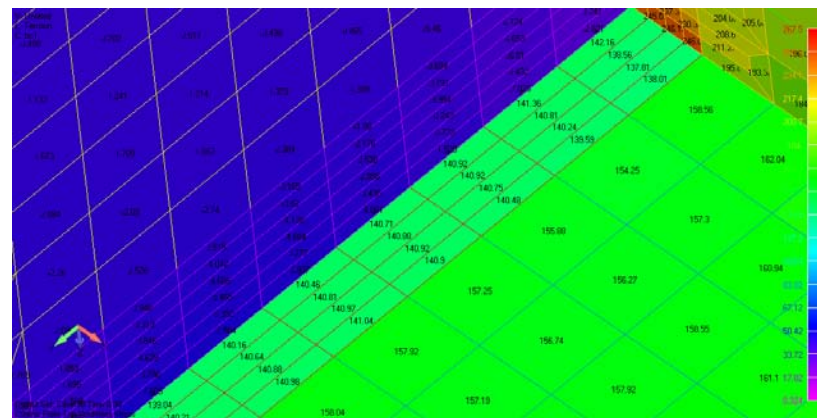


Figure D-32: Tension Yield Points (stiffener) for Model 10

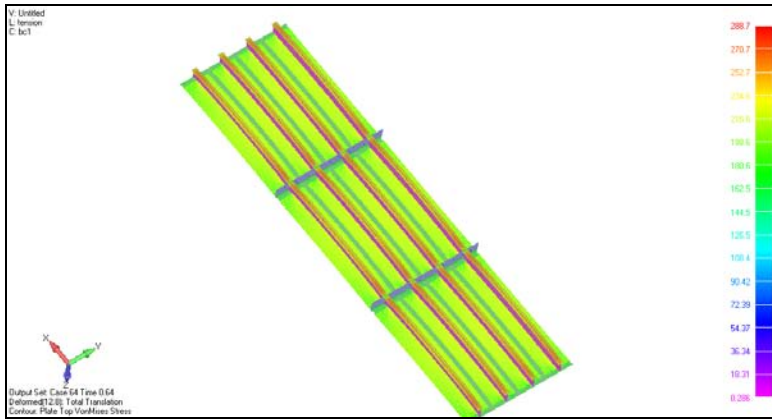


Figure D-33: Stress & Deflection plot for Model 11

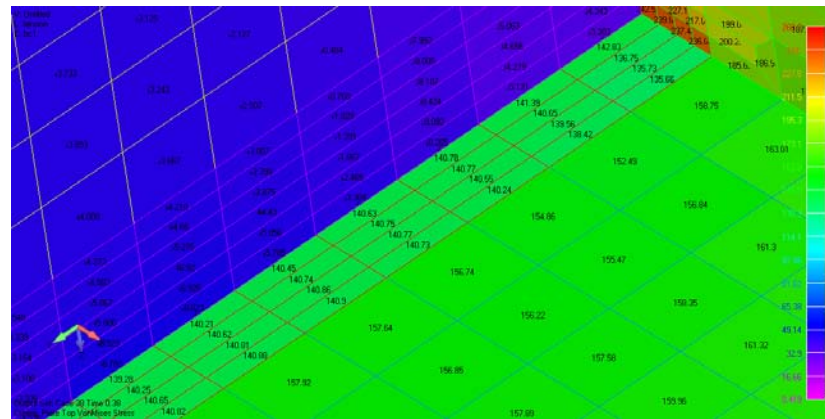


Figure D-34: Tension Yield Points (stiffener) for Model 11

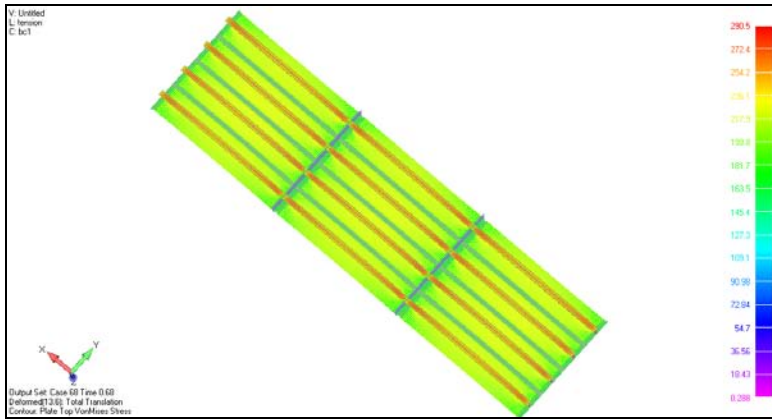


Figure D-35: Stress & Deflection plot for Model 12

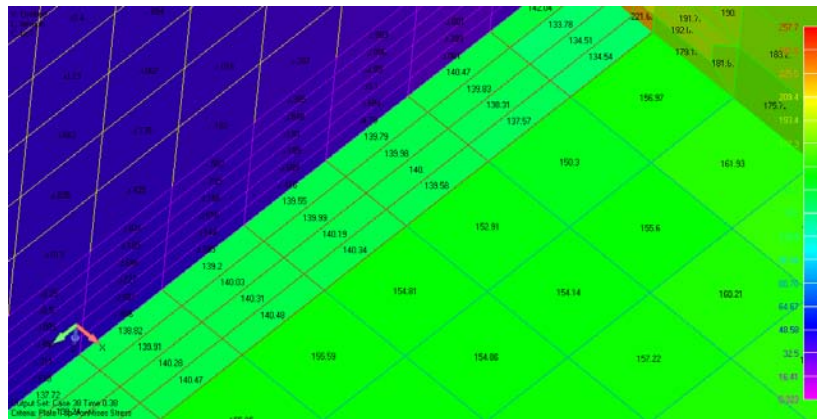


Figure D-36: Tension Yield Points (stiffener) for Model 12

Appendix E

Pressure Load Case: Stress, deflection and Strain Plots

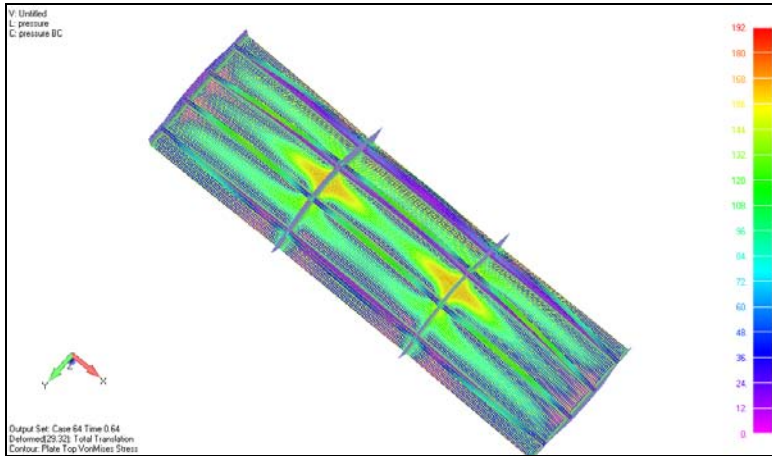


Figure E-1: Stress & Deflection plot for Model 1

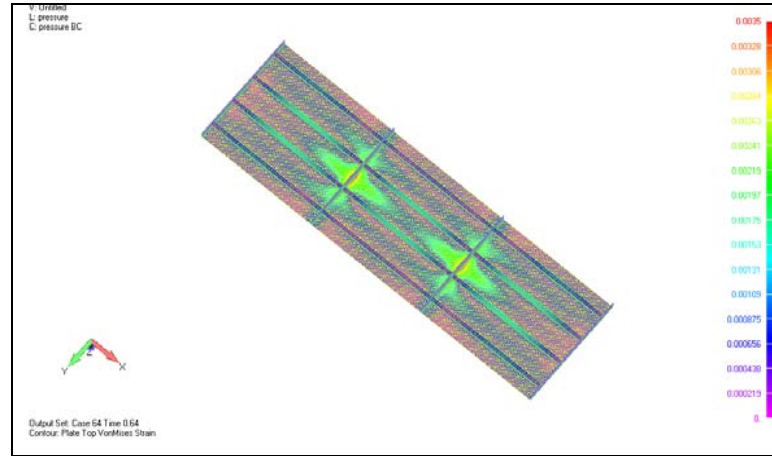


Figure E-2: Strain plots for Model 1

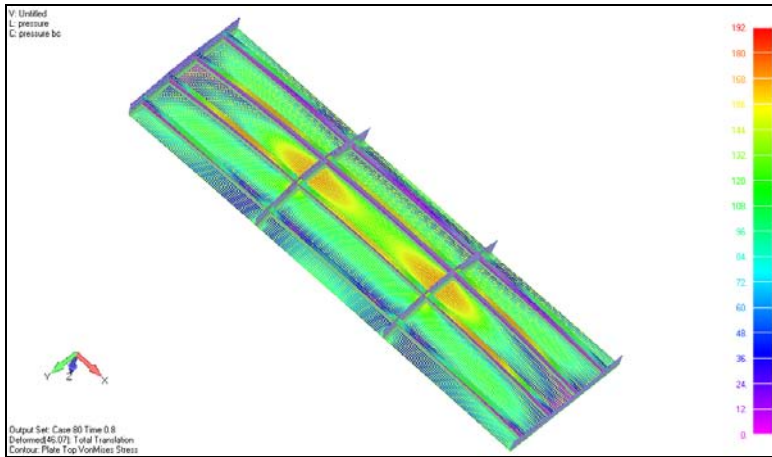


Figure E-3: Stress & Deflection plot for Model 2

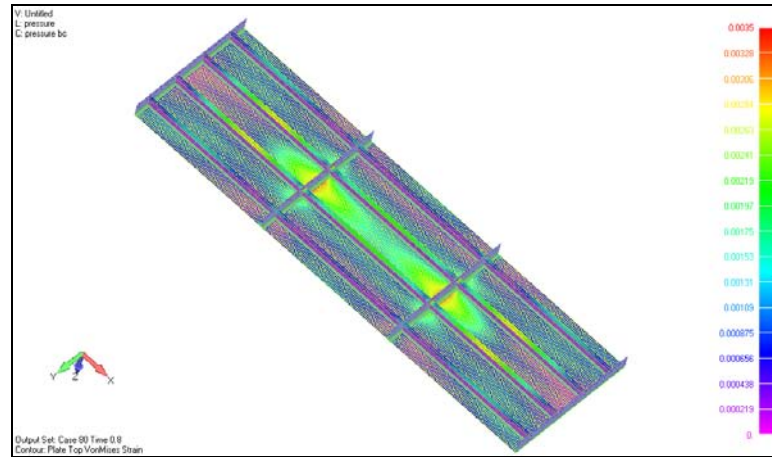


Figure E-4: Strain plots for Model 2

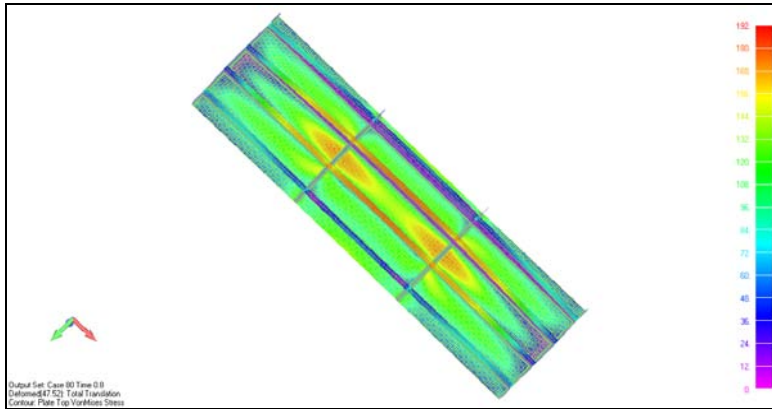


Figure E-5: Stress & Deflection plot for Model 3

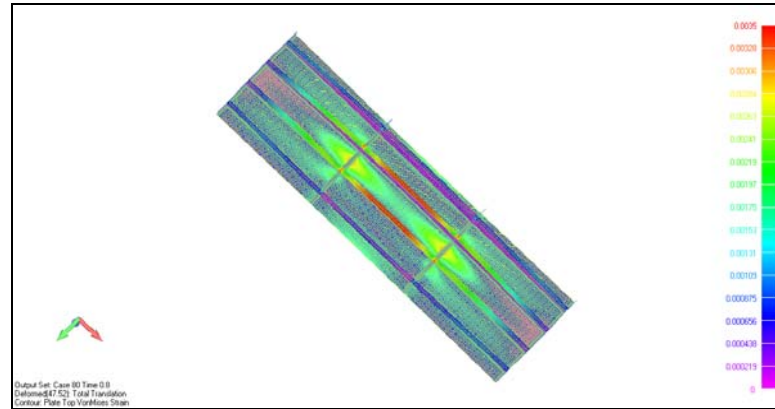


Figure E-6: Strain plots for Model 3

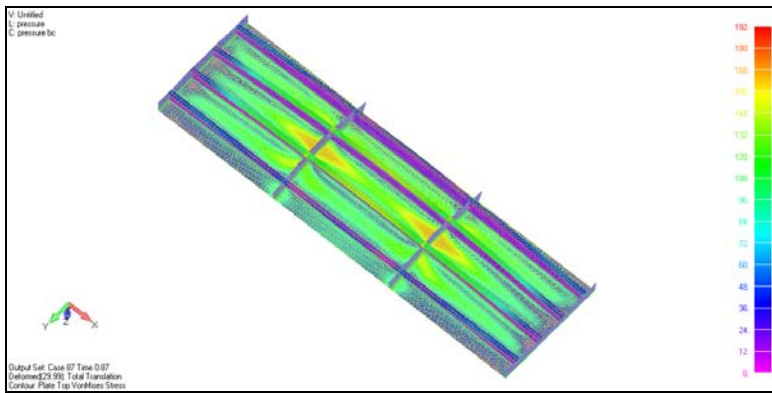


Figure E-7: Stress & Deflection plot for Model 4

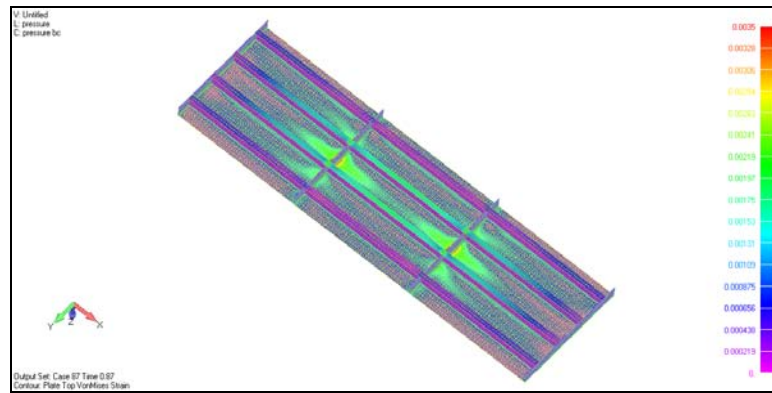


Figure E-8: Strain plots for Model 4

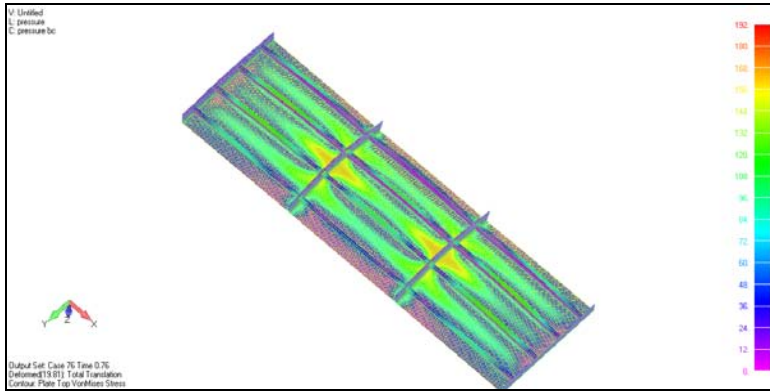


Figure E-9: Stress & Deflection plot for Model 5

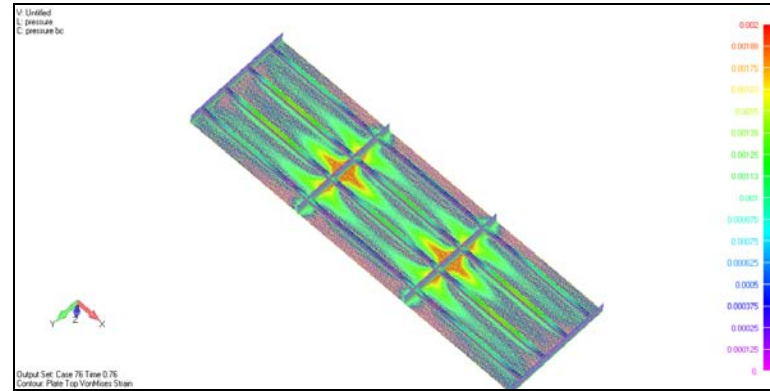


Figure E-10: Strain plots for Model 5

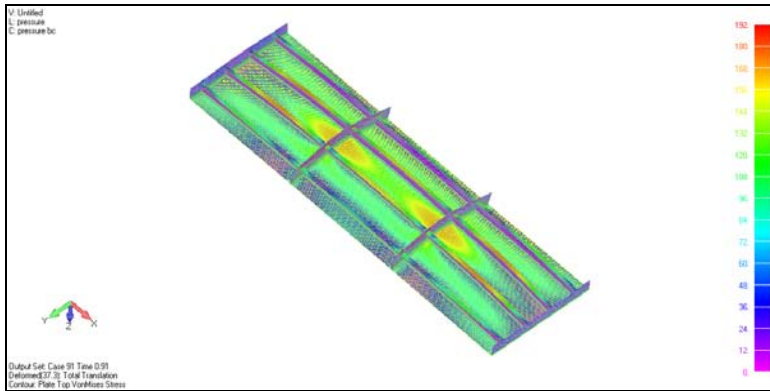


Figure E-11: Stress & Deflection plot for Model 6

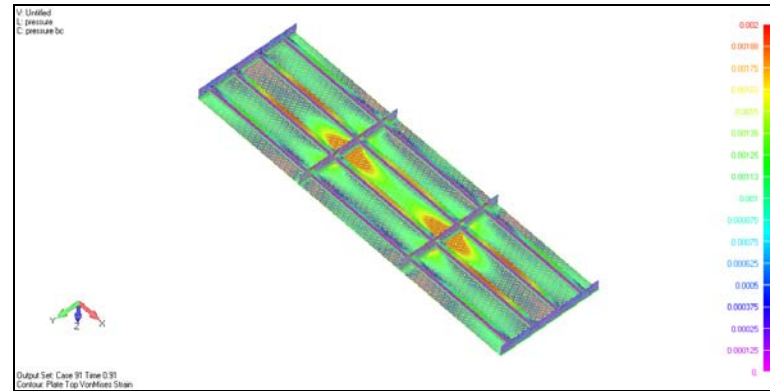


Figure E-12: Strain plots for Model 6

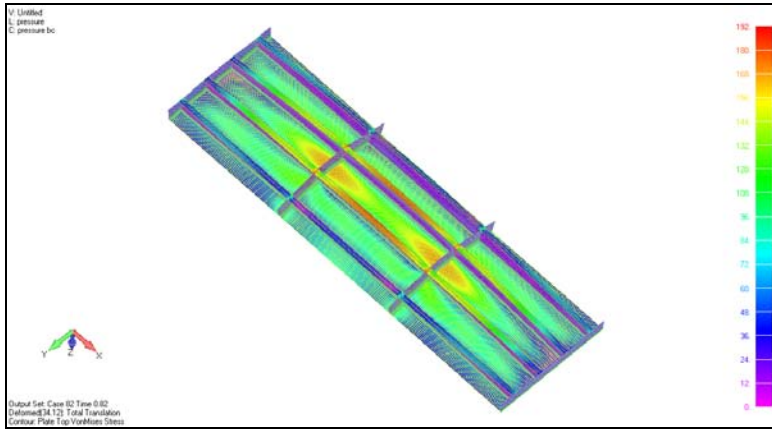


Figure E-13: Stress & Deflection plot for Model 7

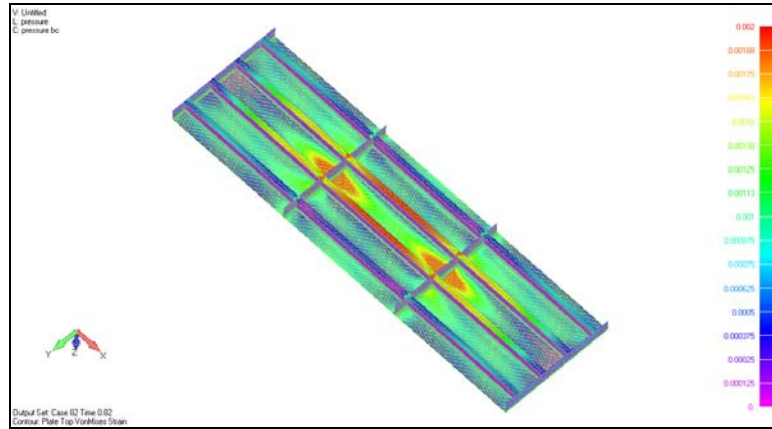


Figure E-14: Strain plots for Model 7

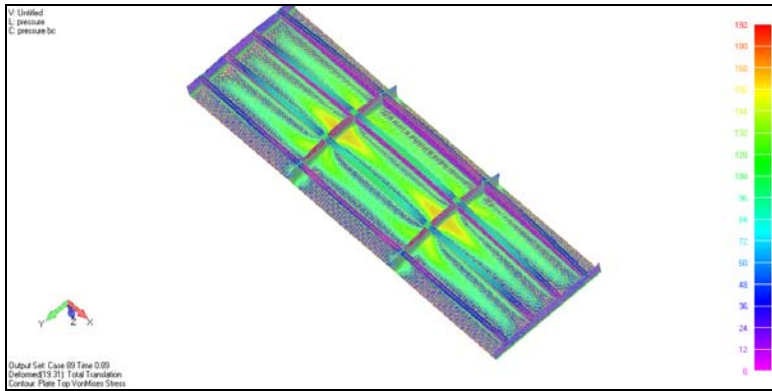


Figure E-15: Stress & Deflection plot for Model 8

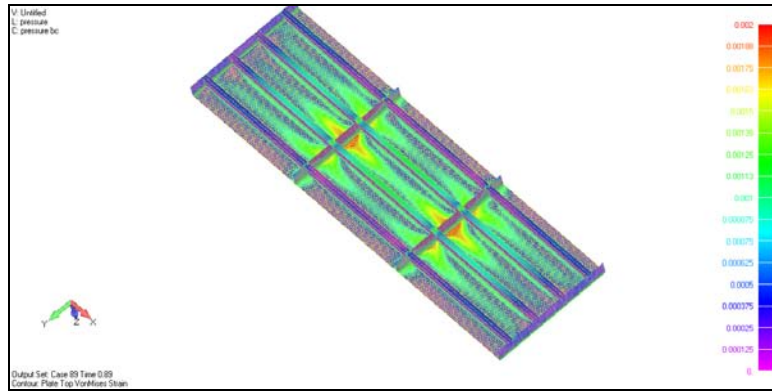


Figure E-16: Strain plots for Model 8

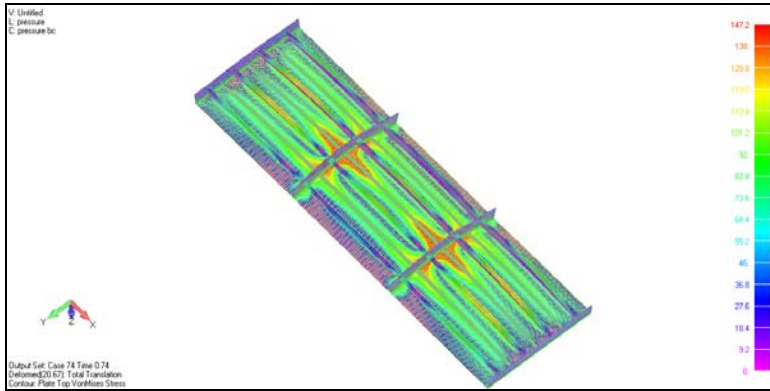


Figure E-17: Stress & Deflection plot for Model 9

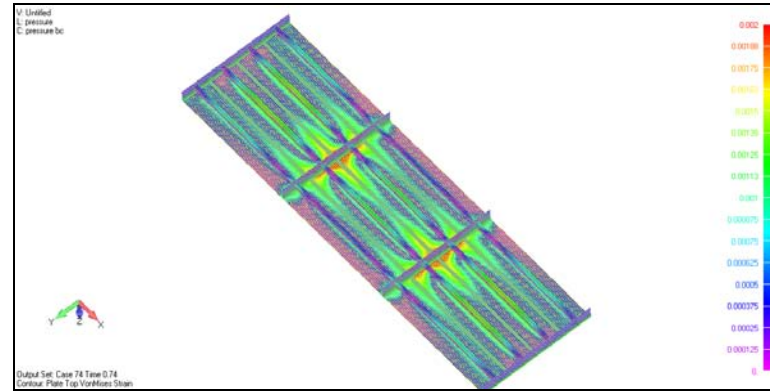


Figure E-18: Strain plots for Model 9

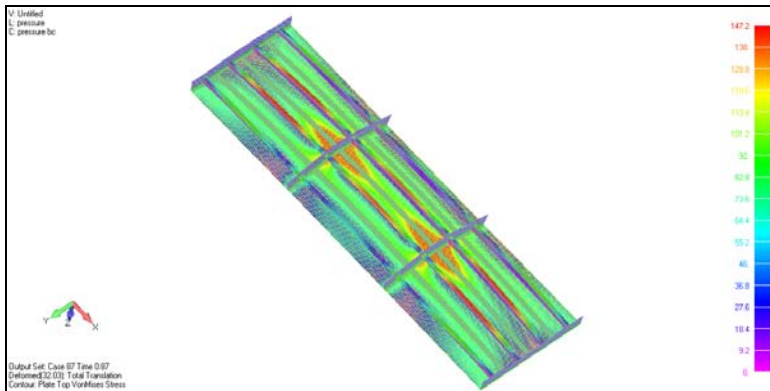


Figure E-19: Stress & Deflection plot for Model 10

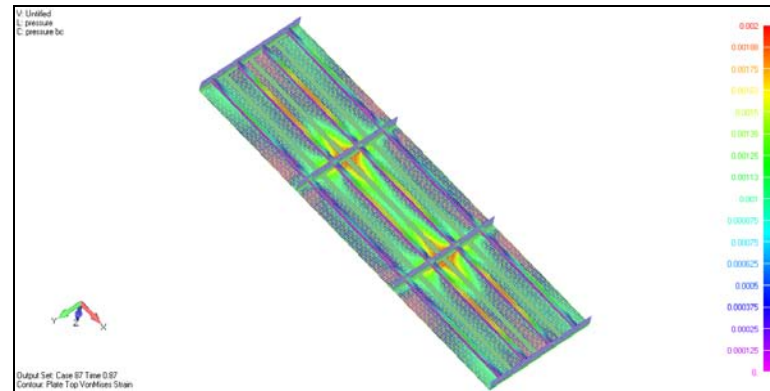


Figure E-20: Strain plots for Model 10

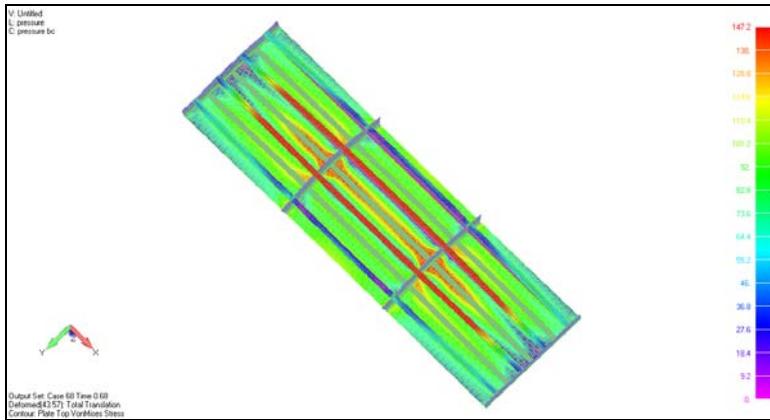


Figure E-21: Stress & Deflection plot for Model 11

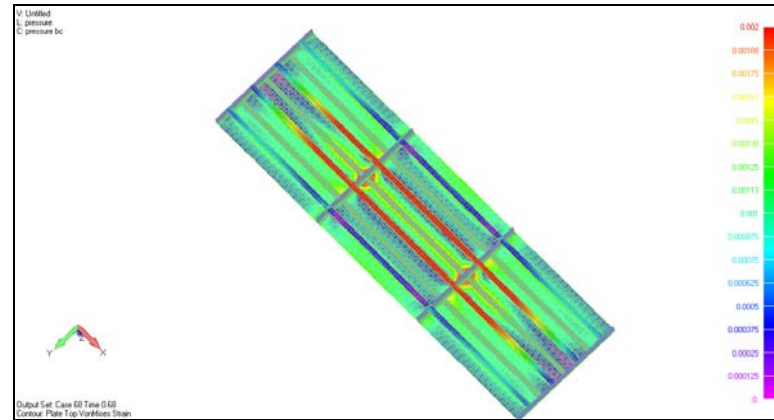


Figure E-22: Strain plots for Model 11

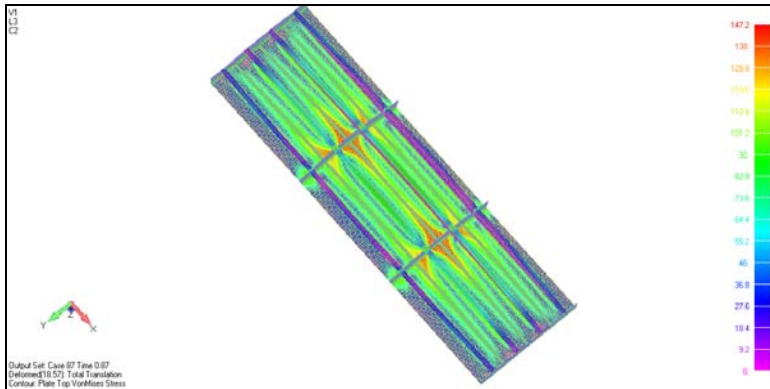


Figure E-23: Stress & Deflection plot for Model 12

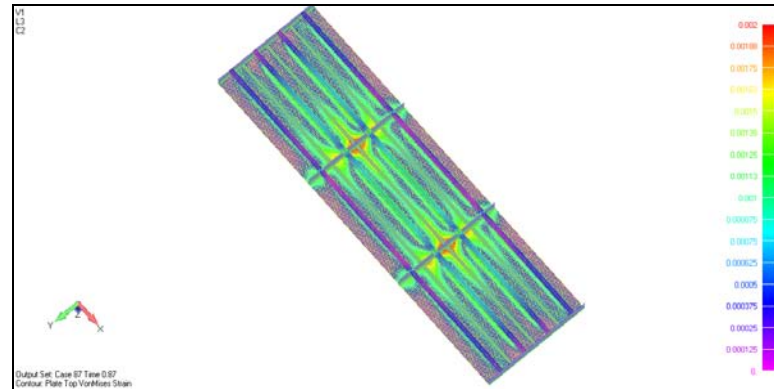


Figure E-24: Strain plots for Model 12

PROJECT TECHNICAL COMMITTEE MEMBERS

The following persons were members of the committee that represented the Ship Structure Committee to the Contractor as resident subject matter experts. As such they performed technical review of the initial proposals to select the contractor, advised the contractor in cognizant matters pertaining to the contract of which the agencies were aware, performed technical review of the work in progress and edited the final report.

Chairman

Members

Contracting Officer's Technical Representative:

Marine Board Liaison:

Executive Director Ship Structure Committee:

SHIP STRUCTURE COMMITTEE LIAISON MEMBERS

LIAISON MEMBERS

American Society of Naval Engineers	Captain Dennis K. Kruse (USN Ret.)
Bath Iron Works	Mr. Steve Tarpy
Colorado School of Mines	Dr. Stephen Liu
Edison Welding Institute	Mr. Rich Green
International Maritime Organization	Mr. Igor Ponomarev
Int'l Ship and Offshore Structure Congress	Dr. Alaa Mansour
INTERTANKO	Mr. Dragos Rauta
Massachusetts Institute of Technology	
Memorial University of Newfoundland	Dr. M. R. Haddara
National Cargo Bureau	Captain Jim McNamara
National Transportation Safety Board - OMS	Dr. Jack Spencer
Office of Naval Research	Dr. Yapa Rajapaksie
Oil Companies International Maritime Forum	Mr. Phillip Murphy
Samsung Heavy Industries, Inc.	Dr. Satish Kumar
United States Coast Guard Academy	Commander Kurt Colella
United States Merchant Marine Academy	William Caliendo / Peter Web
United States Naval Academy	Dr. Ramswar Bhattacharyya
University of British Columbia	Dr. S. Calisal
University of California Berkeley	Dr. Robert Bea
Univ. of Houston - Composites Eng & Appl.	
University of Maryland	Dr. Bilal Ayyub
University of Michigan	Dr. Michael Bernitsas
Virginia Polytechnic and State Institute	Dr. Alan Brown
Webb Institute	Prof. Roger Compton

RECENT SHIP STRUCTURE COMMITTEE PUBLICATIONS

Ship Structure Committee Publications on the Web - All reports from SSC 1 to current are available to be downloaded from the Ship Structure Committee Web Site at URL:

<http://www.shipstructure.org>

SSC 445 – SSC 393 are available on the SSC CD-ROM Library. Visit the National Technical Information Service (NTIS) Web Site for ordering hard copies of all SSC research reports at

URL: <http://www.ntis.gov>

SSC Report Number	Report Bibliography
SSC 461	Structural Challenges Faced By Arctic Ships, Kendrick A., Daley C. 2011
SSC 460	Effect of Welded Properties on Aluminum Structures, Sensharma P., Collette M., Harrington J. 2011
SSC 459	Reliability-Based Performance Assessment of Damaged Ships, Sun F., Pu Y., Chan H., Dow R.S., Shahid M., Das P.K. 2011
SSC 458	Exact Mapping of Residual Stress in Ship Hull Structures by Use of Neutron Diffraction Das. S. Kenno S. 2009
SSC 457	Investigation of Plastic Limit States for Design of Ship Hull Structures, Daley C., Hermanski G. 2009
SSC 456	Buckling Collapse Testing on Friction Stir Welded Aluminum Stiffened Plate Structures, Paik J.K. 2009
SSC 455	Feasibility, Conceptual Design and Optimization of a Large Composite Hybrid Hull, Braun D., Pejcic M. 2008
SSC 454	Ultimate Strength and Optimization of Aluminum Extrusions, Collette M., Wang C. 2008
SSC 453	Welding Distortion Analysis Of Hull Blocks Using Equivalent Load Method Based On Inherent Strain, Jang C.D. 2008
SSC 452	Aluminum Structure Design and Fabrication Guide, Sielski R.A. 2007
SSC 451	Mechanical Collapse Testing on Aluminum Stiffened Panels for Marine Applications, Paik J.K. 2007
SSC 450	Ship Structure Committee: Effectiveness Survey, Phillips M.L., Buck R., Jones L.M. 2007
SSC 449	Hydrodynamic Pressures and Impact Loads for High Speed Catamaran / SES, Vorus W. 2007
SSC 448	Fracture Mechanics Characterization of Aluminum Alloys for Marine Structural Applications, Donald J.K., Blair A. 2007